TAMPEREEN TEKNILLINEN YLIOPISTO
TAMPERE UNIVERSITY OF TECHNOLOGY

MIKKO HALLOMAA

# ELECTRICAL MODELING OF DEEP BRAIN STIMULATION

Master of Science Thesis

Examiner: Prof. Hannu Eskola
Examiner and topic approved by the Faculty Council of the Faculty of Computing and Electrical Engineering on 8th of June 2016

# ABSTRACT

**MIKKO HALLOMAA**: Electrical modeling of deep brain stimulation
Tampere University of Technology
Master of Science Thesis, 68 pages, 4 Appendix pages
April 2017
Master's Degree Programme in Electrical Engineering
Major: Biomeasurements and Bioimaging
Examiner: Prof. Hannu Eskola

Keywords: deep brain stimulation, anterior nuclear group of thalamus, volume of tissue activated, encapsulation

Deep brain stimulation (DBS) is a relatively new and effective method for treating patients suffering from severe and refractory neurological disorders, such as Parkinson's disease and epilepsy. In a DBS treatment, stimulation electrode is implanted into the patient's deep brain structures, which is commonly the subthalamic nucleus in the Parkinson's disease treatment and the anterior nuclear group of thalamus in the epileptic treatment. Major challenges in the procedure are the correct electrode placement and the proper stimulation parameters. Failure in either one may provoke adverse effects or prevent the effective treatment from occurring.

The objective of this thesis was to create a model that could be used to observe the electrical behavior of the deep brain stimulation. Stimulation response was measured with the concept of volume of tissue activated (VTA), which describes the level of neuronal activation. 3D uniform and 2D anatomical models were created for the task. Model included encapsulation, inhomogeneous tissue and anisotropy to give a proper estimate on the electrical behavior.

Misplaced electrodes are one of the major concerns in DBS surgeries and 1/3 mm misplacement may correspond to a few volts in amplitude increase. Encapsulation had an impact of requiring stimulation amplitudes to be increased by over 100% of the initial value. Anisotropic fiber tracts and conductivity variations significantly altered the shape of the VTA. In some cases, changing the electrode configuration or active electrode in a DBS lead proved to be more effective alternative than attempting to increase VTA by increasing the stimulation amplitude.

# TIIVISTELMÄ

**MIKKO HALLOMAA**: Aivojen syvästimulaation sähköinen mallintaminen
Tampereen teknillinen yliopisto
Diplomityö, 68 sivua, 4 liitesivua
Huhtikuu 2017
Sähkötekniikan diplomi-insinöörin tutkinto-ohjelma
Pääaine: Biomittaukset ja -kuvantaminen
Tarkastaja: professori Hannu Eskola

Avainsanat: aivojen syvästimulaatio, thalamuksen etummainen tumakeryhmä, aktivoitunut kudostilavuus, kapselointi

Aivojen syvästimulaatio on kohtalaisen uusi ja tehokas menetelmä potilaiden hoitoon, jotka kärsivät vakavista ja vaikeasti paranevista neurologisista sairauksista, kuten Parkinsonin taudista ja epilepsiasta. Aivojen syvästimulaatiohoidossa potilaan aivojen syvärakenteisiin implantoidaan stimulointielektrodi, joka on yleisesti thalamuksen alainen tumake Parkinsonin taudin hoidossa ja thalamuksen etummainen tumakeryhmä epilepsian hoidossa. Menetelmän suurimmat haasteet ovat elektrodin asettaminen oikeaan kohtaan sekä oikeiden stimulointiparametrien valinta. Epäonnistuminen toisessa näistä voi johtaa epäsuotuisien sivuvaikutusten ilmaantumiseen tai tehottomaan hoitotulokseen.

Tämän diplomityön tavoitteena oli luoda malli, jolla voidaan tarkkailla aivojen syvästimulaation sähköistä käyttäytymistä. Stimulointivastetta arvioitiin aktivoituneella kudostilavuudella, joka kuvaa neuronien aktivaatiotasoa. Malliin luotiin yhdenmukainen 3D-, sekä anatomiaa kuvaava 2D-malli. Malli sisälsi kapseloinnin, epähomogeenisen kudoksen, sekä anisotropian arvioidakseen sähköistä vastetta kunnollisesti.

Väärin sijoitetut elektrodit ovat yksi suurimmista huolista syvästimulaatio-operaatioissa ja 1/3 mm väärä sijoittelu voi vastata muutaman voltin amplitudin kasvua. Kapselointi vaikutti amplitudiin aiheuttaen jopa 100 % noston tarpeen amplitudin alkuarvoon verrattuna. Anisotroppiiset hermosäikeet ja muutokset johtavuudessa muuttivat aktivoituneen kudostilavuuden muotoa merkittävästi. Eräissä tapauksissa elektrodikonfiguraation tai aktiivisen elektrodin muuttaminen oli tehokkaampi vaihtoehto kuin stimulointiamplitudin nostaminen aktivointitilavuuden kasvattamiseksi.

# PREFACE

This Master of Science thesis was conducted at the Tampere University Hospital (TAYS) and Tampere University of Technology (TUT). This study was done for the staff at the TAYS working on the deep brain stimulation treatment. I would like to thank Professor Hannu Eskola for this great opportunity to be able to work on such an interesting and meaningful project and for the understanding during the long process of finishing the thesis. I would also like to thank Professor Jukka Peltola and Neurosurgeon Kai Lehtimäki at the TAYS for the consultation they provided. Finally I would like to thank my family for supporting me throughout my studies and the thesis process.

Tampere, 22.3.2017

Mikko Hallomaa

# TABLE OF CONTENTS

1. INTRODUCTION ..... 1
2. THEORETICAL BACKGROUND ..... 3
2.1 Anatomy and functions of the brain and thalamus ..... 3
2.1.1 Anatomy of the brain and thalamus ..... 3
2.1.2 Neurons ..... 6
2.1.3 Electrical activity of the thalamus ..... 8
2.2 Electric fields in biological tissue ..... 11
2.3 Epilepsy ..... 13
3. DEEP BRAIN STIMULATION ..... 14
3.1 Introduction to DBS ..... 14
3.2 DBS procedure ..... 14
3.3 Effects of DBS on brain ..... 16
3.4 Electrode placement ..... 17
3.4.1 Anatomical atlases ..... 17
3.4.2 Microelectrode recordings ..... 18
3.5 Stimulation parameters ..... 19
3.5.1 Stimulation amplitude ..... 19
3.5.2 Stimulation pulse width ..... 20
3.5.3 Electrode polarity ..... 21
3.5.4 Stimulation frequency ..... 23
4. MATERIALS AND METHODS ..... 25
4.1 Structure of the model ..... 25
4.1.1 Electrode model ..... 26
4.1.2 Uniform model ..... 27
4.1.3 Model of the anatomy ..... 28
4.1.4 Encapsulation model ..... 32
4.1.5 Material properties ..... 35
4.2 Boundary conditions ..... 37
4.3 Volume of tissue activated ..... 39
4.4 Simulation parameters ..... 41
5. RESULTS AND DISCUSSIONS ..... 42
5.1 VTA demonstration ..... 42
5.2 Polarity and amplitude ..... 45
5.3 Encapsulation ..... 48
5.4 Anatomical structures ..... 55
5.5 Model improvements ..... 61
6. CONCLUSION ..... 62
REFERENCES ..... 63

APPENDIX A: MONOPOLAR VTA CONSTITUENTS

APPENDIX B: BIPOLAR VTA CONSTITUENTS

# TABLE OF FIGURES

***Figure 1.*** *Midsagittal section of the human brain.....4*
***Figure 2.*** *Diencephalon seen ventrally. .....5*
***Figure 3.*** *Left thalamus and its major subdivisions.....6*
***Figure 4.*** *Illustration of a neuron (alpha α motoneuron). .....7*
***Figure 5.*** *Action potential propagation in an unmyelinated and a myelinated axon.....8*
***Figure 6.*** *Schematic representation of the functions of the T-type Ca2+-channel paired with K-channel. .....9*
***Figure 7.*** *Membrane potential of the thalamic relay cell with respect to time.....10*
***Figure 8.*** *Membrane potential with respect to time during tonic and burst firing of the relay cells. .....10*
***Figure 9.*** *Illustration of an implanted DBS system.....15*
***Figure 10.*** *T1 weighted 3 T MRI image from the coronal plane on the left and the corresponding atlas representation on the right.....18*
***Figure 11.*** *Typical strength-duration curve of a neuron. .....20*
***Figure 12.*** *Monopolar and bipolar electric potential field patterns as cross sectional views.....22*
***Figure 13.*** *Monopolar, bipolar and tripolar electric potential field patterns from left to right.....23*
***Figure 14.*** *Middle cut plane and the 3D model of the DBS lead used in the model.....26*
***Figure 15.*** *Model geometry of a uniform gray matter domain and the electrode described in the section 4.1.1. .....27*
***Figure 16.*** *Atlas image to geometry process phases 1-3. .....29*
***Figure 17.*** *Atlas image to geometry process phases 4-6. .....30*
***Figure 18.*** *Atlas image to geometry process phases 7-9. .....31*
***Figure 19.*** *Two different levels of magnifications of the meshed border showing the polygonal nature of the border.....32*
***Figure 20.*** *Middle cut plane and the 3D model of the stimulation lead surrounded by symmetrical encapsulation layer. .....34*
***Figure 21.*** *Middle cut plane and the 3D model of the stimulation lead surrounded by an asymmetrical encapsulation layer. .....35*
***Figure 22.*** *Monopolar and bipolar stimulation illustrating the ∂x∂x component of the VTA.....43*
***Figure 23.*** *VTA isosurfaces in a homogenous and isotropic medium generated with a -5 V monopolar stimulation.....43*
***Figure 24.*** *VTA isosurfaces in a homogenous and isotropic medium generated with a -5 V monopolar stimulation.....44*
***Figure 25.*** *VTA isosurfaces in a homogenous and isotropic medium generated with a bipolar stimulation with cathode at -5 V and anode at 5 V. .....44*

***Figure 26.*** *Monopolar VTA union of all constituents of equation (25).* ..... *45*
***Figure 27.*** *Bipolar VTA union of all constituents of equation (25).* ..... *45*
***Figure 28.*** *VTA dependence of the stimulation voltage in monopolar and bipolar stimulations.* ..... *46*
***Figure 29.*** *Difference between a constant activation function and a voltage dependent action function.* ..... *48*
***Figure 30.*** *VTA isosurfaces with an encapsulation layer generated with a monopolar stimulation.* ..... *49*
***Figure 31.*** *VTA isosurfaces with an encapsulation layer generated with a bipolar stimulation.* ..... *49*
***Figure 32.*** *VTA dependence of the encapsulation layer thickness in monopolar and bipolar stimulations with a stimulation voltage of -5 V* ..... *50*
***Figure 33.*** *VTA dependence of the stimulation voltage in monopolar and bipolar stimulations with an encapsulation layer of 0.3 mm* ..... *50*
***Figure 34.*** *Voltage in monopolar and bipolar stimulation while the encapsulation layer grows.* ..... *52*
***Figure 35.*** *VTA dependence of the stimulation voltage in monopolar and bipolar stimulations with an encapsulation layer of 0.3 mm* ..... *53*
***Figure 36.*** *Anodal block estimations with and without the encapsulation layer in -5 V monopolar stimulation.* ..... *54*
***Figure 37.*** *VTA dependence of the stimulation voltage in monopolar stimulation with a non-uniform encapsulation layer varying from 0.15 to 0.3 mm* ..... *55*
***Figure 38.*** *Electric fields in monopolar and bipolar stimulation of the ANT* ..... *56*
***Figure 39.*** *Effects of CSF on VTA in monopolar stimulation.* ..... *56*
***Figure 40.*** *Effects of anisotropic white matter on VTA in monopolar stimulation* ..... *57*
***Figure 41.*** *VTA of a -3 V monopolar stimulation, -3 V centered monopolar stimulation and -3 V/3 V bipolar stimulation.* ..... *58*
***Figure 42.*** *Stimulation voltage dependence on the ANT coverage* ..... *58*
***Figure 43.*** *Hypothetical stimulation target and the misplaced electrode.* ..... *59*
***Figure A-1.*** *VTA constituents of a monopolar stimulation in a homogenous and isotropic medium.* $\partial x \partial x$ *and* $\partial x \partial y$ *components* ..... *i*
***Figure A-2.*** *VTA constituents of a monopolar stimulation in a homogenous and isotropic medium.* $\partial x \partial z$ *and* $\partial y \partial y$ *components* ..... *i*
***Figure A-3.*** *VTA constituents of a monopolar stimulation in a homogenous and isotropic medium.* $\partial y \partial z$ *and* $\partial z \partial z$ *components* ..... *ii*
***Figure B-1.*** *VTA constituents of a bipolar stimulation in a homogenous and isotropic medium.* $\partial x \partial x$ *and* $\partial x \partial y$ *components* ..... *iii*
***Figure B-2.*** *VTA constituents of a bipolar stimulation in a homogenous and isotropic medium.* $\partial x \partial z$ *and* $\partial y \partial y$ *components* ..... *iii*
***Figure B-3.*** *VTA constituents of a bipolar stimulation in a homogenous and isotropic medium.* $\partial y \partial z$ *and* $\partial z \partial z$ *components* ..... *iv*

# LIST OF SYMBOLS AND ABBREVIATIONS

### Abbreviations

| | |
|---|---|
| 2D | two dimensions |
| 3D | three dimensions |
| A80 | measure of hardness of the material |
| AC | anterior commissure |
| ANT | anterior nuclear group of thalamus |
| CE | CE marking |
| CSF | cerebrospinal fluid |
| CT | computed tomography |
| DBS | deep brain stimulation |
| DTI | diffusion tensor imaging |
| EEG | electroencephalography |
| FA | fractional anisotropy |
| FDA | Food and Drug Administration |
| FEM | finite element method |
| IPG | internal pulse generator |
| MD | mean diffusivity |
| MRI | magnetic resonance imaging |
| MTT | mammillothalamic tract |
| PC | posterior commissure |
| PET | positron emission tomography |
| WHO | World Health Organization |
| YCbCr | color space |

### Symbols

| | |
|---|---|
| $\alpha$ | angle |
| $C_o$ | extracellular ion concentration |
| $C_i$ | intracellular ion concentration |
| $Ca^{2+}$ | calcium ion |
| $Cl^-$ | chloride ion |
| $d$ | separation distance |
| $\mathbf{d}$ | displacement vector |
| $D_{ij}$ | diffusion tensor element |
| $\boldsymbol{D}$ | diffusion tensor |
| $\varepsilon$ | permittivity |
| $\varepsilon_0$ | permittivity of the vacuum |
| $\varepsilon_r'$ | real part of the relative permittivity |
| $\varepsilon_r''$ | complex part of the relative permittivity |
| $\bar{\varepsilon}$ | eigenvector |
| $E$ | transmembrane potential |
| $\mathbf{E}$ | electric field |
| $f_{act}$ | activation function |
| $F$ | Faraday's constant |
| $\theta$ | polar angle |
| $I$ | current |

| | |
|---|---|
| $I_{rh}$ | rehobase current |
| $I_T$ | T-channel inward current |
| $\mathbf{J}_e$ | externally generated current density vector |
| $\mathbf{J}$ | current density vector |
| $K^+$ | potassium ion |
| $\lambda$ | eigenvalue |
| $\mathbf{n}$ | normal vector |
| $Na^+$ | sodium ion |
| $\pi$ | pi |
| $\rho$ | volume charge density |
| $P$ | permeability |
| $r$ | radius |
| $R$ | universal gas constant |
| $\sigma$ | conductivity |
| $\sigma_L$ | longitudinal conductance |
| $\sigma_T$ | transverse conductance |
| $t$ | time |
| $t_{PW}$ | pulse width |
| $T$ | temperature |
| $T_{ch}$ | chronaxie time |
| $U$ | electric potential |
| $U_{bi}$ | electric potential in bipolar stimulation |
| $U_{mono}$ | electric potential in monopolar stimulation |
| $U_{tri}$ | electric potential in tripolar stimulation |
| $V$ | electric potential |
| $x,y,z$ | spatial coordinates |

**Mathematical expressions**

| | |
|---|---|
| $k_{ij}$ | matrix element |
| $\boldsymbol{K}$ | matrix or tensor |
| $\boldsymbol{K}^{\mathbf{T}}$ | matrix transpose |
| $\nabla$ | gradient operator |
| $\nabla\bullet$ | divergence operator |
| $\partial$ | partial derivative operator |

# 1. INTRODUCTION

Brain is the most complex organ in the human body, and thus been under an intense research by both scientists and physicians alike for centuries. Since the discovery of electricity, its interactions with all living beings have fascinated scholars and ordinary people throughout the history. First records of using electricity in medical applications date back to 47 A.D., when Scribbonius Largus used eels and torpedo fish to treat headaches and gouty arthritis. Medical use of electricity began to nourish in the late 1700s, when scientists discovered how electricity could be generated artificially. During the following years, physicians experienced on electricity with animals and humans for both research and treatment purposes. First electrical stimulations of the human brain were performed in 1874 by Roberts Bartholow, who locally provoked cortical excitations with electricity. [1]

Brain has a direct connection to countless chronic disorders that affect people everywhere and at every age. Diseases such as epilepsy, Parkinson's disease, dystonia, essential tremor among others, have a significant impact on an individual's everyday life. Person's quality of life is reduced by inabilities to overcome daily tasks and routines, as well as interaction with the society are hindered. Severe chronic disorders also have a massive economic impact. In addition to medical costs, inabilities decrease work time and productivity and increase the probability of premature deaths. Medications and surgical operations alleviate the symptoms of these diseases to some degree, but certain patients are either inapplicable or resistant to most treatment methods. Deep brain stimulation (DBS) is an effective alternative for these patients. [1, 2]

Deep brain stimulation is a field of neurotherapeutics where regions of the brain are stimulated with electricity. First implanted DBS surgery was performed in the 1990s by Alim Benabid. He implanted a pacemaker and electrodes into the brain and observed the successful results, which has been considered as the first successful DBS operation. DBS has been approved as a treatment method in EU and USA since the late 1990s, and it was initially used to treat patients suffering from movement disorders such as Parkinson's disease and essential tremor. The initial success of the DBS treatments paved the way for new DBS applications for other neurological disorders like dystonia, Tourette syndrome, epilepsy, obsessive compulsive disorder and depression. [1, 3]

DBS, just like any other surgical treatment, involves challenges and risks. Electrical stimulation can cause both excitation and inhibition in the target and the surrounding neurons, and therefore increases susceptibility to severe side effects or failures to provide treatment. This problem can be mitigated with correct electrode placement and stimulation parameters. However, optimal stimulation parameters are difficult to determine as balance has to be found between symptom reduction, side effects and stimulator

power consumption [4]. In addition to stimulation parameters, the final position of the electrode cannot be precisely determined even with the latest targeting software, microelectrode recordings and post-operative imaging [1].

Eventually, a successful DBS treatment requires knowledge of the electrical behavior of the stimulation. This allows the staff to adapt into situations when the treatment results are not occurring or are overshadowed by the adverse effects. The goal of this thesis was to give an insight into neuronal activation by stimulation and how the different properties of tissue and implantation affect the results. Finite element model was used to evaluate the effects of electrode placement, stimulation parameters and encapsulation tissue on the excitation of neurons. Stimulation target was the anterior nuclear group of the thalamus (ANT), which a target commonly used to treat epileptic patients.

The structure of the thesis is divided into 5 chapters. In the first chapter, the theoretical backgrounds for the subject are discussed. The chapter begins with the discussion of the structure and primary functions of the brain and specifically of the anterior nuclear group of the thalamus. Then the nerve cells are explained and the focus is on the relay cells of the thalamus. Next the fundamentals of electrostatics are explained. And finally in the first chapter, the basics of the epilepsy are discussed. The second chapter introduces the basics of DBS, what a typical procedure includes and what are possible side effects. Later in the second chapter, common methods to support electrode placement are discussed and the effects of adjusting stimulation parameters. In the third chapter, materials and methods required to create the model are explained. Chapter begins by describing the different parts involved in the model and how they were created. Then the material parameters and electrical properties included in the model are explained. In the fourth chapter, the results of the simulations are shown and discussed. The chapter begins by illustrating the volume of tissue activated (VTA) around the electrode. Then the encapsulation is added and finally a planar model of the ANT and thalamus is included. In the fifth chapter, the conclusion about the model and results are discussed.

# 2. THEORETICAL BACKGROUND

In the following section, anatomy of the brain is shortly discussed and narrowed towards the structure of the anterior nuclear group of thalamus. It is the anatomical region of interest in this thesis and therefore the electrical activity of neurons and thalamus specifically is further discussed in the following section. Then the basics of electrostatics and electrical behavior of the tissue are review. Finally the epilepsy is shortly explained, as it is the reason why we are interested in anterior nuclear group of thalamus.

## 2.1 Anatomy and functions of the brain and thalamus

Brain is the most complex organ in the human body and center of the nervous system. It is responsible for many vital and involuntary tasks, such as controlling circulation, respiration and temperature regulation, as well as processing sensory information, managing memory and secreting hormones. Brain also enables consciousness, thinking and emotions. Therefore brain disorders may have a significant impact on individuals' daily life and behavior [5, 6].

### 2.1.1 Anatomy of the brain and thalamus

Brain is an arrangement of over 100 billion nerve cells and lies at the center of the central nervous system. Brain is surrounded by a bony shell, the skull, and three layers of connective tissue membranes called then meninges. Primary blood supply to the brain flows in arteries and veins within these meninges. Brain constitutes of the three major subdivisions, illustrated in the Figure 1. The largest and the most prominent part is the *cerebrum* that involves *cerebral hemispheres* (1) and *diencephalon* (2). Below the diencephalon is the *brainstem* that is an extension of the spinal cord, which includes *midbrain* (3), *medulla* (4) and *pons* (5). Posterior to the brainstem is *cerebellum* (6). Surfaces of the cerebral hemispheres and cerebellum are prominently featured with fissures and ridges that can be recognized from the Figure 1. [5, 6, 7]

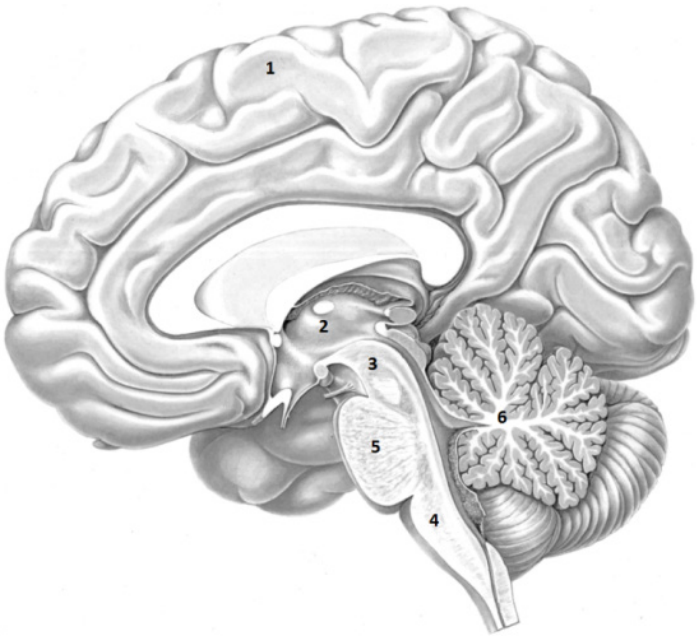


***Figure 1.*** *Midsagittal section of the human brain. Regions shown in the figure are cerebral hemisphere (1), diencephalon (2), midbrain (3), medulla (4), pons (5) and cerebellum (6). Adapted from* [7].

Inside the brain is a ventricular system that is an arrangement of cavities filled with cerebrospinal fluid (CSF). Ventricular system contains paired left and right lateral ventricles, the third ventricle and the fourth ventricle. All ventricles are connected to each other and the CSF eventually flows to the spinal cords' central canal or to the subarachnoid space. CSF provides both mechanical and immunological protection and supplies nutrients for the central nervous system [6, 7].

Diencephalon of the cerebrum is further divided into four subregions, called *hypothalamus*, *ventral thalamus*, *epithalamus* and *dorsal thalamus*. Dorsal thalamus is the largest of these four parts and often referred to just as thalamus [5, 6]. Thalamus (1) is located bilaterally below *lateral ventricles* (2) that are illustrated in the Figure 2. Third ventricle (3) is constrained between thalami. *Massa intermedia* (4) is a gray matter connection between thalami that runs through the third ventricle. *Anterior nuclear group the thalamaus* (5) is partially visible in the Figure 2. On the lateral side of the thalamus resides the internal capsule, which is a large bundle of nerve fibers connecting the lower levels of central nervous system, including thalami, to the cerebral cortex [7].

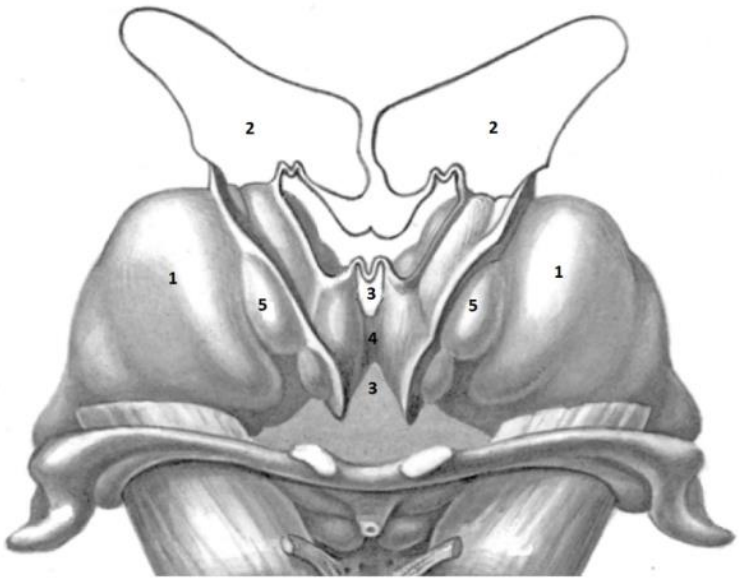


***Figure 2.*** *Diencephalon seen ventrally. Regions shown in the figure are thalamus (1), lateral ventricles (2), third ventricle (3), massa intermedia (4) and anterior nuclear group of the thalamus (5). Adapted from* [7].

Thalamus itself is a group of adjacent nuclei, and therefore can be divided into multiple subdivisions, including nuclear groups and fiber tracts. Each nuclear group can be further divided into even smaller regions [7]. A distinct feature of the thalamus is the *internal medullary lamina,* a layer of white matter that runs through the whole thalamic structure dividing it into conspicuous regions. Figure 3 illustrates thalamus of the left side. In the anterior part of thalamus, internal medullary lamina splits into two branches, forming a Y-shaped structure. Within the bifurcated anterior part lies the anterior nuclear group of the thalamus (ANT, A in the Figure 3). ANT can be further divided into anteroventral, anterodorsal and anteromedial nuclei. Part of the anterior nuclear group extrudes from the thalamic structure, which can be seen in the Figure 2 marked as (5). *Reticular nucleus of the thalamus* (R) is often considered to be part of this group due to its functional relationship with nuclei of the anterior group, even though it is cytoarchitecturally part of the ventral thalamus. On the medial side of the lamina is the *dorsomedial nuclear group* (DM). Lateral side of the lamina can be considered as being a single *ventrolateral nuclear group*, or divided into *ventral nuclear group* (VA, VL, VPL and VPM) and *lateral nuclear group* (LD, LP and P). Within the internal medullary lamina is *centromedian nucleus* (CM). Nomenclature of the thalamic nuclei may vary in different literature [5, 6].

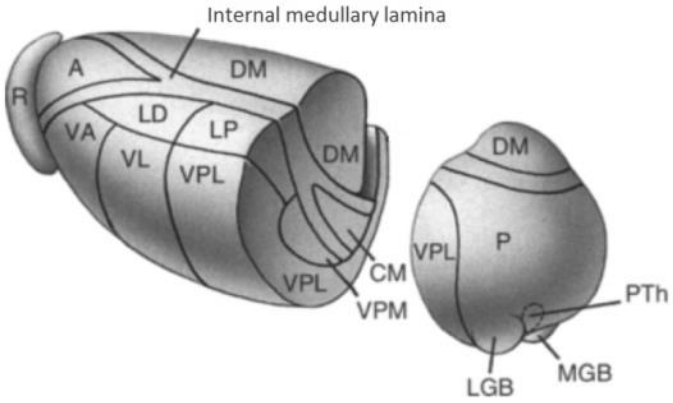


***Figure 3.*** *Left thalamus and its major subdivisions. In the figure, section A points towards the front of the head and section DM towards the center of the head. Adapted from* [6].

Two important neural pathways associated with the thalamus and especially ANT, are the *mammillothalamic tract* (MTT) and *fornix*. Fornix is a fiber bundle that leaves hippocampus and terminates at the mammillary bodies. MTT is an afferent fiber bundle that comes from the mammillary body to the anterior nuclear group. Anterior nuclear group receives information from the limbic system and mammillary bodies through these pathways [5].

Primary function of the thalamus is to relay information to the cerebral cortex. Therefore most of the inputs that cerebral cortex receives, originates from the thalamus. As far as current knowledge of the thalamus goes, each area of the cerebral cortex receives some information from the thalamus. Also most thalamic nuclei have their specific projection area in the cortex [8]. This includes somatic motor information, reticular information and sensory information, but excluding olfactory signals. Thalamus is also assumed to have an essential role in cognition, awareness and arousal. Most connections with thalamus and cerebral cortex are transferred along the previously mentioned internal capsule [5, 9, 10].

### 2.1.2 Neurons

Nerve cells (neurons) are the functional units in the central and peripheral nervous systems. There are approximately 100–200 billion neurons and glial cells in the brain alone. Structure of each neuron is fundamentally similar consisting of 3 basic parts. Cell body (soma) is the center of the neuron and it contains the nucleus and other vital cell organelles. Axon conducts the information from the soma to the presynaptic terminals. Dendrites receive the information from other neurons [6]. Figure 4 illustrates a typical neuron.

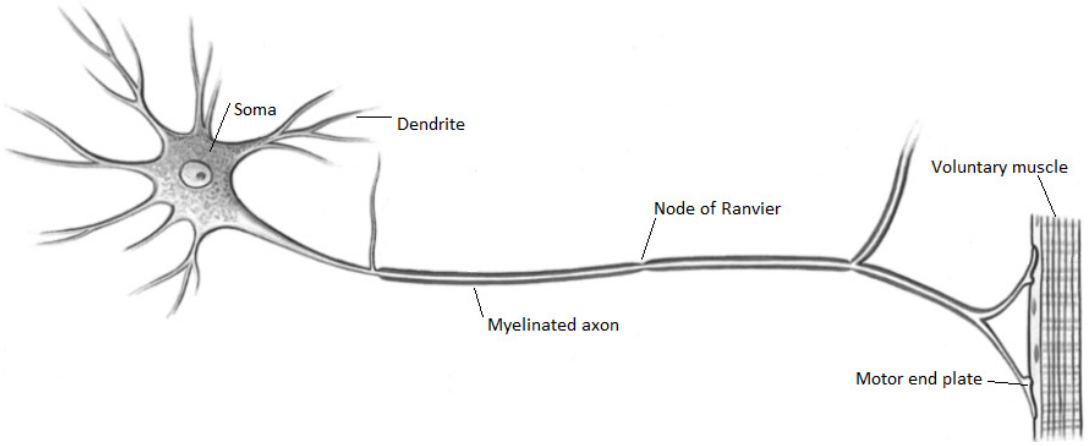


***Figure 4.*** *Illustration of a neuron (alpha α motoneuron). In a motoneuron, presynaptic terminals are located at the motor end plate that connects the axon into a sarcolemma and voluntary muscle. For convenience axon is truncated in the picture. Adapted from* [6].

Neurons possess an electrical potential difference with respect to the extracellular space. This resting potential of a neuron is typically in the range of -60–-70 mV [6]. Resting potential is maintained by the difference in ion concentrations between intra- and extracellular spaces. Unbalanced ion concentration attempts to balance itself by the means of diffusion through the ion channels in the cell membrane. As a result, charges are accumulating on both sides of the membrane, which forms an electric gradient across the cell membrane. Electric gradient opposes the initial ion diffusion, creating a balanced state. At the resting potential, electrical and chemical gradients are equal and ion flux is zero [6, 11]. Membrane potential can be calculated from the Goldman equation (1). Equation (1) shows the Goldman equation in a situation where $Na^+$, $K^+$ and $Cl^-$ ions are permeable through the cell membrane.

$$E = \frac{RT}{F} \ln \frac{P_K[K^+]_o + P_{Na}[Na^+]_o + P_{Cl}[Cl^-]_i}{P_K[K^+]_i + P_{Na}[Na^+]_i + P_{Cl}[Cl^-]_o} \tag{1}$$

In the equation (1), $E$ (V) is the transmembrane potential, $R$ (J/(molK) is the universal gas constant, $T$ (K) is the temperature, $F$ (C/mol) is Faraday's constant, $P_x$ (m/s) is the permeability of ion x and $[X]_y$ (mol/m$^3$) is the concentration of ion X, where the subscript y denotes whether the concentration is inside ($i$) or outside ($o$) of the cell membrane [6].

Cell membranes of neurons contain plenty of voltage gated ion channels that react to electric fields. Increasing the extracellular potential above a certain threshold value, causes ion channels to open and the cell depolarizes. Depolarization propagates along the axon, opening the adjacent ion channels until it reaches a presynaptic terminal. Depolarization last a few milliseconds, ending in a repolarization and possible hyperpolarization [6, 7]. Depolarization of myelinated axon is represented in a Figure 5. Membrane conductance is explained in more detail in section 2.1.3.

Axons are often covered in a fatty substance called myelin. Myelin sheath around the axons gives them their distinctive white color and hence the name white matter. Myelin sheath is not actually part of the never cell, but instead created by glial cells; oligodendrocytes in the central nervous system and Schwann cells in the peripheral nervous system. Myelination electrically insulates the axon from the extracellular space and greatly increases the transmission speed of signals, i.e. the propagation speed of depolarization. Between each myelin sheath there is a region called node of Ranvier that lacks the myelin and allows the conduction of ions through the membrane. In an unmyelinated axon the depolarization propagates continuously, while in a myelinated axon the depolarization jumps from node to node. [7, 10]

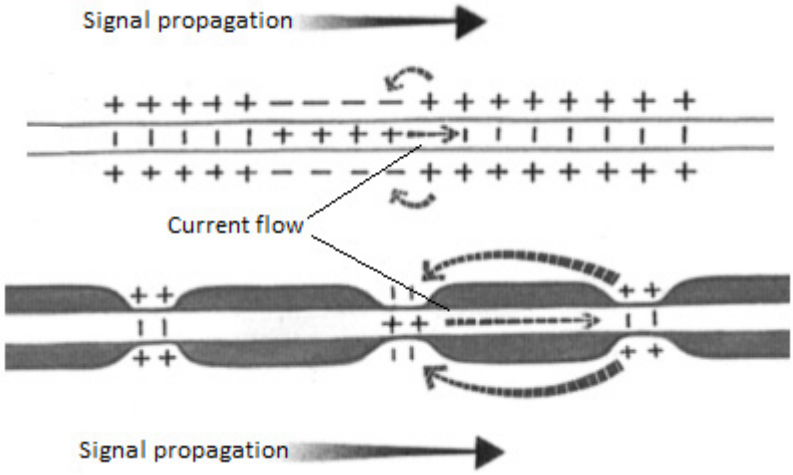


***Figure 5.*** *Action potential propagation in an unmyelinated and a myelinated axon. Signal propagates from soma towards the presynaptic terminals. Dashed arrows represent the intracellular and extracellular current. Adapted from* [6].

Axons terminate into a synapse at the distal end of an axon that is an interface between neurons and the target cells. Neuron also receives information via synapses that connect to its dendrites and soma. Electrical signals cannot pass through the synapse, but instead they cause the release of chemical neurotransmitters to the synaptic cleft, which is small extracellular gap between pre- and postsynaptic cells. If a sufficient amount of neurotransmitters are attached to the postsynaptic neuron, an action potential will be transferred and the signal has been conveyed. [6]

### 2.1.3 Electrical activity of the thalamus

Central nervous system contains multiple types of neurons and each has their countless subtypes. Each neuron also has many ways to enable membrane conductance. These range from membrane voltage controlled and ion concentration dependent gates all the way to synapses. This variety allows cells to respond more dynamically to the inputs and give them control over the type of information that is being transferred. [8]

Primary function of the thalamus is to relay information and hence there is an abundancy of relay cells specifically designed for this type of task. Axons of the relay cells possess the conventional voltage-gated $Na^+$- and $Ca^{2+}$-channels that drive the action potentials. However, soma and dendrites of the relay cells contain plenty of T-type $Ca^{2+}$-channels [8, 12]. The primary difference between the T-type channels and the ordinary voltage gated channels is that the T-channels operate at a slower speed and at a more hyperpolarized region of the membrane potential [10, 12]. Relay cells are not the only neuron type where T-type $Ca^{2+}$-channels can be found, as they are also present in the SA-node of the heart for example [10].

Thalamus has a distinguishable electrical activity manifesting in two firing modes, tonic and burst firing. All excitatory inputs to the relay cells are responded by either of these two firing modes. The fundamental reason for having two distinct firing modes is still unknown, but the mechanics that causes it, is somewhat clear and caused by the T-type $Ca^{2+}$-channels [8, 12]. Due to fundamentally similar nature of an ordinary voltage gated channel and the T-type channel, only the latter is explained here.

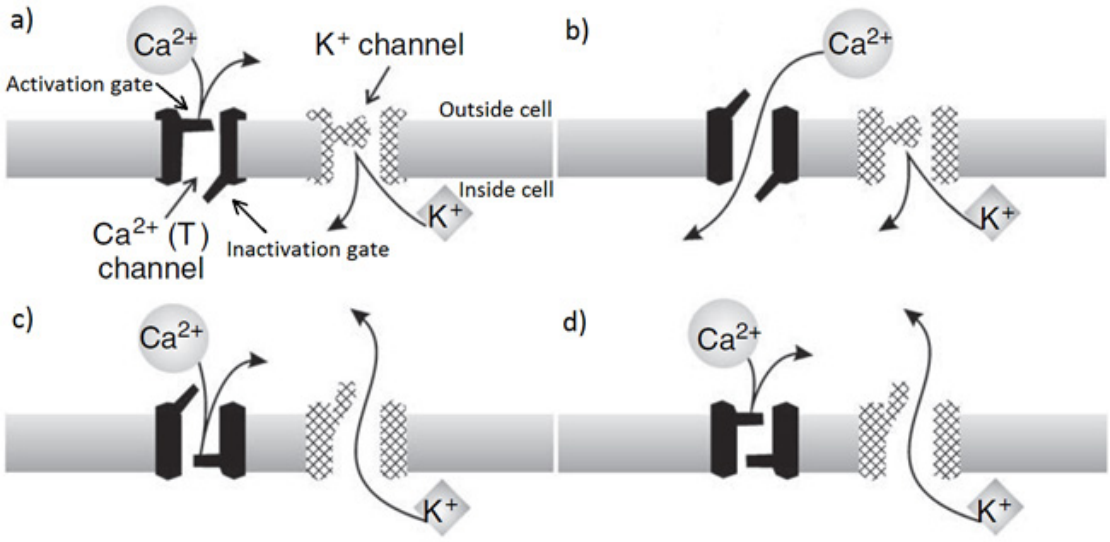


***Figure 6.*** *Schematic representation of the functions of the T-type Ca2+-channel paired with K-channel. Adapted from* [8].

Figure 6 represents the channel activity of the T-type $Ca^{2+}$-channel and Figure 7 the corresponding membrane voltages. T-type $Ca^{2+}$-channel is accompanied by the $K^+$-channels for the complementary ion flux. T-channel has two gates, activation gate and inactivation gate. Both gates have to be open for ion transportation, but if either is closed the influx of $Ca^{2+}$-ions stops. $K^+$-channel has only the activation gate. Both T- and $K^+$-channel activation gates open when the membrane depolarizes, but $K^+$-channel activation gate has a higher depolarization threshold. Inactivation gate opens during hyperpolarization, and also requires about 100 ms of polarization to switch states [8, 12].

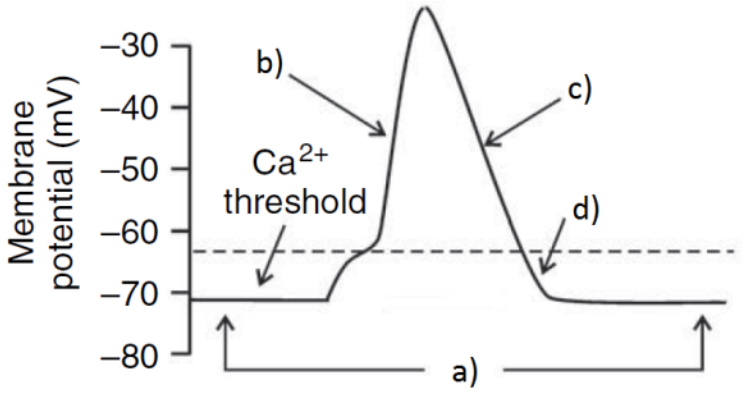


***Figure 7.*** *Membrane potential of the thalamic relay cell with respect to time. Adapted from* [8].

In Figure 6a, the cell membrane is at its resting state and there is no ion flux across the membrane. T-channel activation gate is deactivated and inactivation gate is deinactivated. K+-channel is deactivated as well. In 6b, depolarization of the cell membrane above its threshold opens the activation gate of T-channel. This generates an influx of Ca2+-ions into the cell, which is known as $I_T$-current (T-channel inward current). $I_T$-current depolarizes the cell membrane and the resulting all-or-none Ca2+-spike travels throughout the soma and dendrites, but not in axons as there aren't many T-type Ca2+-channel in the axons. In 6c, the cell membrane has been depolarized sufficiently to activate K+-channel and efflux of K+-ions. At this point the cell membrane has been depolarized long enough for the inactivation gate of the T-channel to close, which takes about 100 ms. $I_T$-current is said to be inactivated when the inactivation gate closes. In 6d, the cell membrane has been repolarized to close the T-channel activation gate. When the cell membrane falls into hyperpolarization, the K+-channel activation gate closes. T-channel inactivation gate opens again after being closed for about 100 ms, and membrane is back to its initial state. [8, 10, 12]

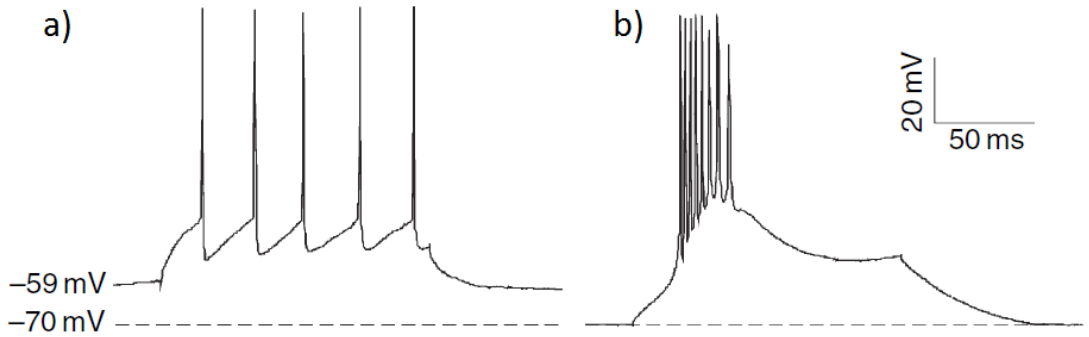


***Figure 8.*** *Membrane potential with respect to time during tonic and burst firing of the relay cells. Adapted from* [8].

Whether the cell responds in tonic or burst mode, depends on the initial membrane voltage and consequently on the $I_T$. Figure 8 clarifies this difference. In the potential (a) of Figure 8, the cell has been depolarized long enough ($\sim$ 100 ms) to inactivate $I_T$ and the excitatory suprathreshold input generates a single action potential. In Figure 6, this corresponds to the membrane state (d) when the new input arrives. This behavior is called the tonic response. In the potential (b) of Figure 8, the cell membrane has been hyperpolarized long enough ($\sim$ 100 ms) for $I_T$ de-inactivate. This activates an all-or-none low threshold spike that usually generates a set of high frequency action potentials. This occurs when the cell membrane is at the state represented by Figure 6a. This is the burst response, which normally involves 2-6 spikes. [8, 12]

## 2.2 Electric fields in biological tissue

Biological tissue acts like a volume conductor at a macroscopic level that transmits electric currents from sources to sinks. Electric current flow in tissue depends on the constitutive medium and material parameters that describe the medium. These parameters are conductivity, permittivity and permeability. Conductivities of biological tissues are primarily determined by free ions at frequencies well below 100 kHz and therefore tissue acts essentially as a conductor. At higher frequencies, electric field induced dipoles begin to dominate and tissue begins to act like a lossy dielectric material [11, 13]. Conductivity of human intracranial tissue typically ranges between 0.06 S/m and 2 S/m.

Permittivity describes materials ability to store and expend electrical energy, which is dependent on tissue type and frequency. Permittivity has two components, real and complex part as shown in equation (2) [11, 14].

$$\varepsilon = \varepsilon_0(\varepsilon_r' - i\varepsilon_r'') \tag{2}$$

In the equation (2), $\varepsilon_0$ (F/m) is permittivity of the vacuum, $\varepsilon_r'$ is real part of the relative permittivity, $\varepsilon_r''$ is the complex part of the relative permittivity and $i$ denotes imaginary number. Complex permittivity describes dielectric losses that arise from polarizations of dipoles in the medium. At frequencies below 100 kHz polarization is minimal in biological tissue and the permittivity can be expressed as in equation (3) [11, 14].

$$\varepsilon = \varepsilon_0\varepsilon_r' \tag{3}$$

Biological tissue is generally non-magnetic and thus its permeability is very close to that of the vacuum and relative permeability is therefore 1 [10, 13]. There are some exceptions to this, such as hemoglobin that contains iron, which is utilized in functional magnetic resonance imaging [10].

Material parameters cannot always be described as a single value, but instead they depend on the forces that act on them and their geometry, for example. If the material

properties are independent of the electric and magnetic fields, or any other force, it is said to be linear and if it is dependent, it is nonlinear. If the material properties are independent of the space coordinates, it is said to be homogeneous, otherwise it is inhomogeneous. If the material parameters are independent of the direction, it is said to be isotropic material, otherwise it is anisotropic [15].

Information in neurons in conveyed by charged particles in the form of action potentials and post- and presynaptic potentials. Electrical stimulation affects these charged particles in the tissue medium. Electric field describes the forces exerted on the charged particles. It can be evaluated by the negative gradient of the electric potential (4) [14].

$$\mathbf{E} = -\nabla U \tag{4}$$

In the equation (4), $\boldsymbol{E}$ (V/m) is the electric field, $\nabla$ is the gradient operator and $U$ (V) is the electric potential. Electric field can be considered as a quasistatic field, if the wavelength of the electric field is significantly larger than the object it interacts with [11, 14]. In a quasistatic approximation, equations of the electrostatics can be applied to a slowly time varying systems. In biological systems, wave nature of the electric and magnetic fields is not apparent in frequencies below 100 kHz [11, 13].

Current density describes the current flowing in a volume conductor per surface area. Current density generated in a material depends on both the strength of the electric field and conductivity of the medium. This is defined by the Ohm's law in equation (5), where $\mathbf{J}$ (A/m2) is the current density, $\mathbf{E}$ (V/m) is the electric field and $\sigma$ (S/m) is the conductivity [14].

$$\mathbf{J} = \sigma\mathbf{E} \tag{5}$$

Current is the flow of electric charges and electric charges cannot be created or destroyed in the observed system. Charges can flow in and out of the system resulting in the net change of charges. This charge conservation law is expressed as equation of continuity shown below (6) [14].

$$\nabla \cdot \mathbf{J} = -\frac{\partial \rho}{\partial t} \tag{6}$$

In equation (6), $\nabla \cdot$ is the divergence operator, $\mathbf{J}$ (A/m$^2$) is the current density and $\rho$ (C/m3) is the volume charge density. Equation (6) states that the flow of current from a closed volume equals the negative rate of change of charge density [14, 15].

## 2.3 Epilepsy

Epilepsy is not one condition, but instead a group of different conditions that may manifest in various ways. Manifestation depends on the locations and ways how it spreads, as well as on the patient's age and causes that provoke the epilepsy. Epilepsy is associated with seizures that emerge from group of cortical neurons discharging excessively in synchrony. The fundamental mechanism that initiates these seizures is still largely unknown. Some theories propose that it is due to the abnormal synchronization and firing of neurons, combined with inhibitory deficiencies in neurons. Distinguishing between seizures and epilepsy is an important aspect in diagnosis, as having a seizure is not an adequate confirmation to make an epileptic diagnosis. Person with epilepsy has a tendency to experience recurrent and unprovoked seizures. [16]

According to world health organization (WHO), nearly 1% of the world's population suffers from some form of epilepsy. Third of that population has a refractory epilepsy. Epilepsy is equally consistent among different nations and races, but occurrence is in low- and middle-income countries and especially in rural areas is higher. Epilepsy might results from brain and head injuries, strokes, infections and abuse of alcohol. [2, 16]

Epilepsy, as well as other neural disorders, rarely has just one location in the brain where the disorder originates, but instead, multiple structures in the brain affect the propagation of the disorder [3]. This allows for many feasible locations for DBS treatment [3]. Various thalamic nuclei have been extensively used for DBS treatment [3, 17, 18]. This is due to vast neural connections between thalamus and cerebral cortex [1]. Especially nuclei of the anterior nuclear group (Anterior nuclei of the thalamus, ANT) has appealing characteristics, as it is involved in seizure generation. Each sub-nuclei of the ANT plays a significant role in the limbic system and Papez circuit [5]. ANT is also relatively small in size, it is easily accessible with electrodes and it is not as close to basal veins as some other structures of the Papez circuit [3, 17].

Despite the ANT being an effective and practical target for epileptic DBS, other targets have been investigated as well. Halpern et al. states that other potential targets would be centromedian nucleus of the thalamus, caudate nucleus, cerebellum, hippocampus, mammillary nuclei and subthalamic nucleus. Alterations in the Papez circuit have been noted during many forms of epilepsy and therefore all region of this circuit are candidates for DBS electrodes in epileptic treatment. [1, 3]

# 3. DEEP BRAIN STIMULATION

In this chapter the basics of deep brain stimulation is explained, as well as typical treatment procedure and the effects it has on the brain. Later in the chapter, electrode placement is discussed as it is a particularly challenging task in a deep brain stimulation procedure. Stimulation parameters are explained in the last section and how they affect the treatment results.

## 3.1 Introduction to DBS

Deep brain stimulation (DBS) is a neurosurgical treatment method, where electrodes are implanted into the brain and electrical current is delivered to the target area. The current to the electrodes is generated by an internal pulse generator (IPG) that is also implanted into the patient's body [19]. DBS method is utilized when the patient suffers from a refractory neurological disorder. Refractory disorder is resistant to most conventional treatment methods, such as medications [3].

Refractory disorders were traditionally treated with more extreme approaches, like resections and ablations. However, only about 60 percent of the patients with refractory epilepsy are even eligible for the resection surgery in the first place, and 4 percent of the patients undergoing the surgery die or get a permanent brain damage. Due to the irreversible nature and high risks of these methods, DBS is a compelling alternative. Deep brain stimulation has a high success chance in alleviating the symptoms; it is reversible and relatively rarely causes severe complications. [1, 3]

Another reversible treatment method for refractory epilepsy is supplementation of antiepileptic medication with vagus nerve stimulation. It can provide up to 50 percent seizure frequency reduction, but it rarely eliminates the symptoms completely [3]. Low reduction in seizure frequency makes it an inferior option compared to DBS [3]. Nevertheless, caution must still be taken when evaluating and comparing DBS treatment results to other options, since it is still a relatively new method and most studies have been done with small patient populations [19].

## 3.2 DBS procedure

Deep brain stimulation methods may vary between different hospitals and clinics, but the core of the procedure remains the same. Figure 9 represents the implanted DBS system after the operation. The process begins by assessing the suitability of a candidate patient to undergo a DBS surgery. Assessment is done by a multidisciplinary council

that may include neurosurgeon, neurologist, psychologist, psychiatrist and nurses. Purpose of the meeting is to evaluate the severity and refractoriness of the symptoms, potential responsiveness to DBS and possible risks and benefits it may provide. [1]

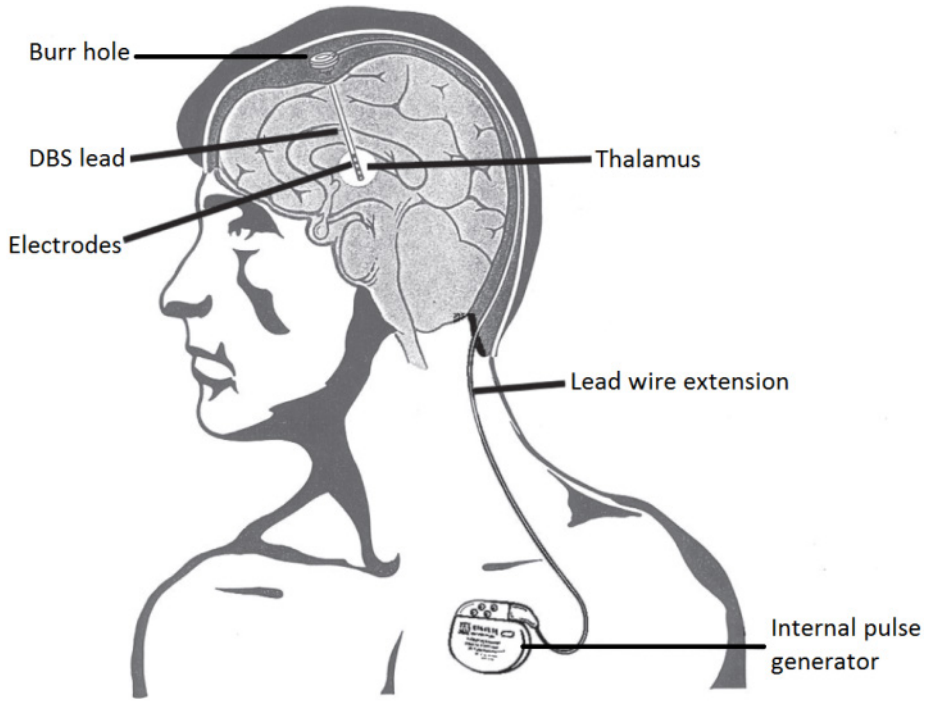


***Figure 9.*** *Illustration of an implanted DBS system. Adapted from* [1].

The surgical procedure begins by setting the patient into a supine or sitting position and fixating his head into a stereotactic frame. Then CT or MRI images are taken from the patients head and the external landmarks in the frame, as well as internal landmarks are identified. Commonly used internal landmarks are anterior commissure (AC) and posterior commissure (PC) and the plane that they define. Fiducial markers of the frame are spatially related to internal landmarks to generate frame based coordinate system. [1, 3]

Next the scalp surface is sterilized and incised and the burr holes are drilled through the skull. Then the meninges are incised and cauterized [3]. Modern DBS procedures involve some form of microelectrode mapping that is used in addition to imaging methods and anatomical atlases to find the correct anatomical target. Microelectrodes can be used to record neuronal activity or to stimulate the target region [1].

A cannula is then inserted through the burr hole close to the target region in the brain, and the recording electrodes are inserted into the cannula. Recording procedure is conducted under a local anesthesia. When the correct location has been confirmed, the microelectrodes are used to find stimulation thresholds for clinical effects. Then the stimulation and measurement electrodes are removed and the actual DBS lead is added via the cannula. When the DBS lead is in place, the cannula is removed. Lead is attached to the burr hole to ensure its stability. [1, 3]

Internal pulse generator (IPG), that drives the stimulation lead, can be placed in during the same surgical session or at a later date. It is conventionally placed into the subclavicular pocket, which is a cavity under the collar bone. Conductor wires of the DBS lead are burrowed under the skin and tunneled to the IPG subcutaneously. Correct lead placement is verified postoperatively with MRI or CT images. Finally the stimulation parameters are adjusted for each patient individually to achieve an effective treatment. [1, 3, 20]

## 3.3 Effects of DBS on brain

Mechanisms behind the DBS treatment are not yet completely understood. There are few prevalent theories that attempt to explain the causes of seizure reduction. One such theory suggests that high frequency stimulation partially disrupts or overrides the unchallenged neural network activity around the stimulation region. It has been found in animal studies that this kind of desynchronizing behavior of the thalamus occurs in response to the high frequency stimulation. This theory is consistent with the preceding treatment methods that involved resections and ablations. Another theory proposes that high frequencies might block the neural activity completely, including activity that evokes seizures. [1, 3, 17, 21]

Because the stimulation always spreads to the surrounding tissues around the stimulation lead, thus the stimulation of these neighboring regions might also contribute to the treatment results. Hence the stimulation effects are likely to be caused by complex changes in the thalamo-cortical networks, of which the stimulation target is part of, rather than simple neuronal excitations and inhibitions. [1]

Positron emission tomography (PET) images taken from patients, who have a DBS electrode implanted, show changes in regional cerebral flood flow and cerebral glucose metabolism in areas where electrode was not implanted. This is expected to indicate the effects of DBS on global cerebral network [1, 19]. Some studies claim that just by implanting the DBS electrode occasionally had an effect of reducing the seizure frequency and in some occasions activating the IPG had no additional effect on the seizure reduction. This is expected to be result of lesioning of the thalamus due to the electrode implantation, just as it was with the ablation and resections [3].

Even though the DBS has proven to be relatively effective method and the process is reversible, it is not completely without complication, as is the case with any surgeries and implantations. Stimulation related side effects may include nystagmus, lethargy, depression, memory decline, anorexia, paranoid ideation and auditory hallucinations. Most of these side effects are mild and temporary. Surgery related complications may become more severe. Examples of these are hemorrhage, scalp erosion, infections and even a stroke [1, 3, 18, 22, 23]. A record of 358 DBS-surgeries suggests that the chance to require a recurrent surgery due to complications is as high as 14%. Supplementary

surgeries were divided into subcutaneous and intracranial surgeries with 8.1% and 5.9% probabilities respectively [1, 22].

Hardware related failures are also a possibility and they include unintentional stimulator turn-offs, lead fractures, lead migrations and erosion [1, 3, 22]. These complications have an occurrence of 8.4% per lead per year [1]. All the risks that a DBS surgery may involve are not so easily identified, as the results may affect person's behavior, mood or even personality. This threat is especially present when DBS is used to treat patients with psychiatric disorders, rather than motor symptoms [19]. Stimulation effects might not be instantly observably either. Bradykinesia symptoms may take hours to observe and the frequency of epileptic seizures even months [4].

## 3.4 Electrode placement

A successful DBS treatment involves both an effective treatment results and minimized side effects. These requirements depend largely on the correct placement of the electrodes and proper stimulation parameters. Electrodes can be either radiographically or clinically misplaced. Radiographic misplacement refers to electrode coordinates that are not what they were supposed to be. Misplaced electrodes can be somewhat verified with postoperative magnetic resonance images (MRI). Starr [1] states that a 2 mm difference in electrode placement and the target anatomical structure can be considered as a radiographically misplaced electrode. However, target structures in DBS are so small that consistent sub-millimeter accuracy is required and the 2 mm misplacement is far from satisfactory. Clinically misplaced electrode fails to produce clinical treatment, even if it was in the correct place regarding to radiographic considerations. If the stimulation provokes adverse side effects, it is also considered to be clinically misplaced; despite the benefits it might produce. [1, 19]

### 3.4.1 Anatomical atlases

Anatomical atlas is a detailed graphical representation of anatomical structures. There are atlases for every region of the human body and even for other species. First anatomical atlas of the human brain was published in 1952 by Spiegel and Wycis, which was specifically made for stereotactic surgeries [1]. Brain atlases provide illustrations of a sliced brain in each sagittal, coronal and transverse direction. Most commonly used atlases are Talairach and Schaltenbrand atlases and their updates and variations [24]. These days there are large variation of atlases in the electronic form as well, such as the Allen brain atlas. Figure 10 below shows an example of an MRI image in the coronal plane and the corresponding atlas representation from the Allen brain atlas [25].

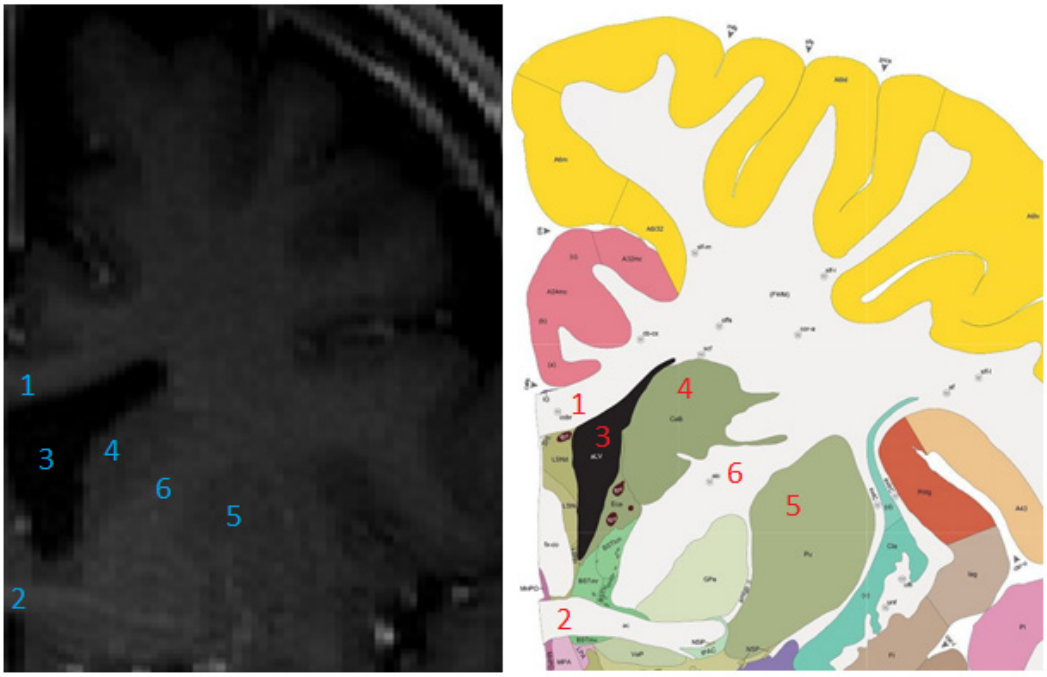


***Figure 10.*** *T1 weighted 3 T MRI image from the coronal plane on the left and the corresponding atlas representation on the right. Some clearly distinguishable structures marked in the images from 1 to 6. 1. Corpus callosum. 2. Anterior commissure. 3. Lateral ventricle. 4. Caudate nucleus. 5. Putamen. 6. Internal capsule. Adapted from* [25].

Most surgeons and planning software rely on these atlases when planning and executing stereotactic surgeries. However, atlas is always a representation of a single individual and due to the variations in size, shape and orientation of anatomical structures, there might be significant differences between patient and the atlas [26]. Postoperative and intraoperative imaging, as well as microelectrode recording can be used to confirm electrode location. Misplaced electrodes can be compensated to some extent by adjusting the stimulation parameters, but in the worst case, reposition surgery is necessary [1].

### 3.4.2 Microelectrode recordings

Electrophysiological mapping is an essential part of every neurosurgery. In a common DBS surgery, it is done before the implantable DBS is lead is inserted into the brain. It may be performed with a microelectrode recording systems or a macrostimulator, or as in many cases using both of them [1].

Microelectrode recording systems provide information about nuclear boundaries by measuring the electrical activity that is distinctive between nuclei, fibers and other structures in the brain. Occasionally, even adjacent sub-nuclei have strikingly different discharge patterns that can be identified. Single microelectrode provides information only from a single trajectory. Therefore recording systems often contains multiple recording electrodes that are parallel or forming another shape, for example a circular

pattern. Multitrajectory recordings give information about the spatial extent of nuclear structures. [1, 19]

Spotting the ANT with microelectrodes is a complicated task. It is small in size and surrounded by multiple other small nuclei, which all have tonic and burst firing modes. There are but few remedies for this task. Close vicinity of the cerebrospinal fluid can be readily distinguished with microelectrode recordings due to its vastly different electrical properties. Thin layer of white matter lamina and MTT are surrounding the ANT, which both lack the burst firing mode of the relay cells. [1, 12, 26]

Macrostimulators are also an essential part of the mapping procedure. Temporary macrostimulator can be inserted into the brain along the same trajectory after the microelectrodes have found the correct location. Macrostimulation provides information about the clinical effects and possible adverse effects, and therefore it is performed with the same stimulation parameters as the implantable stimulation electrodes [1, 19]. Some researches claim that electrode placement can be verified by measuring cortical electroencephalography (EEG) simultaneously. This is due to the reason that stimulating the ANT provokes recruiting rhythms on the cortex [3]. But in fact, many thalamic nuclei can induce similar patterns on the cortex, and therefore measuring an EEG pattern is not a consistent and reliable verification method [3].

## 3.5 Stimulation parameters

The other important factor for the successful treatment is the correct stimulation parameters. The purpose of the deep brain stimulation is to deliver electricity to the target location in brain, and at the same time restrict it from spreading to the unwanted areas. The size and shape of the electric field are key properties in defining where the current flows, because the impedance of the medium cannot be adjusted. Electric field can be influenced by modifying polarity, amplitude, pulse width and pulse frequency of the stimulation [1, 4].

### 3.5.1 Stimulation amplitude

Stimulation voltage defines how far neurons can be recruited from the electrode. The higher the voltage, the better chance that the target region will be covered by sufficient electric field, but at the risk of higher tendency for adverse effects [1]. It is difficult to estimate how distant neuronal elements are excited as it depends on the tissue properties, such as linearity, homogeneity, anisotropy and whether axons are slowly or rapidly conducting [27]. Neurons are influenced more by the peak value of the stimulation rather than the average power delivered [11].

Commonly used therapeutic amplitudes used in DBS treatment range from 1 V to 5 V [3, 21, 22, 23, 28]. Some studies claim to use amplitudes up to 7 V [18]. However, most

pulse generators used in DBS systems utilize 3.6 V batteries, and hence the stimulation voltage should not be increased above that level regarding to certain guides [27]. Even a slight increment of voltage above 3.6 V, results in a reduced battery life of about 50% due the voltage doubler circuit being activated in the IPG [27]. This should only be considered if the clinical effect resulting from the increased voltage is significant or if there have not been any clinical effects with lower voltages. This will most likely be a result of the misplaced electrode or due to attenuating encapsulation tissue [29].

### 3.5.2 Stimulation pulse width

Pulse width is the duration of the stimulating electrical pulse, and it normally varies between 60 μs and 210 μs in DBS treatment [21, 23, 30]. Pulse width is closely related to the sensitivity of neurons to react to stimulation. Duration of the exposure to electric field greatly affects the threshold of excitations, and this dependence is represented in the strength-duration curve in Figure 11. Stimulation current required to excite neuronal cells decreases when the pulse width increases like an inverse exponential function [1, 11].

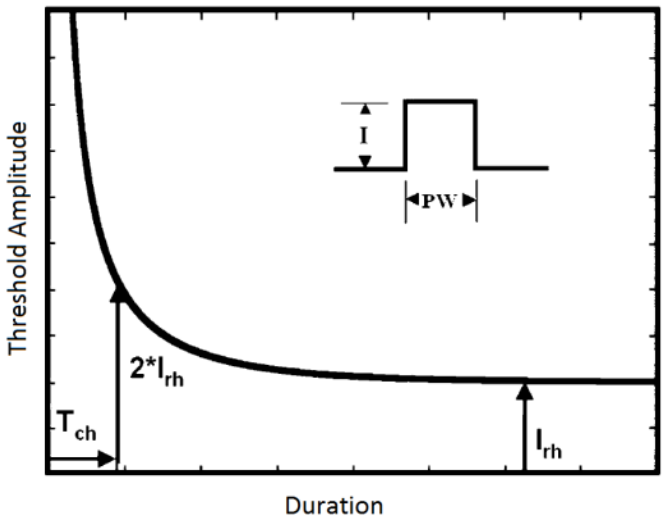


***Figure 11.*** *Typical strength-duration curve of a neuron. $I_{rh}$ is the rheobase current, $T_{ch}$ is the chronaxie time, I is the stimulation current and PW is the pulse width of the stimulation. Adapted from* [4].

Threshold current for neuronal stimulation can be calculated from the Weiss equation (7). It allows us to choose stimulation current and pulse width that suits the requirements of the anatomical target. In the equation (7) $I$ (A) is the stimulation current, $I_{rh}$ (A) is the rheobase current, $T_{ch}$ (s) is the chronaxie time and $t_{PW}$ (s) is the pulse width.

$$I = I_{rh}\left(1 + \frac{T_{ch}}{t_{PW}}\right) \tag{7}$$

Rheobase is the minimum current that can cause the excitation of a neuron with an infinitely long pulse. Chronaxie measures the excitability of neuronal structures and is defined as the minimum time required, with a current twice the rheobase, to excite a neuron [1, 11]. Chronaxie varies depending on the target neuronal structure. Whether it is soma, dendrites or axons that are being stimulated; Pulse width can be chosen so that it affects just the target neuronal elements. Chronaxie of the soma is typically 1-10 ms, small myelinated fibers have a chronaxie in the range of 200-700 µs and large myelinated fibers have a chronaxie in the range of 30-200 µs. Chronaxie of a thalamus is approximately 65 µs [1, 4]. Chronaxie of an average axon is lower than that of a soma, and rapidly conducting axons may have a significantly lower chronaxie. Therefore, increasing pulse duration will direct the neuronal excitation from axons towards the cell bodies [27, 31].

### 3.5.3 Electrode polarity

Stimulation current flows into the tissue and out of it through the electrodes on a DBS lead. Extracellular space near cathode gets depolarized and hyperpolarized near anode, and at a sufficient magnitude it will excite the neurons. Most efficient neural excitation takes place near the cathodal surface [19, 27, 32]. Anodal excitation is possible, but it requires larger stimulation amplitudes [19].

Monopolar stimulation generates spherical electric field in an isotropic and homogenous medium. Electric field generated by bipolar stimulation generates narrower and more directed field than monopolar stimulation. This can prevent some adverse effects, if the electric field can be directed only to the target volume. Ideal placement of the electrodes near the target region can be extremely difficult and therefore monopolar stimulation is used more often, due to the lower stimulation intensity it requires to achieve the same clinical effect [27, 33]. However, as the monopolar stimulation spreads further, misplaced electrodes may consequently require such a large voltages for target activation that it excites unnecessary neurons in the surroundings as well [1]. Potential fields generated by monopolar and bipolar electrodes are expressed in equations (8) and (9) respectively [13].

$$U_{mono} = \frac{I}{4\pi\sigma r} \tag{8}$$

$$U_{bi} = \frac{I\mathbf{d}\cos\theta}{4\pi\sigma r^2} \tag{9}$$

In equations (8) and (9), $I$ (A) is the source current, $\sigma$ (S/m) is medium conductivity, $r$ (m) is the distance from the source, $\mathbf{d}$ (m) is the displacement vector between the electrodes and $\theta$ is the polar angle between the observed point and an axis perpendicular to the displacement vector [13]. Figure 12 represents the -1 V monopolar and -1 V/1 V

bipolar electric fields as cut planes from the midpoint of the source. The narrower field pattern of the bipolar electrode is clearly observable from these images, even with twice the potential difference.

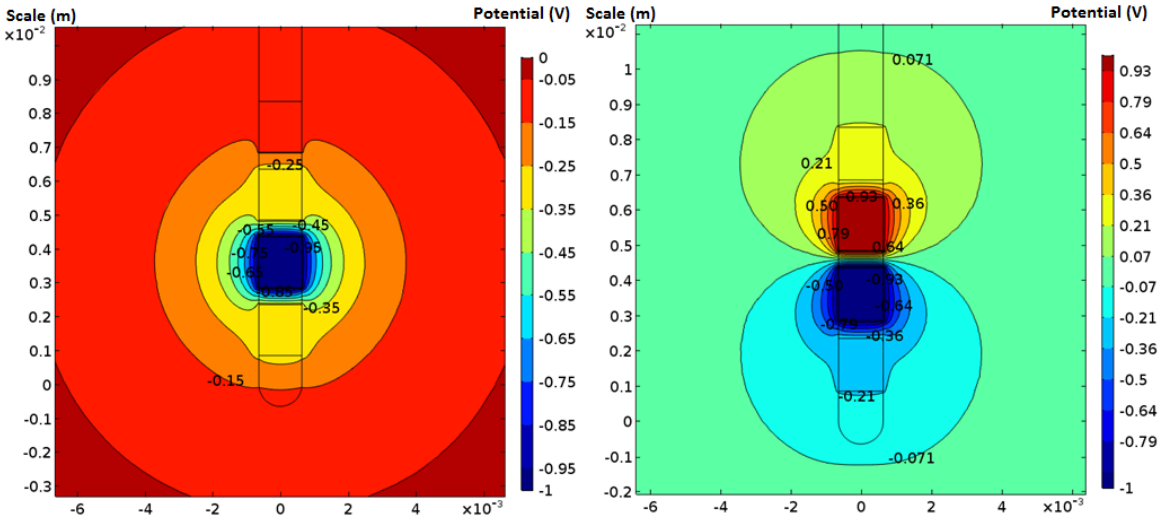


***Figure 12.*** *Monopolar and bipolar electric potential field patterns as cross sectional views. Images are created with Comsol 5.2 using Medtronic electrodes.*

The closer the neurons are to the stimulating electrode the higher is the probability that they will get activated. Monopolar electric field strength attenuation is inversely proportional to the distance from the electrode $U_{mono} \propto 1/r$. In bipolar stimulation, the electric field attenuation is inversely proportional to the square of the distance $U_{bi} \propto 1/r^2$, and in tripolar stimulation, the relationship is to the cube of the distance $U_{tri} \propto 1/r^3$ [1]. Figure 13 illustrates the electric potential field patterns in monopolar, bipolar and tripolar electrode configurations.

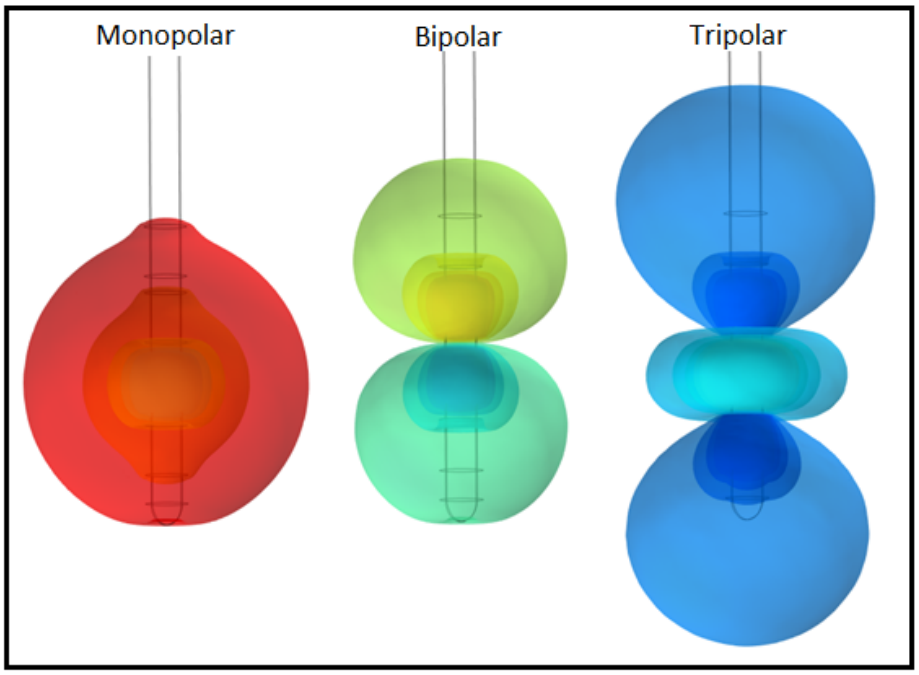


***Figure 13.*** *Monopolar, bipolar and tripolar electric potential field patterns from left to right. In the images, blue color corresponds to negative potential and red positive potential, while all other colors are potentials between these two extremes. Images are created with Comsol 5.2 using Medtronic electrodes.*

Separation distance of the electrodes in a DBS lead also has an effect on the generated electric field patterns in multipolar stimulations. The further the electrodes are from each other, the higher voltages can be generated. Equation (10) describes this relationship in bipolar configuration [1].

$$U_{bi} \propto d^2/r^2 \tag{10}$$

In equation (10), $U_{bi}$ (V) is the stimulation voltage, $d$ (m) is the separation distance between two electrodes and $r$ (m) is the distance from the electrode. In most DBS systems, electrode polarities can be set to any combination of the four attached electrodes in a DBS lead; ranging from monopolar to quadripolar stimulation. Any electrode of the lead can be set to either cathode or anode in multipolar stimulations, or as cathode in monopolar stimulation [20]. In monopolar stimulation, the IPG acts as anode [20].

### 3.5.4 Stimulation frequency

Direct current has a tendency to damage all living tissue in a long-term exposure, regardless of the magnitude of the current. One directional electrochemical processes cause excess electrical charges and toxic substances to accumulate and also alters tissue pH locally. Therefore stimulation pulse should always be biphasic in long-term stimulations. Rectangular pulse is typically used in DBS stimulations [19]. Frequency refers to stimulation pulses per second and it affects the treatment efficiency. Generally in DBS

treatments the therapeutic effects are detected above 90 Hz frequencies with abrupt thresholds. For epileptic treatment, frequency ranges from 90 to 140 Hz and for the Parkinson's between 100 and 150 Hz [21, 27, 28]. Some treatments may require frequencies to go even up to 185 Hz [34, 23]. Low frequency stimulations have not been found to alleviate symptoms, and occasionally they even become worse. Increasing the frequency beyond the conventional range might have a small influence on treatment efficiency, but due to increased power consumption, frequency should rarely be increased beyond 130 Hz [27]. The impedance of the biological tissue is frequency dependent, decreasing as the frequency increases [11, 13]. Tissue impedance has also been observed to change within months from surgery date. This change occurs most likely due to healing of implantation lesions and growth of encapsulation tissue around the electrode [1].

# 4. MATERIALS AND METHODS

Purpose of the modeling is to explain experimentally acquired research data by simplifying complex systems and excluding variables that have no significant impact on the phenomena under examination. Conversely, modeling can provide hypotheses that can be tested with experiments. The scale of modeling of neuronal systems can vary from individual ionic channels and neurons into complete organs and neural networks. Even though the model is always just an approximation, it can still be used to describe, predict and explain the reality. [35]

Simulation is a method to solve models and evaluate the results and responses to given inputs. Simulations are recommended when the experiments are too difficult to perform or they would require long periods of time to obtain results. Some experiments could even be too dangerous and ethically inappropriate to perform on the living subjects. [35]

In this chapter, the structure of the model is first explained and then the details how it was created. Next the electrical properties concerning the model and solution are described. Finally simulation parameters that were changed to get the desired solutions are described.

## 4.1 Structure of the model

The model consists of three different subsystems, geometry that resembles tissue, stimulation electrode and the encapsulation layer. Finite element models (FEM) of each of the subsystems were created with COMSOL 5.2 software. Two tissue models were created, 3D model of uniform tissue type and planar model of the thalamus. Construction of each model is explained in the following sections.

COMSOL is a FEM solver. After the geometry has been created, each geometrical domain is divided into a number of non-overlapping finite elements in a process called finite element discretization. Elements are often triangles or tetrahedrons depending on the number of dimension being used. Finished result is known as a mesh and seen later in Figure 18 and Figure 19. The more elements are being used, the finer the mesh and more accurate is the solution, but at the cost of increased computation time. [15, 36]

Solution for the problem is calculated from the mesh rather than from the actual geometry. To get the solution, concerning partial differential equations are solved on each node of every finite element tetrahedron. This process is repeated until the solution con-

verges or pre-defined requirements are met. As a result, the solution at any point within the mesh is known when the value at each node is evaluated. [15]

### 4.1.1 Electrode model

Stimulation electrodes were modeled based on those currently used in practice. Most commonly used stimulation electrodes for DBS are Medtronic models 3387 and 3389 (registered trademarks of Medtronic, Inc.). Both models have CE and FDA approvals, and at the time of writing they were the only electrodes that had those approvals for DBS surgeries [1, 20].

In the stimulations, the model 3389 was used as it is more popular of the two options. The only difference is that the model 3389 has a 0.5 mm electrode spacing while model 3387 has 1.5 mm electrode spacing. Closely located electrodes make it easier to target correct anatomical regions. Figure 14 represents the lead geometry of Medtronic model 3389. Bulk of the lead is a long polyurethane tube with a diameter of 1.27 mm. Its length is significantly larger than the dimensions of the thalamus and ANT, and therefore it is truncated at the edge of the model space. There are a total of four cylindrical electrodes in a polyurethane housing. Each electrode is 1.5 mm long with a separation distance of 0.5 mm. Electrodes and the conductor wire inside the tubing is made of platinum-iridium alloy [20]. Conductor wire was not included in the model, since the internal behavior of the lead is not a relevant in this model.

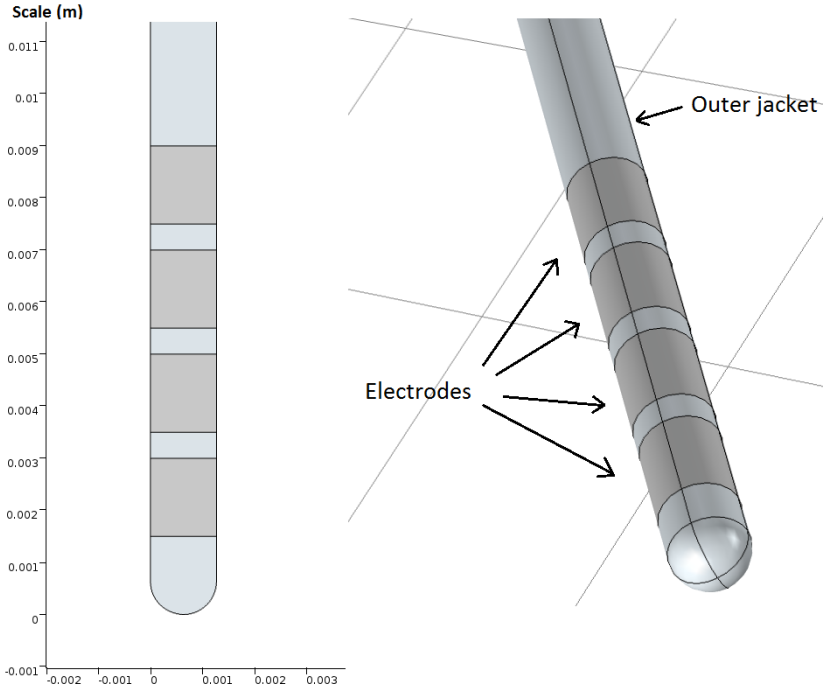


***Figure 14.*** *Middle cut plane and the 3D model of the DBS lead used in the model.*

Conductivity of platinum-iridium alloy depends heavily on the ratio of used metals. 90% of platinum and 10% of iridium is the most commonly used platinum-iridium alloy ratio used in biomedical electrodes. It has a conductivity of $4\times10^6$ S/m and relative permittivity of 1 [37]. Polyurethane housing was made from hardness A80 polyurethane [20]. Polymer material properties depend on the internal structure, processing methods and testing methods that vary between different manufacturers and trademarks [37]. Electrical properties of polymers varied significantly and therefore average values of material properties were used in the model. Geometric mean was used with conductivities due to values differing more than $10^9$ S/m. Conductivity of A80 polyurethane was $4\times10^{-12}$ S/m and relative permittivity was 5.28 [37, 38].

### 4.1.2 Uniform model

Uniform model was first created to study the behavior of electric fields and stimulation parameters without the distortions of the anatomical domains and boundaries. Uniform domain was chosen to be cylinder, because the electrode itself is cylindrical in shape. In this manner the distances between boundaries and voltage sources remain relatively constant. Figure 15 represents the uniform domain and the electrode.

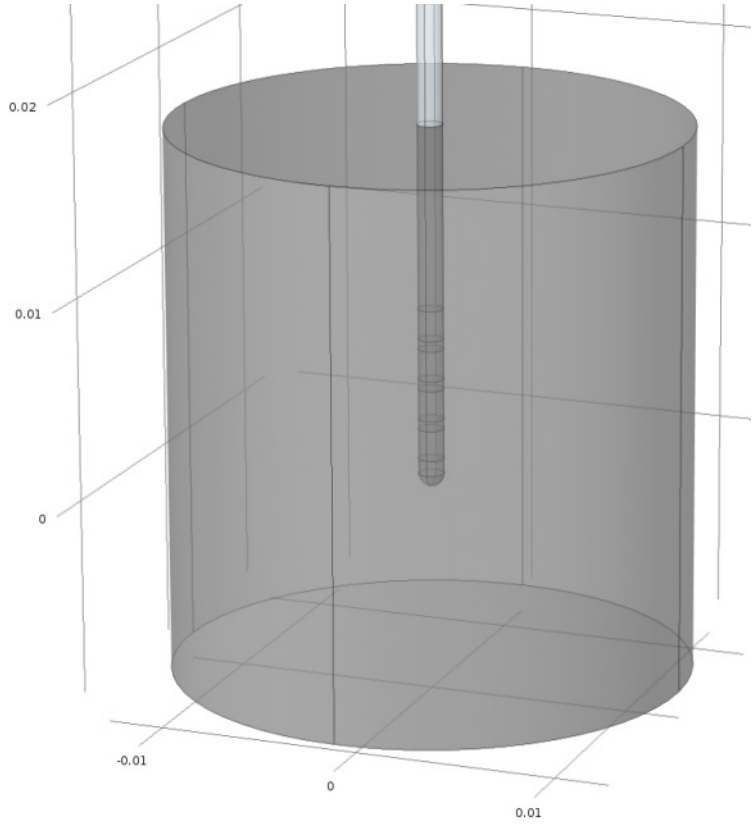


***Figure 15.*** *Model geometry of a uniform gray matter domain and the electrode described in the section 4.1.1. Scale in the figure is in meters and the origin is at the center of the electrode tip.*

Cylinder domain was modeled as a mass of homogenous and isotropic gray matter that represented the brain tissue. Cylinder was 25.4 mm in diameter or 20 times larger in diameter than the electrode. Length of the cylinder was 27 mm, which is 3 times the distance from electrode tip to proximal electrode. Lengthwise electrode was placed in the middle of the cylinder. Cylinder dimensions are arbitrary but large enough to reduce the electrode interactions with the boundaries, but not too large to increase computational time noticeable. Both cylinder and the electrode were oriented concentrically with respect to each other. Gray matter conductivity in this model was 0.343 S/m and permittivity was $3.5\times10^6$ in the uniform domain [39].

### 4.1.3 Model of the anatomy

Uniform model gives an insight into electrical behavior of stimulation in the brain. However, different anatomical structures in the brain have different electrical properties, and therefore have an effect on the electric field propagation [40]. Uniform model is not satisfactory to predict interactions on the material borders, nor can it predict the sufficiency of neural activation of realistically shaped and sized regions.

Planar model was used to simulate anatomical properties of the thalamus rather than a 3D volume. Creating a 3D model from thalamus where one could distinguish ANT and MTT based on the MRI images, is an unfeasible alternative. Even with a highly accurate 3 T MRI multiplanar reconstruction methods, one can have voxel sizes in the sub millimeter range. MRI Image in the Figure 10 had a voxel size of 0.459x0.459x0.9 mm, which may seem adequate. However, MTT for example, is 1-1.5 mm thick, which means that it would provide just 1 to 3 planes where the MTT would show up [25]. Creating a 3D model from only a few images is not a reasonable alternative, and even then it would not resemble the anatomy any more than a 3x3 pile of cubes.

Geometry of the anatomy was created by using Matlab, LiveLink for Matlab and COMSOL softwares. Model geometry can be created from any plane required, but the most used plane in this thesis was the one described below. Transverse plane does not show the ANT, MTT and lateral ventricles in the same image, as they are located in different transverse planes. Sagittal planes on the other hand, cannot display the DBS lead properly, because the lead does not come straight down but is instead aimed through the lateral ventricles. Therefore, coronal plane is the most suitable option for a planar model. Among all coronal planes, the one that shows ANT and MTT properly was used.

Acquiring the geometry of the anatomical structure for modeling was composed of 9 primary phases. Images in the Figure 16, Figure 17 and Figure 18 represent the results of each phase. In the first step, the region of interest is decided and the most suitable plane is chosen from the anatomical atlases. Allen brain atlas was used in the creation of our image [25]. Then the image is cropped to contain only the surroundings of the target

region. In the second phase, denotations are removed by either utilizing atlas properties to hide them or using image processing software. In Matlab, this can be done by adding Gaussian filtering to the image which is a type of blur filter [41].

In the third phase, the image is segmented by using the YCbCr color thresholding. The purpose of the segmentation is to separate regions of interest, which are ANT, MTT and rest of the thalamus. LiveLink commands that generate geometry from images operate with surface contours and therefore it is more feasible to create empty regions where ANT and MTT are, rather than segmenting each part individually. YCbCr is a type of thresholding where you can control blue-yellow and red-green color spectrum. Any other method can be chosen if necessary, but YCbCr was used because of the color map of the original image [41].

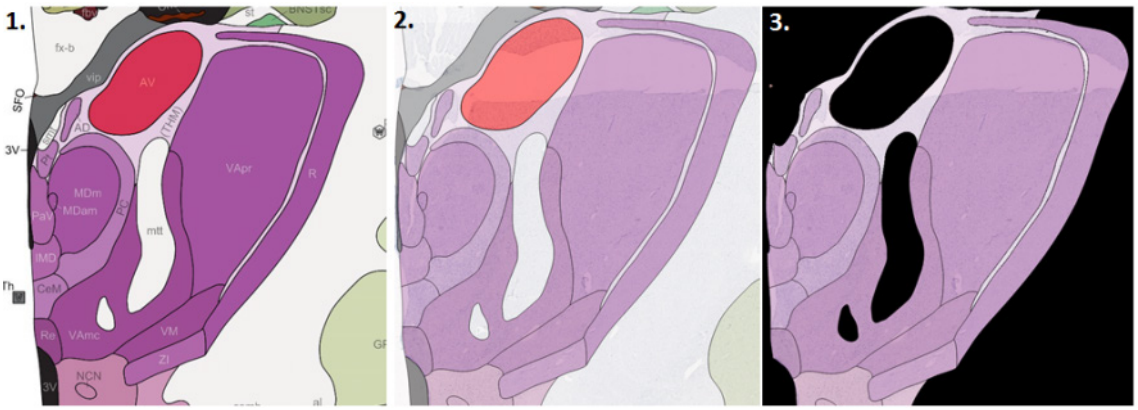


***Figure 16.*** *Atlas image to geometry process phases 1-3.1. Original atlas image. 2. Atlas image where denotations are removed. 3. Segmented image.*

In the fourth phase, a binary image is created by changing every pixel value except 0, to 1. From the image 4 (Fig. 17), it can be clearly seen that every subnuclei of the thalamus were bordered in the atlas for clarity. This will cause problems in the following stages and thus they must be removed.

In the fifth phase, all pixels with a value of 0 that were constrained within the thalamus are separated into a new image. This affects the ANT and MTT as well. We can prevent those regions from being removed, by using a Matlab function that discards all the pixels that have a pixel connectivity below certain threshold value. The resulting image is then subtracted from the modified image 4 where all the internal holes are filled. The result is seen in the image 6 (Fig. 17). Smaller objects were also removed in the phase 6 that were still visible in the top and left boundaries of the image 4.

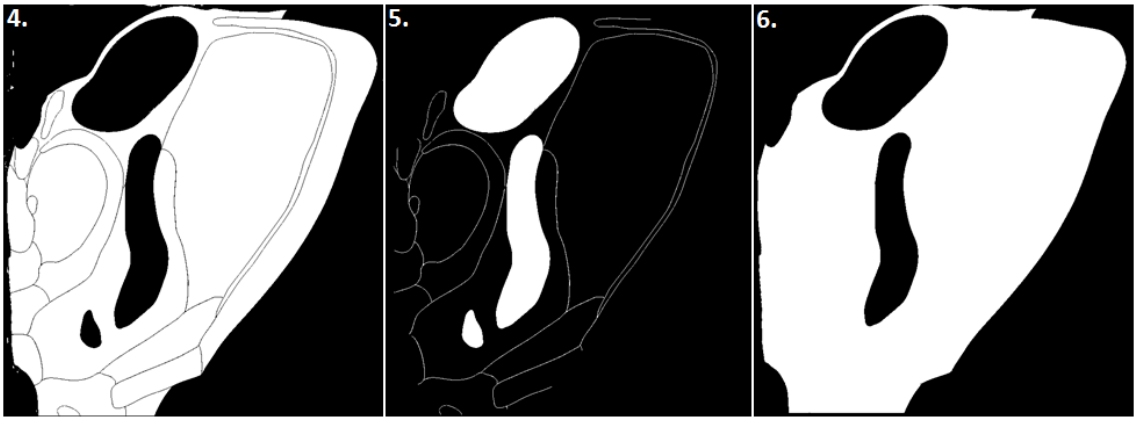


***Figure 17.*** *Atlas image to geometry process phases 4-6. 4. Image converted to binary image. 5. Redundant areas identified. 6. Image with all imperfections removed.*

In the seventh phase, a value for contour threshold is chosen. In the case of a binary image, 0.5 is chosen, but generally any value between 0 and 1 would work. Next the image must be mirrored and scaled before transfering it into COMSOL. Images in Matlab are handled as arrays and the pixel numbering begins from the top left corner. In COMSOL however, geometry is built into a coordinate system, beginning from lower left corner. Using the flip function in Matlab, allows an easy mirroring with respect to x-axis.

An unscaled image that is transferred into COMSOL interprets every pixel to be a square with a side of 1 m. Atlas that was used to get the intial picture, contained a movable measuring scale that was used to measure the length of the ANT. Corresponding distance in pixels was measured in Matlab. Dividing the atlas distance with the number of pixels in Matlab gives the scaling factor of the thalamus. In the phase 8, geometry is transferred into COMSOL and the polygons representing the ANT and MTT holes were replicated to fill them again. In the last phase, a finite element mesh is created onto the transferred geometry.

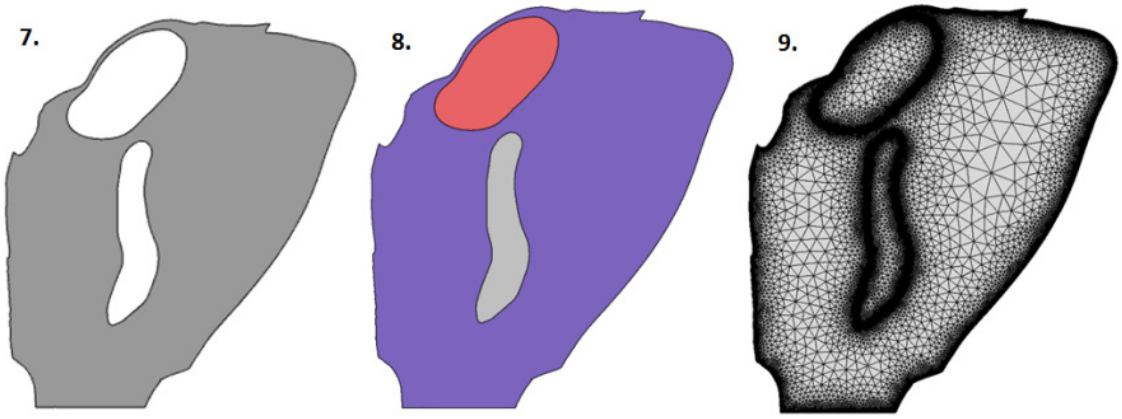


***Figure 18.*** *Atlas image to geometry process phases 7-9. 7. LiveLink image of the thalamus in Matlab. 8. Thalamus geometry transferred to COMSOL with ANT and MTT added. 9. Meshed geometry of the thalamus.*

While creating any type of geometry for modeling, despite the software that is being used, extreme caution must be taken to void geometrical singularities. Sharp corners and cracks in the geometry may create discontinuities that cause gradients to become near infinite. As can be seen from the equation (4), electric field is the negative gradient of the potential which is being calculated in our solution and therefore singularities should be avoided in our model as well [36]. Pixelwise reconstruction of anatomical targets has a tendency for sharp edges and corners, which is especially prevalent when the reconstruction is made from images. Singularities can be one reason if the solution does not converge in the simulation. This may also be noticed if the solution involves abnormally large values that should not exist. This was taken care of in the process phase 6, where all imperfections and cracks were removed.

From the images in Figure 18, it may seem like the border of the thalamus is smooth, but instead is made of 3650 different boundaries. LiveLink commands that convert contours into geometry utilize polygons instead of polynomials. Figure 19 below shows an example of the meshed geometry border.

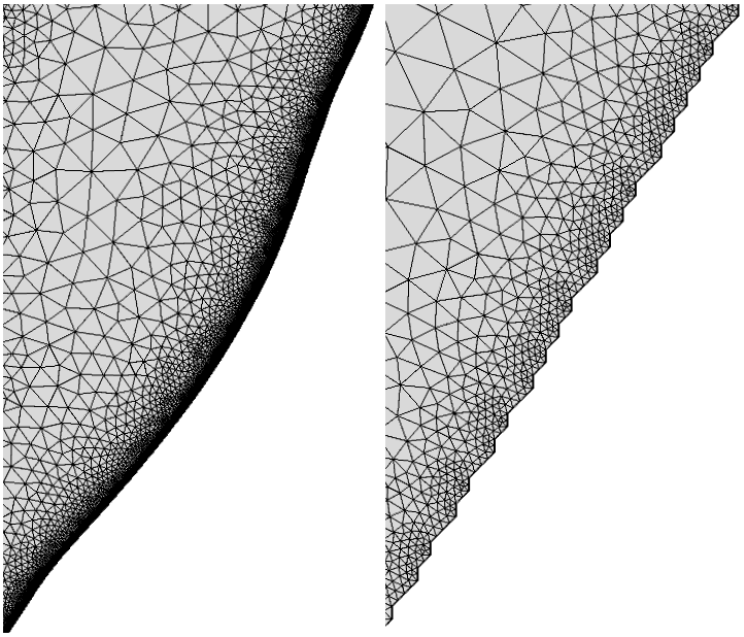

***Figure 19.*** *Two different levels of magnifications of the meshed border showing the polygonal nature of the border.*

Numerous edges and borders cause the mesh to become extremely dense where it should not be, because the jagged border is just a false interpretation of the anatomical border. As previously mentioned, computation time depends on the amount of mesh elements and therefore unnecessary mesh elements should be minimized. COMSOL provides multiple premade meshing options, but due to the jagged borders, some modifications to the meshes were made. Predefined fine quality mesh was used as a frame and it was modified by increasing the maximum element growth rate from 1.3 to 1.5 and minimum element size by 10 fold. This resulted in domain element reduction from 112146 to 37181 elements.

### 4.1.4 Encapsulation model

Human body can react to foreign objects in various ways, ranging from adverse toxic effects to vital reactions. Ideally, electrode would be perfectly biocompatible and unaffected by the human body. However, ideal electrodes do not exist and therefore, well designed electrode provokes a vital reaction. In vital reaction, body initiates a defensive reaction by growing a fibrous tissue encapsulation around the electrode. [42, 43]

Encapsulation tissue has a significant impact on both stimulations and measurements of living tissues. It affects the spread of electric field, recording specificity, selectivity and signal to noise ratio by increasing the impedance at the electrode-tissue interface [29, 30, 42]. The increase in impedance depends on the thickness and morphology of the tissue. Capsule thickness and morphology consequently depends on the electrode shape, material and surface texture [29]. Adequately biocompatible electrodes will provoke a thin and tightly packed encapsulation layer generation, while the less biocompatible

electrodes generate large macrophages, giant cells and overall looser collagen and fibroblast structure [29].

Encapsulation can be further divided into acute and chronic states. Acute encapsulation takes place right after the stimulation lead is implanted, and is resulted from the implantation process. Implantation process causes fluids, such as blood and CSF, to flow into newly created cavities. Implanting the DBS lead also compresses cells around it and may cause cell deaths. This state lasts about 1 to 3 weeks [44]. Chronic encapsulation is a more stable state [30]. Chronic encapsulation often grows within the first few months after the implantation and is permanent while the implant is in the body. Both states can be detected as a changed demand in supply voltage [44].

DBS studies that included encapsulation, reported that the effects of encapsulation tissue layers are so substantial that it should always be included into the models. The encapsulation tissue was modeled as a homogenous and isotropic resistive layer surrounding the stimulation lead [44]. Figure 20 illustrates the encapsulation sheath. In the reference studies, the encapsulation thickness typically varied between 100 μm and 300 μm and absolute extremes are from 25 μm to 1000 μm [30, 32, 44]. Thickness was chosen to be 300 μm that was the largest of the commonly used values found in the previous studies. Encapsulation tissue properties cannot be measured after the stimulation leads have been implanted. Information about the thicknesses and material properties can only be obtained when the stimulation lead is removed. Pfingst et al. investigated the encapsulation tissue on cochlear implants and suggested that increased voltage requirements during the first few months might actually be the result of the decreased sensitivity of neural tissue, which will seem as if the impedance had increased [42].

Grill et al. studied different macrostructures and found that a tightly layered fibroblasts and collagens had a frequency independent resistivity of 627 ± 108 Ωcm. Mixture of different layers, consisting of macrophages, foreign body giant cells, loose collagen and fibroblasts, formed a frequency dependent resistivity ranging from 454 ± 123 Ωcm at 10 Hz to 193 ± 98 Ωcm at 1 kHz [29, 43]. Acute and chronic encapsulation conductivities were studied by Polikov et al., which were 1.7 S/m and 0.125 S/m respectively [44]. High conductivity of the acute encapsulation is consequence of the extracellular fluids surrounding the DBS lead in the acute phase [45]. Butson et al. recorded tissue conductivities clinically and observed them ranging from 0.2 S/m to 0.07 S/m [32].We were not modeling different macrostructures on the encapsulation tissue and therefore used the value 0.07 S/m as it describes the least conducting situation and it was also referred to in many other publications. Values described by Polikov were used to simulate encapsulation growth from acute to chronic phase.

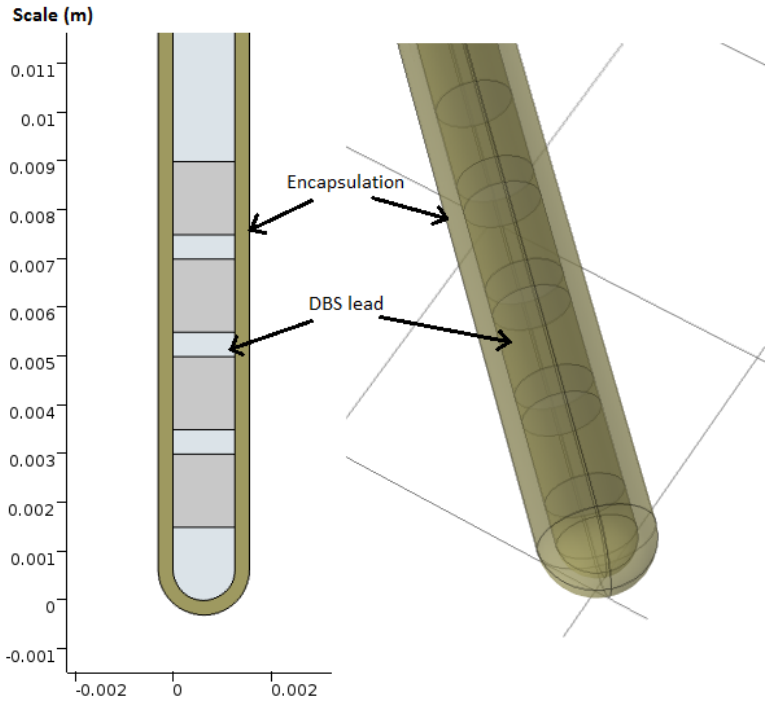


***Figure 20.*** *Middle cut plane and the 3D model of the stimulation lead surrounded by symmetrical encapsulation layer.*

Encapsulation might provide some serious setbacks during the treatment, as tissue might not grow uniformly around the electrode. Therefore thicker encapsulation layer towards the target region will require larger voltages, which consequently may have severe impact on collateral neurons if there was a thinner layer on any other side [30, 44, 45]. Asymmetrical encapsulation growth was modeled as one side having half the maximum thickness (150 µm) that can be seen in Figure 21. In the lead model, 150 µm encapsulation thickness transitions steadily towards normal thickness by the half way of the stimulation lead.

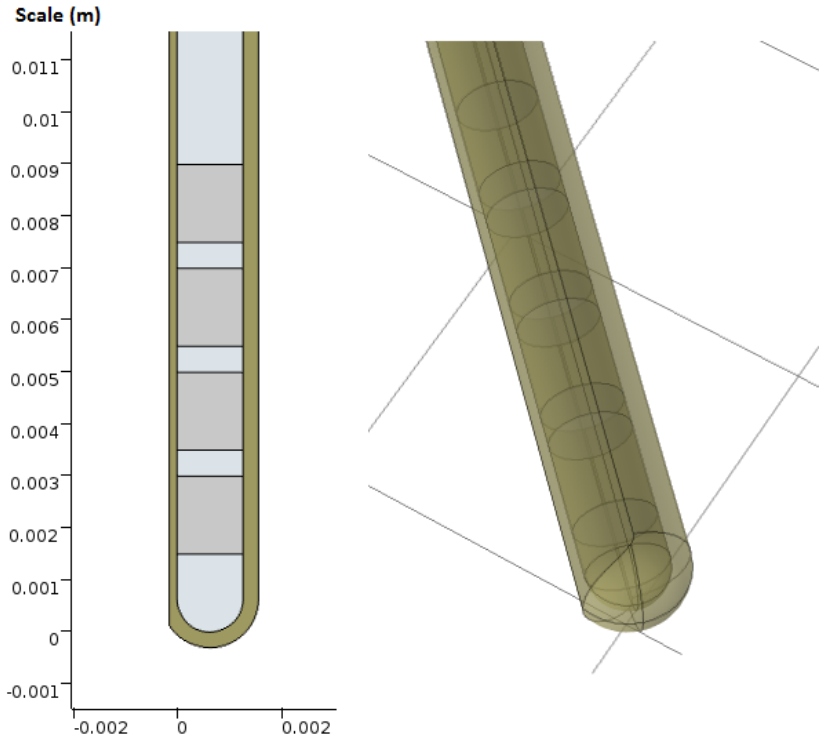


***Figure 21.*** *Middle cut plane and the 3D model of the stimulation lead surrounded by an asymmetrical encapsulation layer.*

### 4.1.5 Material properties

Material parameters for the model were explored from multiple sources. Most widely accepted parameters were often chosen, unless they were particularly not suitable for this model. When multiple parameters were found, an average was taken and significant outliers were discarded. In a quasistatic electrical model, permittivity values are not required for the solution, however, software that was used demands certain permittivity as a default value. Therefore, permittivity values that were applied are also presented in the text.

Tissue properties had some variations between different studies, but it is noteworthy that most researches refer to few prevailing studies. Gray matter conductivities were between 0.09 S/m and 0.455 S/m and average being 0.343 S/m [13, 21, 34, 39, 46, 47]. White matter conductivities ranged from 0.06 S/m to 0.255 S/m and the average value was 0.185 S/m [13, 32, 34, 39, 46, 47]. Conductivities of cerebrospinal fluid varied between 1.25 S/m and 2 S/m and the average was 1.52 S/m [13, 34, 39, 46, 47, 48]. Relative permittivity for gray matter, white matter and CSF were $3.5\times10^6$, $1.49\times10^6$ and 109 respectively [39].

Anisotropy of a material describes its dependence on the direction. Most axons of the central nervous system are myelinated on the outer surface. Myelination has higher im-

pedance than extracellular space and therefore tissue impedance is higher in the perpendicular direction with respect to myelination. Many thalamic nuclei are surrounded by other nuclei or white matter fiber tracts that create inhomogeneous and anisotropic volumes [33]. These properties distort the electric fields and change the size and shape of VTA, and therefore affect the neural responses. Especially areas that are in close proximity to fiber bundles like MTT, internal capsule and stria medullaris, may be greatly affected by tissue anisotropy [34].

White matter is always anisotropic, even though material parameters such as conductivity are often given as a single value. Therefore, there might be large variations in white matter values in different literature unless the direction of fibers is known, which rarely is. Anisotropy is expressed as a rank 2 tensor, which is essentially a vector with 2 directions. Anisotropy in 3 dimensions has 6 different elements in a 3 by 3 symmetric matrix, which shown in equation (11) [49, 50].

$$\boldsymbol{K} = \begin{bmatrix} k_{xx} & k_{xy} & k_{xz} \\ k_{xy} & k_{yy} & k_{yz} \\ k_{xz} & k_{yz} & k_{zz} \end{bmatrix} \tag{11}$$

In 2 dimensions, tensor matrix is also symmetric, but only 3 elements that include x and y subscripts exist. Those are shown below in equations (12), (13) and (14) [49].

$$k_{xx} = \sigma_L \cos^2\alpha + \sigma_T \sin^2\alpha \tag{12}$$

$$k_{xy} = (\sigma_L - \sigma_T)\cos\alpha\sin\alpha \tag{13}$$

$$k_{yy} = \sigma_T \cos^2\alpha + \sigma_L \sin^2\alpha \tag{14}$$

In the equations (12), (13) and (14), $\sigma_L$ is the longitudinal conductivity, $\sigma_T$ is the transverse conductivity and α is the angle between fibers and the x-axis [49]. For example, if the fibers run parallel to the y-axis, sinα equals 1 and cosα equals 0 and the three equations are reduced to following equations (15).

$$k_{xx} = \sigma_T, k_{xy} = 0, k_{yy} = \sigma_L \tag{15}$$

Both $\sigma_T$ and $\sigma_L$ can be obtained from experimental data or calculated from the information acquired in DTI imaging [34]. Kwon et al. studied mammillothalamic tracts with DTI methods, and reported mean values for fractional anisotropy (FA) and mean diffusivity (MD) of MTT [51]. Mean FA for both sides was 0.37 and mean MD for both sides was 0.87. FA and MD do not give diffusion direction information, but they can be used to calculate the degree of anisotropy. This gives a good estimate of the anisotropic properties of the tissue, since we know the principal fiber direction of MTT. Diffusion tensor is expressed as 3 by 3 matrix in equation (16), just like conductivity tensor in (11). Eigenvalues of the diffusion tensor, also shown in the equation (16), describe dif-

fusivity along tissue based coordinate system [51]. Corresponding eigenvectors $[\bar{\varepsilon}_1, \bar{\varepsilon}_2, \bar{\varepsilon}_3]$ represent the direction of the aforementioned diffusivity. Each voxel in the tissue has its individual diffusion tensor [52].

$$\boldsymbol{D} = \begin{bmatrix} D_{xx} & D_{xy} & D_{xz} \\ D_{yx} & D_{yy} & D_{yz} \\ D_{zx} & D_{zy} & D_{zz} \end{bmatrix} \rightarrow \begin{bmatrix} \lambda_1 & 0 & 0 \\ 0 & \lambda_2 & 0 \\ 0 & 0 & \lambda_3 \end{bmatrix} \tag{16}$$

Mean diffusivity can be calculated from the equation (17), which is simply an average diffusion of each voxel [52].

$$MD = \frac{\lambda_1 + \lambda_2 + \lambda_3}{3} \tag{17}$$

Fractional anisotropy gives information about the degree of anisotropy and it can be calculated for each voxel with the equation (18) [52].

$$FA = \sqrt{3/2}\, \frac{\sqrt{(MD - \lambda_1)^2 + (MD - \lambda_2)^2 + (MD - \lambda_3)^2}}{\sqrt{\lambda_1^2 + \lambda_2^2 + \lambda_3^2}} \tag{18}$$

In a 2 dimensional model where the plane is parallel to the principal fiber direction, we can make an approximation that minor axes of diffusion tensor are equal, or in other words $\lambda_2 = \lambda_3$. Now the average eigenvalues for MTT can be calculated from equations (17) and (18). As a results $\lambda_1$= 1.2599 (0.4801) and $\lambda_2$= 0.6750 (1.0650). Second roots, which are shown in the parenthesis, must be discarded as $\lambda_1$ would not be primary axis [52]. Diffusion tensors and anisotropic conductivity are directly proportional and therefore the ratio of $\lambda_1$and $\lambda_2$ gives the ratio of longitudinal and transverse conductivity [34, 21, 33, 53]. Ratio of eigenvalues was 1.867.

White matter conductivity in longitudinal direction was calculated from the average isotropic white matter conductivity, which was 0.185 S/m. Because white matter is always anisotropic, also this value has longitudinal and transverse components in it. We are expecting white matter measurements to be randomly measured, i.e. there are no sense of the directional relationship between measurement probes and neural fibers. Taking this into account, 1/3 of the white matter conductance is in longitudinal direction on average, resulting into a $\sigma_L$=0.268 S/m. Transverse conductance will consequently be $\sigma_T$=0.144 S/m.

## 4.2 Boundary conditions

After the geometry and mesh has been built, proper physics are applied to the model. Boundary conditions are a set of constraints that allow the solving of partial differentia equations. Following boundary conditions were applied in the FEM model. [15]

In monopolar stimulations, the outer boundaries of the tissue were grounded and the active electrode was set as a negative voltage source. In bipolar stimulation, two electrodes were set to an equal but opposite voltage. Voltage sources and ground planes were constants and independent of the surrounding, thus fulfilling the Dirichlet boundary condition. Any of the four electrodes can be set as an active or inactive contact surface. When the electrode is active, the outer surface of the electrode cylinder is set as a voltage source. Active electrode surfaces can have any arbitrary voltage value, depending whether it is cathode or anode. Simulation parameters are discussed in more detail in section 4.4. [14, 15]

Internal material boundaries and insulations were specified with a normal derivative with respect to the surface or border, and therefore following the Neumann boundary conditions explained below [15]. Borders of the model were electrically insulated satisfying the equation (19) [14, 36].

$$\mathbf{n} \cdot \mathbf{J} = 0 \tag{19}$$

In the equation (19), $\mathbf{n}$ is the normal vector of the boundary and $\mathbf{J}$ is the current density. Equation (19) essentially states that the angle between normal vector and the current density vector has to be 90° or 270° to satisfy the condition by the definition of dot product. Therefore, the current at the border flows along the edge and no charges gets through the boundary. Internal boundaries between different media and domains must satisfy the boundary condition equation (20), which states that all the charges exiting medium 1 will enter medium 2 and vice versa. Applying equation (20) prevents no charges accumulating or getting destroyed at the internal boundaries. [14, 36]

$$\mathbf{n_{12}} \cdot (\mathbf{J}_1 - \mathbf{J}_2) = 0 \tag{20}$$

In the equation (20), $\mathbf{n_{12}}$ is the normal vector of the internal boundary from medium 1 to medium 2, $\mathbf{J}_1$ is the current density from medium 1 towards the boundary and $\mathbf{J}_2$ is the current density from medium 2 towards the boundary [15, 36].

Each domain in the model satisfies the charge conservation law applying equation (6) into every node in the FEM model. Ohm's law (5) is modified to include externally generated currents $\mathbf{J}_\mathrm{e}$ as shown in equation (21). These currents originate from outside of the domain boundaries [15, 36].

$$\mathbf{J} = \sigma\mathbf{E} + \mathbf{J}_\mathrm{e} \tag{21}$$

Values of charge density are not always known and therefore continuity equation (6) can be expressed without it. First equation (4) is substituted into Ohm's law, resulting in the equation (22).

$$\mathbf{J} = -\sigma \nabla \mathrm{U} + \mathbf{J}_{\mathrm{e}} \tag{22}$$

Then equation (22) is substituted into equation (6).

$$\nabla \cdot \mathbf{J} = -\nabla \cdot (\sigma \nabla \mathrm{U} - \mathbf{J}_{\mathrm{e}}) \tag{23}$$

Resulting equation (23) is an alternative way of expressing continuity equation (6), which can be calculated without the information about charges [36].

## 4.3 Volume of tissue activated

Volume of tissue activated (VTA) describes the extent of brain tissue that can be excited with the stimulation [33]. It is the one of the most important concepts of the DBS treatment. VTA defines the efficiency of treatment results, as well as likehood of possible side effects [33]. VTA depends on the tissue properties, electrode placement and stimulation parameters, stimulation voltage, pulse width and frequency [19, 33].

DBS functions like a local delivery treatment, and is therefore highly dependent on the tissue volume that can be affected [34]. Regions that are not target areas of the stimulation will be affected by the electric fields as well. This might induce adverse effects like an excitation of the corticospinal tract [33]. There are some debates on the correct electrode locations and stimulation parameters, thus modeling the VTA and knowledge of the behavior of electric fields is necessary in treatment planning [33].

Current density is often used in conjunction with neural stimulation, but since it is not directly related to it, most studies prefer other methods for calculating the VTA. Current density distribution is also difficult to model because we are not using point sources and the distribution is non-uniform on the electrode surface [21]. VTA can be evaluated by calculating the second spatial derivative of the potential in the extracellular space and comparing that value to an activation function $f_{act}$ [54]. While the equation (24) holds, the neuronal elements will have a high probability to become activated in that specific location. [33]

$$f_{act} \leq \frac{\partial^2 V}{\partial x^2} \tag{24}$$

Activation function depends on the type of neural tissue, its geometry and possible myelination, as well as stimulation amplitude and pulse widths. Values of activation functions are obtained primarily from neuronal models and simulations. Although, the cell bodies can be stimulated, it is believed that the axons attached to the cell bodies are being excited more commonly, even when the stimulation electrodes are closer to soma [55]. Therefore VTA calculations are performed with the activation functions of myelinated axons [34, 33].

Axon models are primarily linear and non-linear cable models that are fundamentally based on the earliest works Hodgkin and Huxley [11, 13]. The most prevalent axon model for DBS simulations and modeling was created by McIntyre et al.. However, in McIntyre's model the diameter of the axon could be varied from 5.7 µm to 16 µm, but the axons in the brain are much smaller than that on average [32, 40]. Axon diameters in the brain range from 0.2 µm to over 10 µm, while majority of the diameter distribution occurs below 1 µm [56]. Therefore we used activation function values acquired from another model created by Åström et al. They created a detailed model for activation functions with multiple axon diameters and stimulation voltages. Median activation function values with different stimulation voltages for 2.5 µm, 5 µm and 7.5 µm diameter myelinated axons were 0.309 V/mm$^2$, 0.634 V/mm$^2$ and 0.307 V/mm$^2$ respectively. Activation function for 2.5 µm axon and 5 V amplitude was 0.277 V/mm$^2$, which is the most commonly used value in our simulations [57].

Electric field propagates into every direction in the brain and therefore the neuronal activation can also occur in any direction. VTA can induce both depolarization and hyperpolarization, since it has positive and negative component in any given direction [21]. In the VTA evaluation, the equation (24) has to be calculated with respect to each spatial variable. Instead of a single value, result of each voxel (pixel) is a Hessian matrix as shown in the equation (25).

$$\boldsymbol{H} = \begin{bmatrix} \frac{\partial^2 V}{\partial x^2} & \frac{\partial^2 V}{\partial x \partial y} & \frac{\partial^2 V}{\partial x \partial z} \\ \frac{\partial^2 V}{\partial y \partial x} & \frac{\partial^2 V}{\partial y^2} & \frac{\partial^2 V}{\partial y \partial z} \\ \frac{\partial^2 V}{\partial z \partial x} & \frac{\partial^2 V}{\partial z \partial y} & \frac{\partial^2 V}{\partial z^2} \end{bmatrix} \tag{25}$$

In the matrix (25), each element is a second spatial derivative of the potential. Most materials are symmetric and therefore the Hessian matrix is also symmetric and satisfies the transpose condition in equation (26) [14, 58]. As consequence, only 6 elements need to be calculated.

$$\boldsymbol{H} = \boldsymbol{H}^{\boldsymbol{T}} \tag{26}$$

In COMSOL 5.2, second spatial derivative of the potential or VTA are not premade solutions, but the value can be derived by setting a custom solution in the expression section of derived values option. Complete VTA in the Hessian matrix can also be solved by setting a logical condition that checks whether any of the matrix elements meets the VTA threshold in a mesh element, and then marking that element as either 1 or 0, depending whether the condition was met or not. This threshold checking is done to each mesh element and the result is a binary space. The resulting binary space can then be volume integrated to get the total VTA value.

## 4.4 Simulation parameters

Simulations were executed to evaluate the electric field behavior in different circumstances by modifying various simulation parameters. Affected parameters included lead location and orientation, encapsulation layer thickness and uniformity, electrode polarity and amplitude.

Lead orientation can rarely be affected after the initial trajectory is decided and burr hole has been drilled. Safest trajectory is always chosen to avoid it from intersecting with other basal nuclei and internal cerebral veins that run close to thalamus [6]. Lead was allowed to move slightly while constraining the shaft to remain roughly within the lateral ventricle, corresponding to about 5° change in angle. Lead location was within the ANT, except in simulations when lead misplacements were modeled.

Encapsulation thickness was varied from 100 µm to 1000 µm in a uniform encapsulation model and from 100 µm to 500 µm (200 µm to 1000 µm) in a non-uniform state. In a non-uniform state, the thicker side of the encapsulation was always twice the thickness of the thinner side. Thickness at the 1000 µm range is an exaggeration, but some similar studies included thicknesses up to 1000 µm, and for the sake of comparability the range here is extended to those values as well.

Electrode polarity was either monopolar and bipolar in most simulation and tripolar in misplacement simulation. Even though quadripolar configuration is available in most DBS systems, it is rarely used and therefore it was not included in the simulations. In bipolar stimulations, cathodal and anodal electrode locations were altered to observe the effects of distant and close electrodes and possible correcting actions in the case of misplaced lead. Commonly used amplitudes in epileptic DBS range from 1.5 V to 5 V, which was further extended to observe some extremes. Voltage amplitude range was from (-)1 V to (-)10 V in 0.2 V steps.

# 5. RESULTS AND DISCUSSIONS

In this section, the most significant simulation results are presented and their importance is discussed. From the section 4.4, it is clear that there would be too many different simulation parameter combinations to present them all in this section. First, the size and shape of the VTA is presented to give reader an understanding of its manifestation. Then the effects of stimulation voltage and polarity are analyzed. After that, the encapsulation is added to the subsequent simulations. Effects of uniform encapsulation and its irregularities are studied. Finally the planar model of thalamus and the effects of tissue properties are examined.

Simulation parameters in this chapter are constant throughout every section unless specifically mentioned, which allows us to compare the results more easily. In a monopolar stimulations, cathode was mostly at -5 V and the reference was grounded. In a bipolar stimulations cathode was at -5 V and anode at 5 V. In the anatomical geometry section the corresponding potentials were -3 V and 3 V. The VTA of a small diameter (2.5 μm) axon is roughly 0.277 V/mm$^2$ at -5 V stimulation amplitude, which is the value used in this section [57]. Encapsulation thickness was 300 μm in the simulations where it was present, which is on the higher end of the commonly used values [30].

## 5.1 VTA demonstration

Shapes and sizes of the VTA and its components are illustrated here. Sheer purpose of this section is to give reader an insight into activation volumes, which will later become distorted in the presence of material boundaries. Figure 22 represents the VTA in -5 V monopolar and -5 V/5 V bipolar stimulation. VTA is presented as a color map. Purpose of this simulation is to show where the VTA gets largest values and how it spreads. In every simulation afterwards, the VTA is presented only as isosurface or isoline that equals the activation function value. Because VTA is the second gradient of the potential and also the first gradient of the electric field, it is obvious that the largest VTA values are found at the material interfaces where electric field lines converge.

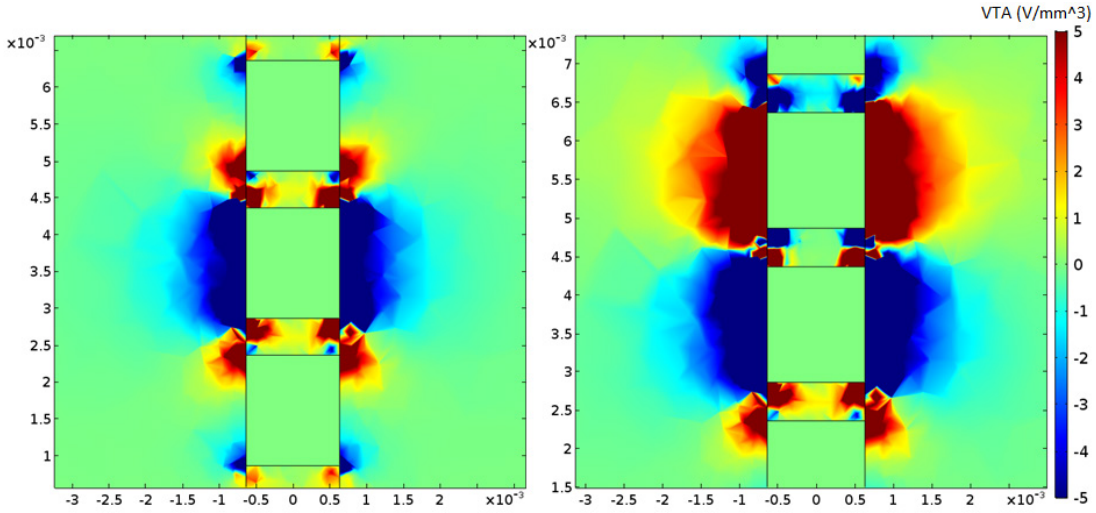


***Figure 22.*** *Monopolar and bipolar stimulation illustrating the ∂x∂x component of the VTA.*

Volume of tissue activated (VTA) was simulated for both monopolar and bipolar electrode configurations and the results are shown as cut planes in Figure 23, Figure 24 and Figure 25. Color map in the aforementioned figures represents the potential field. Cut planes are primarily used as they provide a better illustration of the actual VTA. In addition to primary isosurfaces shown in all figures below, smaller separate regions of the VTA appear near each border of the polyurethane and platinum-iridium electrode due to high difference in conductivity. Examples of these regions can be seen in the Figure 22 where the small blue or red areas appear. These areas are filtered out from the images for clarity, but included in graphs and calculations.

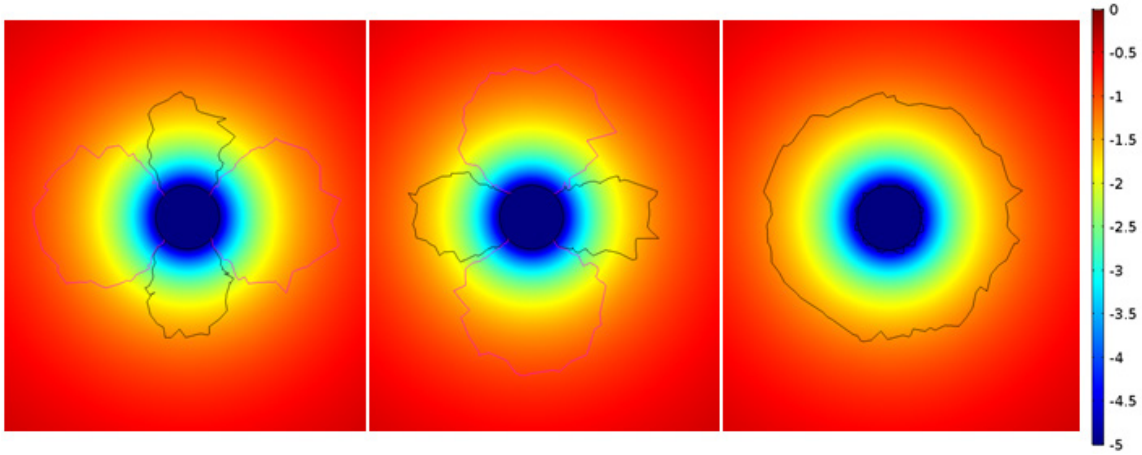

***Figure 23.*** *VTA isosurfaces in a homogenous and isotropic medium generated with a -5 V monopolar stimulation. Black outlines are activation due to depolarization and magenta outlines are activation due to hyperpolarization. Images from left to right represent horizontal, vertical and perpendicular potential gradients. Images are cut planes from middle of the active cathodal electrode in the xy-plane. Color scale on the right represents the voltage variation.*

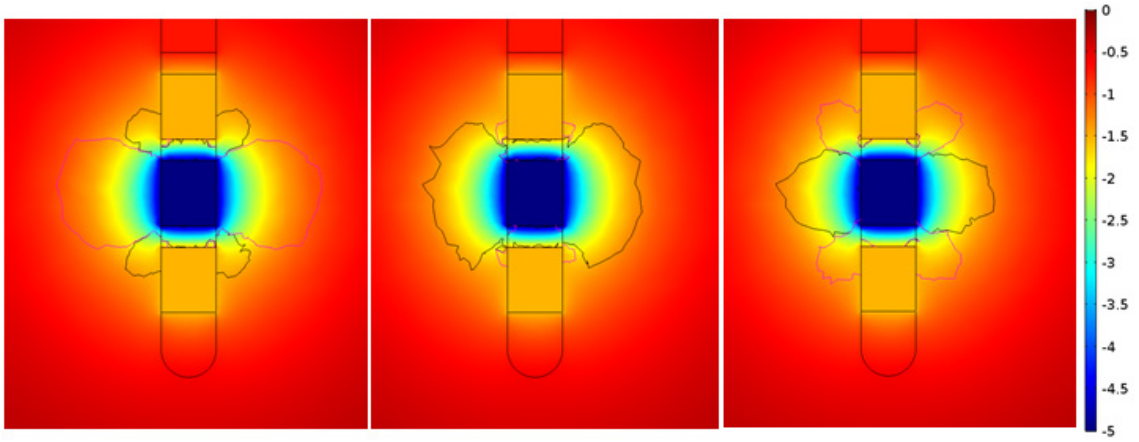


***Figure 24.*** *VTA isosurfaces in a homogenous and isotropic medium generated with a -5 V monopolar stimulation. Black outlines are activation due to depolarization and magenta outlines are activation due to hyperpolarization. Images from left to right represent horizontal, vertical and perpendicular potential gradients. Images are cut planes from middle of the active cathodal electrode in the xz-plane. Color scale on the right represents the voltage variation.*

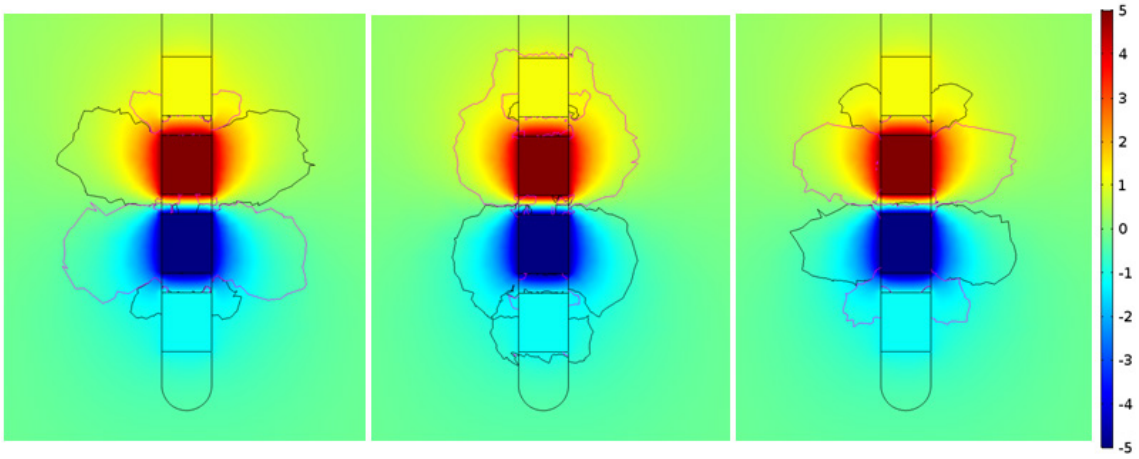


***Figure 25.*** *VTA isosurfaces in a homogenous and isotropic medium generated with a bipolar stimulation with cathode at -5 V and anode at 5 V. Black outlines are activation due to depolarization and magenta outlines are activation due to hyperpolarization. Images from left to right represent horizontal, vertical and perpendicular potential gradients. Images are cut planes from middle of the active cathodal electrode in the xz-plane. Color scale on the right represents the voltage variation.*

VTA in 3 dimensions for both monopolar and bipolar stimulations are shown in the Figure 26 and Figure 27. The fundamental constituents of these complete VTA are shown in appendices A and B.

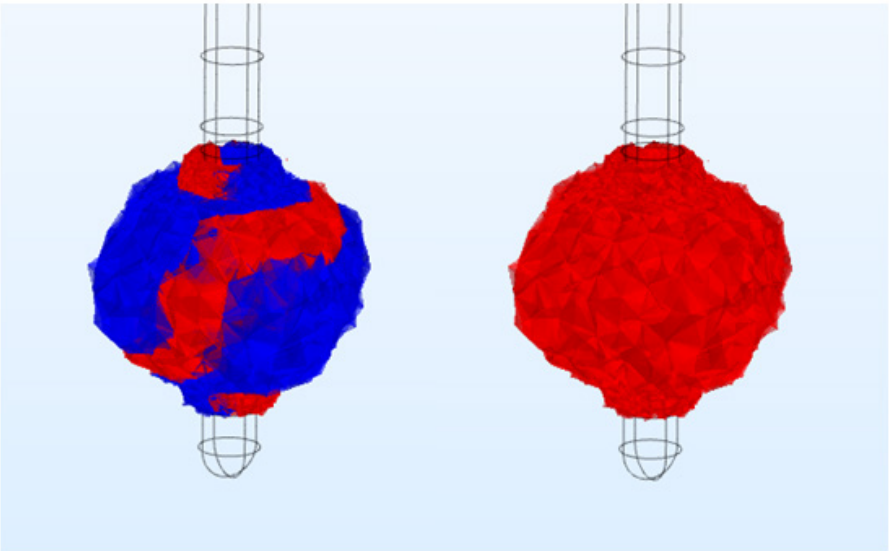

***Figure 26.*** *Monopolar VTA union of all constituents of equation (25).On the left, red represents the depolarization and blue represents the hyperpolarization. On the right both activation functions are merged as one color for clarity.*

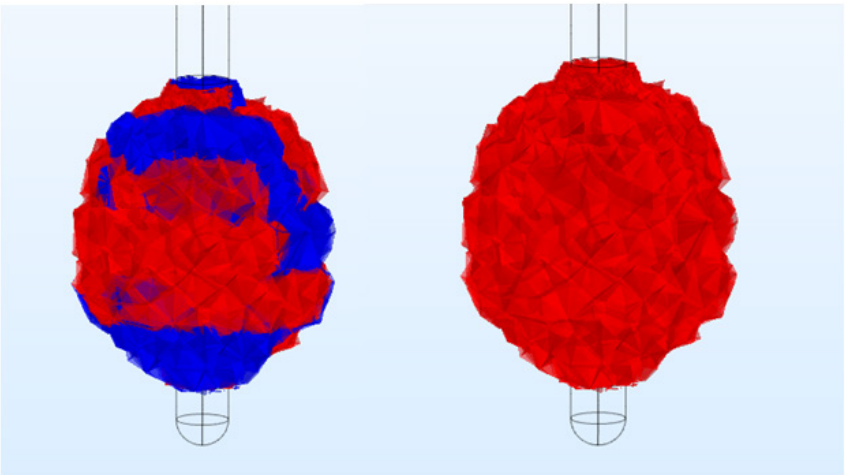

***Figure 27.*** *Bipolar VTA union of all constituents of equation (25). On the left, red represents the depolarization and blue represents the hyperpolarization. On the right both activation functions are merged as one color for clarity.*

## 5.2 Polarity and amplitude

Electrode polarity and amplitude are clearly the most important factors to understand, as they are the only parameters that can be changed post-operatively, of those included in this model. VTA calculations may reach the activation function threshold inside the DBS lead and encapsulation tissue, but since there are no neurons in those volumes, they are discarded from the calculations.

Figure 28 shows the relationship between stimulation voltage and VTA. From the Figure 28 it is clear that larger volume is activated with bipolar stimulation. When comparing the stimulation voltages, one has to take into account that the potential difference is twice as large in bipolar stimulation when the cathodal voltages are equal. Bipolar stimulation at -5 V/5 V has the VTA value of 116.4 $mm^3$ and the monopolar at -10 V has the VTA of 119.64 $mm^3$. Therefore VTA values are roughly equal when comparing potential differences rather than cathodal voltages. The size of the VTA must not be mixed up with electric potential field, which is larger in monopolar stimulation that can be seen in the Figure 12 in section 3.5.3.

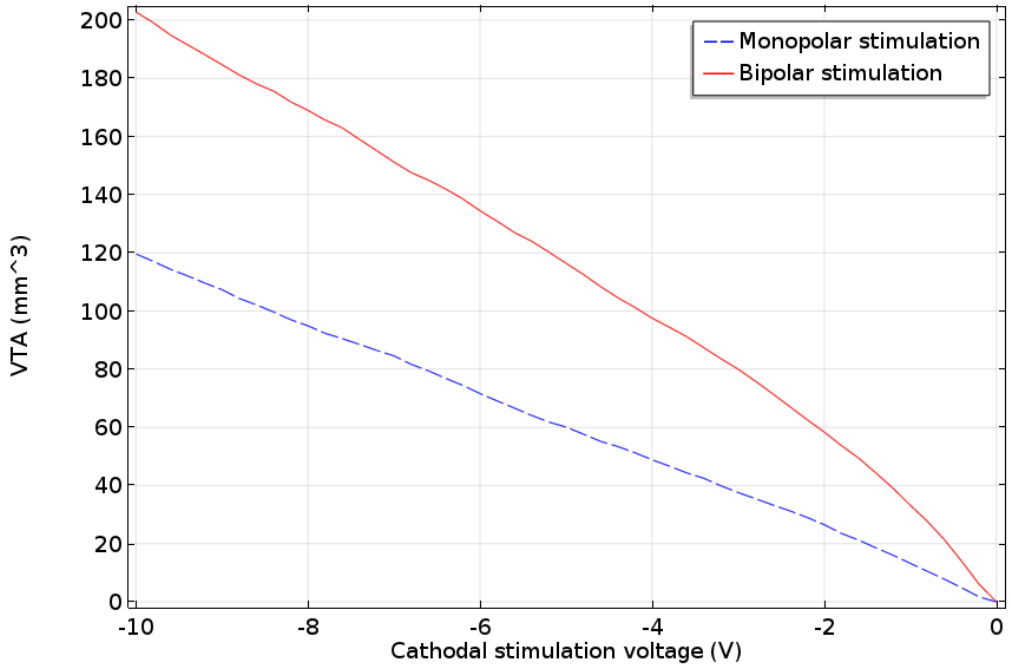


***Figure 28.*** *VTA dependence of the stimulation voltage in monopolar and bipolar stimulations.*

Due to linear nature of the voltage-VTA relationship, linear regression of data points of the Figure 28 provides the following voltage-VTA dependencies. Equations (27) and (28) are relationships for monopolar and bipolar stimulations respectively and $U$ is the stimulation voltage.

$$VTA_{mono} = -11{,}73U + 1.66 \tag{27}$$

$$VTA_{bi} = -19.10U + 17.06 \tag{28}$$

3D illustrations of the VTAs in Figure 26 and Figure 27 indicate them to be relatively spherical, which is more prominent in the monopolar VTA. Previous equations can used to estimate the voltage required to mitigate misplaced electrodes. For example, if the amplitude has to be increased from -4 V to -6 V for clinical effects to show up, then the total VTA increases by 23.46 $mm^3$ in monopolar and 38.2 $mm^3$ in bipolar stimulation. In a perfectly spherical VTA this would correspond to an additional distance of 0.32

mm and 0.34 mm reached in monopolar and bipolar stimulation respectively. As a comparison, volume of each electrode on the DBS lead is 1.9 $mm^3$ [20], so this increased VTA may seem large at first. However, if the anatomical target is located at one particular direction then the increased volume into any other direction is worthless. Therefore, the distances 0.32 mm and 0.34 mm matter more than the volumes.

Both Medtronic DBS leads have 4 electrodes and they span in 7.5 mm distance in the Model 3389 and in 10.5 mm distance in Model 3387. This clearly implies that in most cases it should be far more beneficial to change the active electrodes rather than increasing the amplitude to extremely large values. This evaluation did not include the encapsulation layer, so the actual volumes and distances are going to be even smaller and the benefit of varying electrodes even larger.

Increasing the VTA does not just require larger voltages to be used, but it also drains battery life more. Most programming guides suggest that voltages should not be raised above 3.6 V due to voltage doubler circuits getting activated [4, 27]. Looking at voltage-VTA dependence graph and the example voltage-distance results, this seems an extremely hard goal to achieve. Numerous DBS reports have stimulation amplitudes in the range of 5 V or 5 mA, so in practice this can rarely be achieved either [18, 28, 59]. In an epileptic DBS, the suggested default value for the amplitude is 5 V to begin with. Having a stimulation voltage below 3.6 V would require almost perfectly placed electrode. Or in some cases, have some other than the intended target in the neural network to activate and cause the treatment. This leads us to the most severe drawback of increasing stimulation voltage, the adverse effects of the stimulations that were discussed in section 3.3. Fundamentally, when the stimulation amplitude is increased to increase the VTA, so is the influence on unwanted neurons as well. When it comes to that point, we can't even be sure whether it was the intended target that caused the clinical effect or some other mechanism [30].

Even though we are using a constant activation function in this thesis, in reality it is a function of multiple parameters. Comparison of a constant activation function and a voltage dependent activation function in monopolar stimulation is shown in the Figure 29. Constant activation function gives larger VTA in every voltage value with average difference of -0.353 $mm^3$. This difference could be included into other simulations as a correction factor, but the presence of so many other variables, such as dependence on the axon diameter, would merely increase the uncertainty of the calculations.

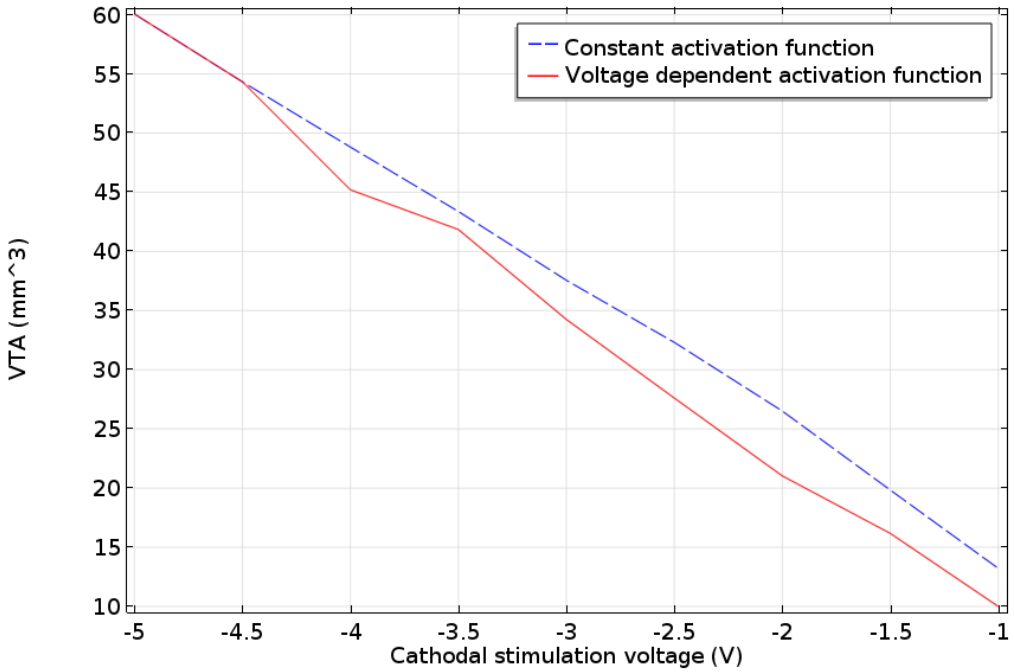


***Figure 29.*** *Difference between a constant activation function and a voltage dependent action function. Activation function values are derived from the works of Åström et al.* [57].

## 5.3 Encapsulation

In the results from here on, the encapsulation layer is always included, because it is always present on the objects implanted in the body. However, the thickness, uniformity and cell structure is rarely known. Encapsulation properties have been measured from the DBS leads that have been removed from the body or grown in vitro. Here encapsulation thickness was first changed from 0.1 mm to 1 mm to observe its effects on the VTA in both monopolar and bipolar stimulations. Figure 30 and Figure 31 represent the xz-cutplanes of the electrode and VTA with the encapsulation thickness of 0 mm, 0.1 mm and 0.3 mm. From these figures it observable how the VTA is drastically reduced in the presence of an additional resistive layer, which represents a more realistic interaction of the DBS lead and tissue.

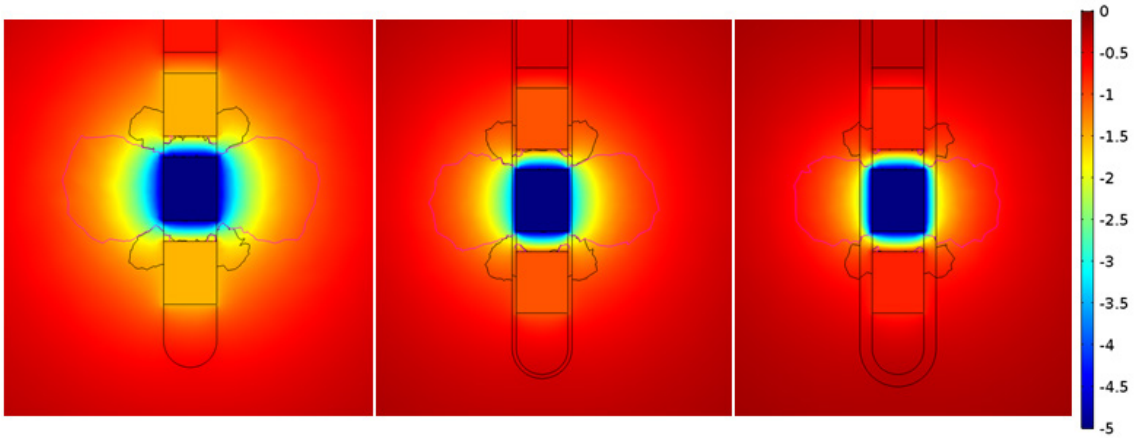


***Figure 30.*** *VTA isosurfaces with an encapsulation layer generated with a monopolar stimulation. Black outlines are activation due to depolarization and magenta outlines are activation due to hyperpolarization. Images from left to right contain 0 mm, 0.1 mm and 0.3 mm encapsulation layer respectively. Images are cut planes from middle of the active cathodal electrode in the xz-plane. Color scale on the right represents the voltage variation.*

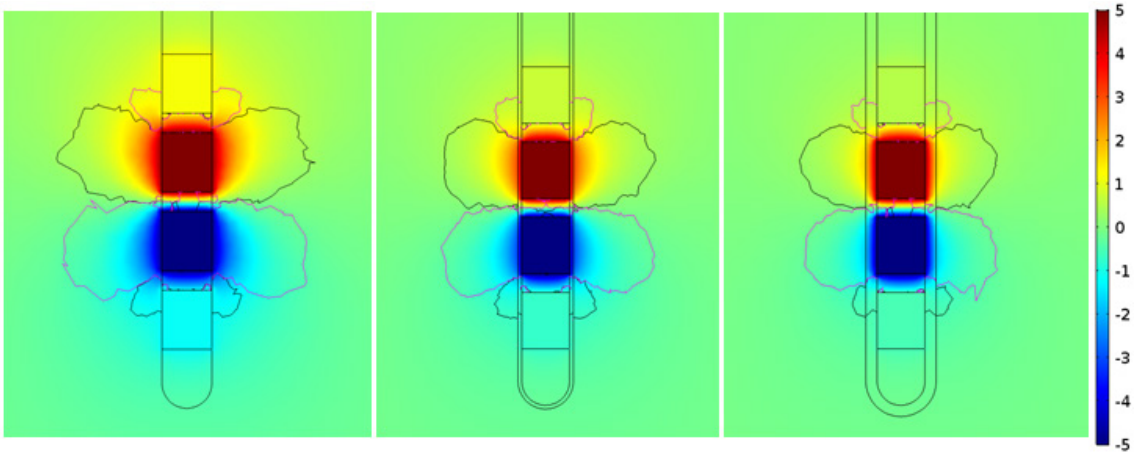


***Figure 31.*** *VTA isosurfaces with an encapsulation layer generated with a bipolar stimulation. Black outlines are activation due to depolarization and magenta outlines are activation due to hyperpolarization. Images from left to right contain 0 mm, 0.1 mm and 0.3 mm encapsulation layer respectively. Images are cut planes from middle of the active cathodal electrode in the xz-plane. Color scale on the right represents the voltage variation.*

In the graphs below, the volume inside the encapsulation tissue that met the activation threshold was not included the calculations. Therefore, in addition to attenuating properties of the encapsulations layer, the ignored volume was also larger. Figure 32 represents the VTA dependence of the encapsulation thickness. Thickness was simulated up to 1 mm to show how drastically it reduces the VTA. Realistic encapsulation thicknesses are in the range of 0.1 mm to 0.3 mm.

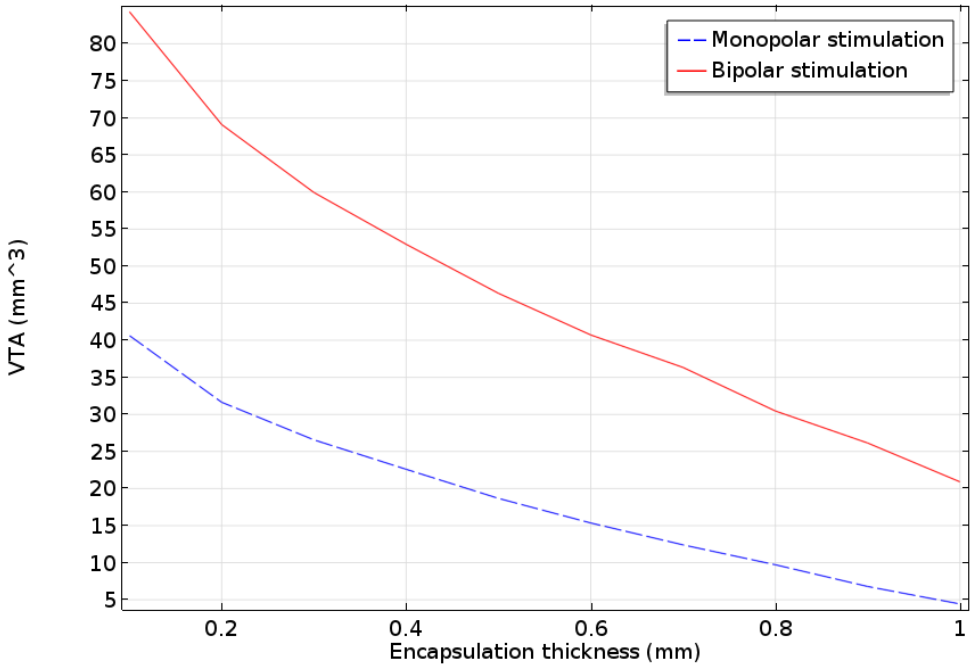


***Figure 32.*** *VTA dependence of the encapsulation layer thickness in monopolar and bipolar stimulations with a stimulation voltage of -5 V.*

Figure 33 represents the VTA dependence of the voltage with an encapsulation layer of 0.3 mm.

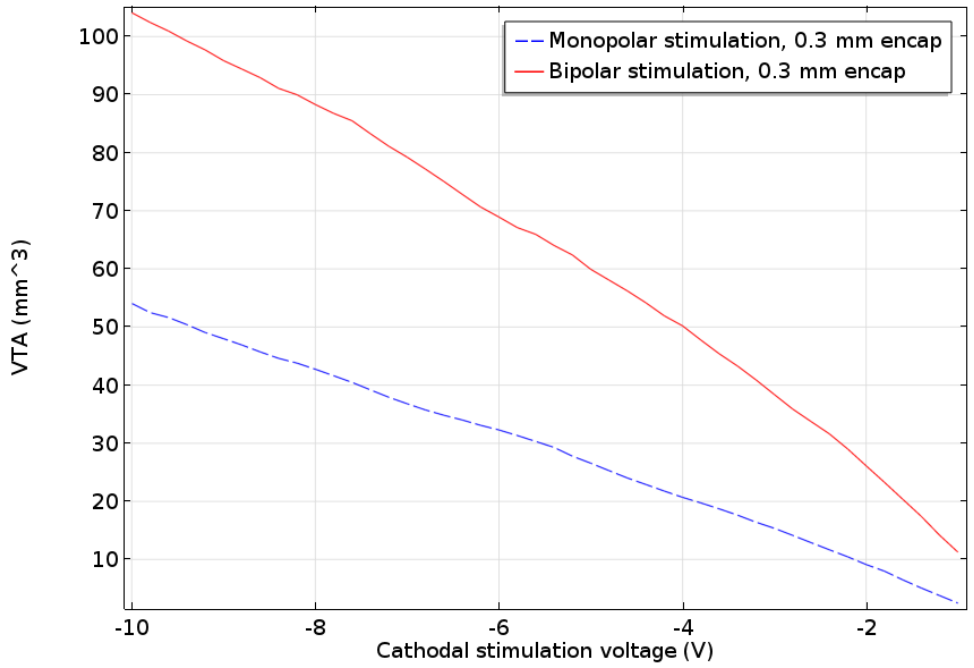


***Figure 33.*** *VTA dependence of the stimulation voltage in monopolar and bipolar stimulations with an encapsulation layer of 0.3 mm.*

Linear regression of data points of the Figure 33 provides the following voltage-VTA dependencies. Equations (29) and (30) are relationships for monopolar and bipolar stimulations respectively and $U$ is the stimulation voltage.

$$VTA_{mono} = -5.58U + 1.81 \quad (29)$$

$$VTA_{bi} = -10.06U + 7.42 \quad (30)$$

Comparing these equations to those acquired in section 5.2, one can notice the reduction by roughly a double the amount. This implies that the 0.3 mm encapsulation layer requires the amplitude to be increased twice the amount to get the same increase in VTA, as it would require without the encapsulation layer. As an example, the VTA without the encapsulation layer was 60.059 $mm^3$ and 69.331 $mm^3$ in monopolar (-5 V) and bipolar stimulation (-2.5 V/2.5 V) respectively. Corresponding values with the 0.3 mm encapsulation layer were 26.567 $mm^3$ and 32.675 $mm^3$. These are equal to 44.2% and 47.3% reductions, which is so significant that encapsulation should not be ignored from any DBS models.

Increasing encapsulation thickness causes a steep decrease in VTA and looking at the Figure 32; it is obvious that stimulation would require unfeasible amplitudes very rapidly when the thickness grows. Therefore, the implantation procedure should cause as minimal trauma as reasonably possible to avoid scar tissue growth. Some suggest using pharmacological agents or electrode surface patterning to minimize encapsulation growth. However, electrode surface patterning would require lead manufacturers effort, as the leads need to be approved for DBS surgeries [30].

Clinicians report that the stimulation amplitudes are often needed to be increased within the first few weeks after the implantation [28]. There are two types of encapsulation layers, the acute and the chronic, which are described in more detail in section 4.1.4. VTA drop that requires the amplitude to be increased is caused by the state change from acute to chronic encapsulation [30]. Figure 34 shows the results of a multiparameter sweep that illustrates the required need to increase stimulation voltage to maintain constant VTA during the first weeks after the implantation. Y-axis represents the cathodal voltages despite the positive values. Encapsulation conductivity decreased from 1.7 S/m to 0.125 S/m in the 3 week acute phase succeeded by 5 week period when the chronic layer was forming [44]. Final conductivity value of 0.125 S/m is on the other extreme of the realistic values and the need to increase voltage may not be as much as shown in Figure 34. From the graph it is apparent that shortly after the implantation, the response to the treatment needs to be constantly monitored and adapted to encapsulation growth. Required voltage increase in the monopolar stimulation was from (-) 3.136 V to (-) 6.8618 V which equals (-) 3.7258 V or 119% increase. Corresponding bipolar values were from (-) 1.4252 V to (-) 2.848 V equaling (-) 1.4228 V or 99% increase. After the 8 week period the voltage values plateau, as the encapsulation has reached its long term

conductivity. In the previous calculations, the VTA was expected to initially barely cover the anatomical target and hence require the constant amplitude increments. Back et al. measured postoperative voltage drops in DBS patients suffering from idiopathic Parkinson's disease. Measurements were detected by the electrode during the first 7 days after implantation and they found insignificant voltage drops in the range of tens of millivolts [60]. This result is consistent with the data in Figure 34 and it describes the initiation of the acute encapsulation.

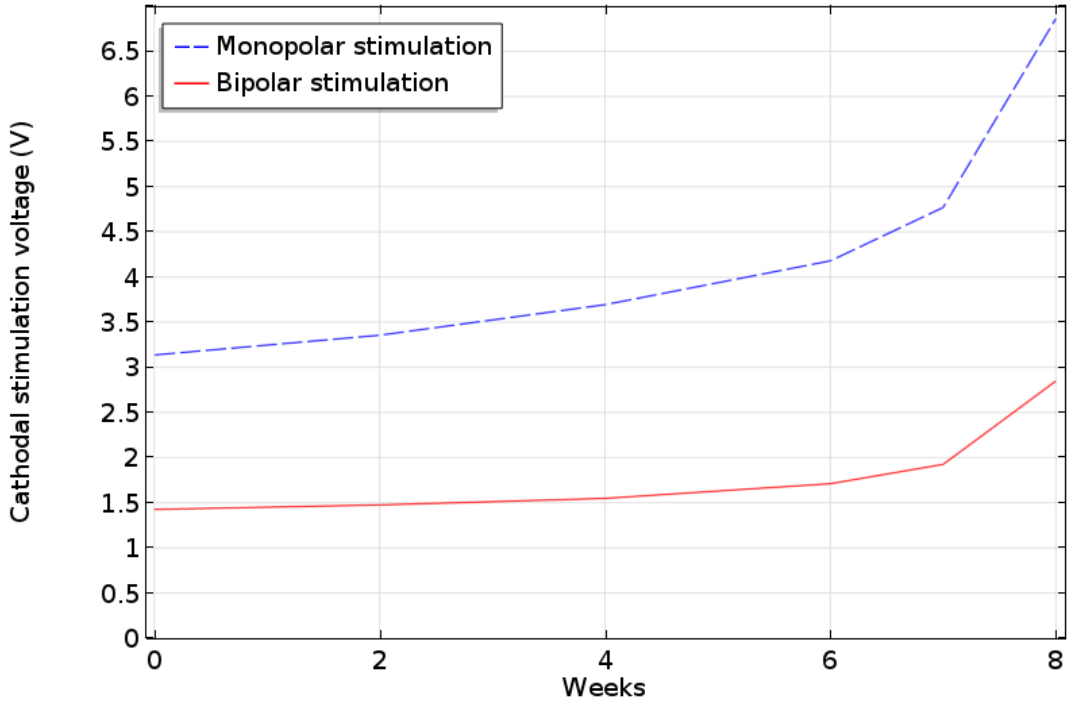


***Figure 34.*** *Voltage in monopolar and bipolar stimulation while the encapsulation layer grows.*

Predicting the VTA by calculating volumes up to activation threshold might not give the correct results. It is known that stimulation amplitudes large enough might even block the generations of action potentials [55]. This is called the anodal surround block, which prevents the escape of an action potential impulse in the cathodal stimulation [13]. There aren't any exact values for these blocking current, but some studies claim that currents exceeding 8 times the threshold current may begin to block the action potentials [55, 61]. Activation current thresholds depend on the pulse duration and axon diameter, which makes it hard to estimate exact blocking values. Also the larger the axon diameter the wider is the anodal block region and from further the excitation will occur. However, anodal stimulation experiences no blocking activity [13]. Figure 35 shows the effect of anodal block in monopolar and bipolar stimulations. Blocking value was chosen to be 2.216 V/mm$^2$ that is 8 times the activation function value.

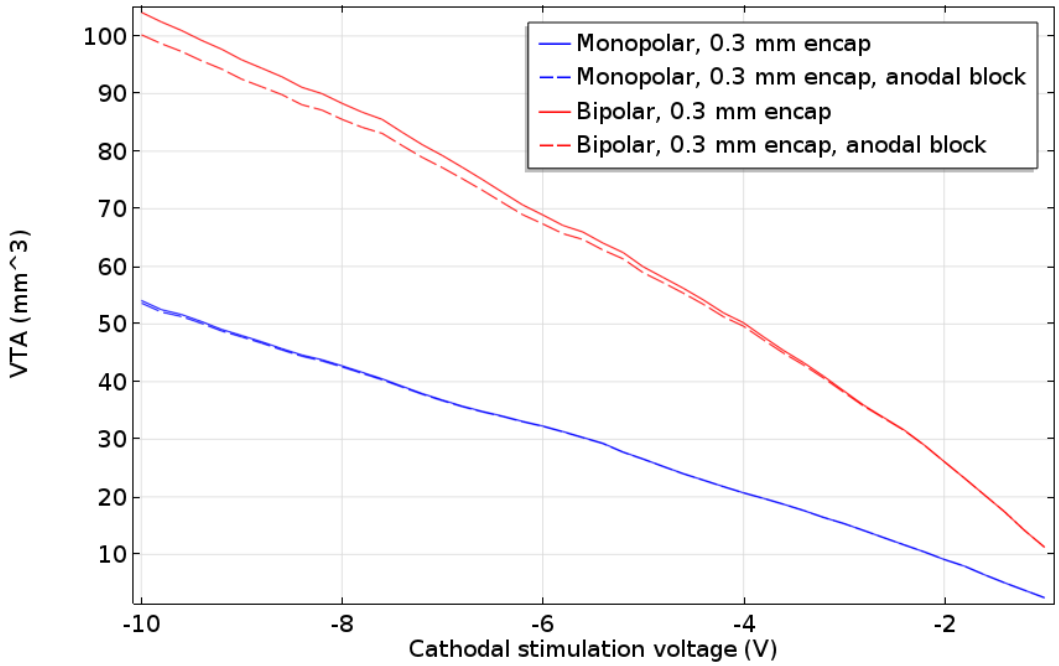


***Figure 35.*** *VTA dependence of the stimulation voltage in monopolar and bipolar stimulations with an encapsulation layer of 0.3 mm. Dashed lines are stimulations with anodal block included.*

Anodal block reduces the chance of neuronal activation near the electrode surface. Since the encapsulation layer attenuates it so extensively, that volume where the activation does not occur remains relatively small. Even the smallest blocked areas are mostly contained within the encapsulation layer itself. It can be seen from the Figure 35 that in monopolar stimulation the effect of anodal block is almost non-existent and in bipolar stimulation also relatively small. The higher the stimulation amplitudes get, the more its effect is increased. Figure 36 shows the effects of anodal block in monopolar stimulation with and without the encapsulations layer.

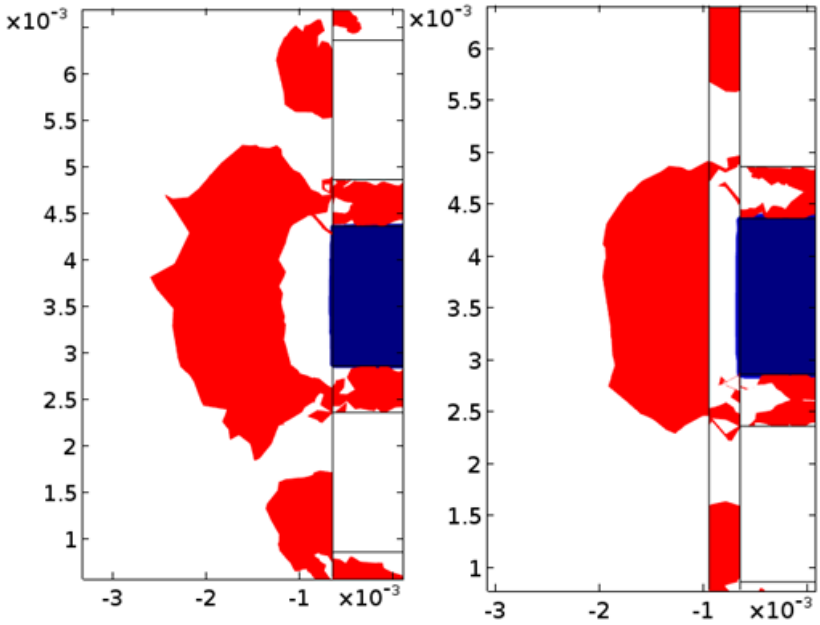


***Figure 36.*** *Anodal block estimations with and without the encapsulation layer in -5 V monopolar stimulation. Blue region is the active electrode. Image shows only ∂y∂y component.*

From the left image in Figure 36, VTA is clearly reduced by the huge open areas where the second derivative of the potential gets the largest values. In the right image of the Figure 36, open areas are inside the encapsulation layer and the VTA that overlaps the tissue remains unaffected. Therefore, the effect of anodal block is negligible when the encapsulation is present. Anodal block is not included in most other studies, but as just mentioned it would not bias the results until at very large amplitudes.

Encapsulation thickness cannot be controlled on the implanted DBS lead and it might grow unevenly. Voltage-VTA dependence of a non-uniform encapsulation layer is shown in the Figure 37. This encapsulation was described earlier in the section 4.1.4. Uneven encapsulation layer would be greatly beneficial, if the thin side would be towards the target anatomical region. This would allow lower stimulation amplitudes to be used and it would also mitigate the adverse effects by activating unwanted regions. However, this is going to be a severe setback if the thick side grows towards the target region, which would require larger amplitudes and higher tendency to activate unwanted regions.

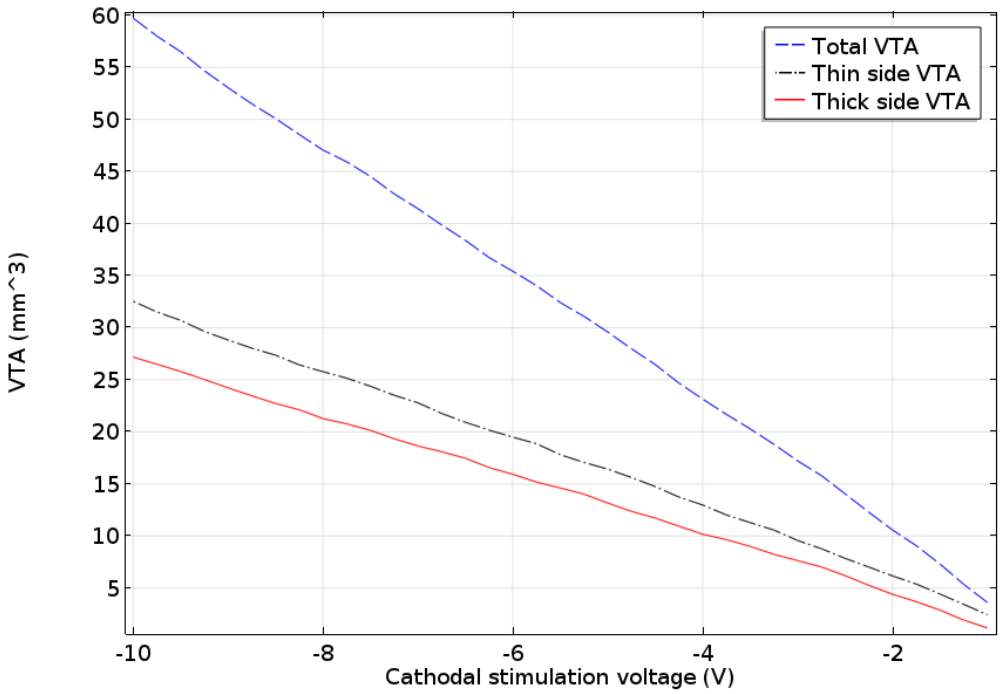


***Figure 37.*** *VTA dependence of the stimulation voltage in monopolar stimulation with a non-uniform encapsulation layer varying from 0.15 to 0.3 mm. In the graph, thicker and thinner sides of the encapsulation layer are separated to show their individual effect.*

Buhlmann et al. created an experimental DBS lead based on the Medtronic model, which had each electrode split into four separate entities. This allows controlling the direction of electric field spread in addition to amplitude. Uneven encapsulation layer would be no risk anymore and the side effects could be minimized [23].

## 5.4 Anatomical structures

In the following section, different tissue properties are added into thalamus plane model. Electric field is affect by differences in conductivity and as a result the VTA becomes distorted as well. Figure 38 represents the electric potential fields in monopolar and bipolar stimulation of the ANT with -3 V/3 V amplitudes.

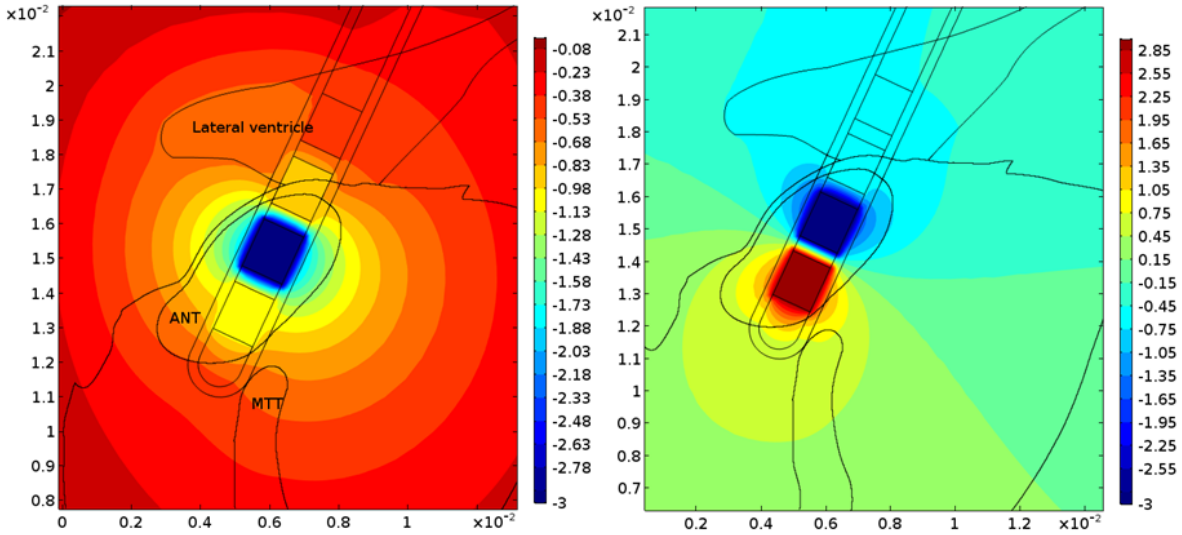


***Figure 38.*** *Electric fields in monopolar and bipolar stimulation of the ANT.*

Figure 39 illustrates the effects of CSF on stimulation. In the following figures, VTA color scale is reduced to a range from -1 to 1 in order to elicit even the smallest changes in VTA. Only $\partial x \partial x$ component is included in the images for clarity. Black borders in the red areas represent the VTA isosurface. CSF has an extremely high conductivity among materials of the human body. In the left image of the Figure 39, lateral ventricle has the same material properties as the surrounding materials and therefore has no effect on the VTA. In the right image of the Figure 39, lateral ventricle contains CSF and strongly affects the VTA size and may possibly activate unwanted neurons.

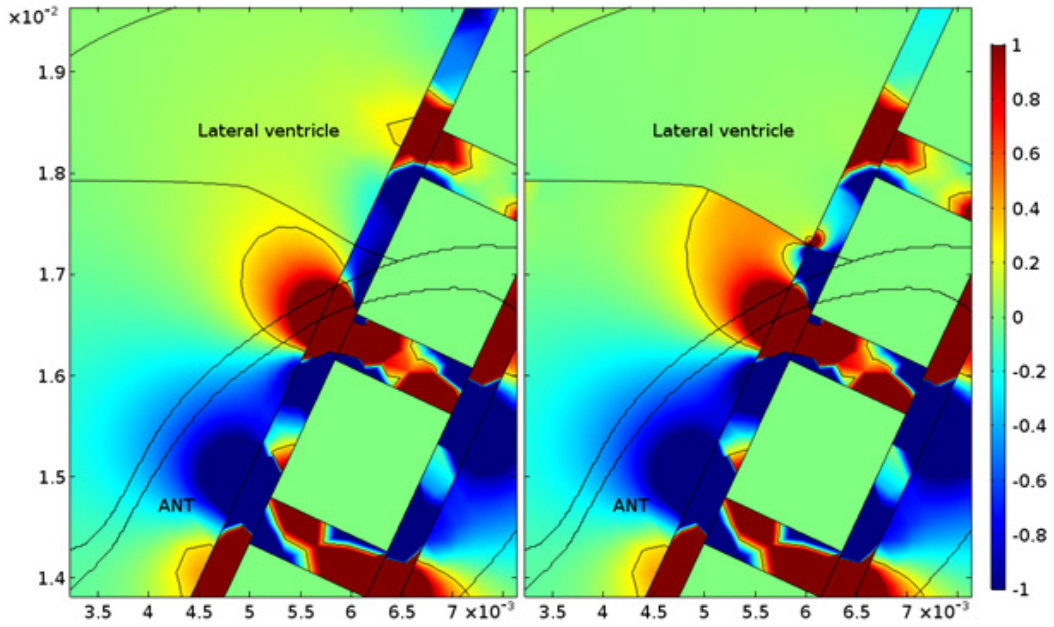


***Figure 39.*** *Effects of CSF on VTA in monopolar stimulation. On the left image, lateral ventricle has the properties of the surrounding material and on the right image, it contains CSF.*

Figure 40, represents the effects of tissue on anisotropy on the VTA in monopolar stimulation. Left image of the Figure 40 has an MTT with isotropic white matter and on the right it has an anisotropic MTT. Fiber direction of the MTT is along the y-axis. DBS lead in these images is implanted deeper than in the previous images for illustrative purposes. If the lead would ever be this close to white matter, the anisotropy would have a significant impact on the VTA. This may result into spreading of the neuronal excitation further into unwanted regions. Because of our incomplete knowledge of the mechanisms behind the treatment, we cannot be sure whether it is advantageous for the treatment or not. MTT being part of the Papez circuit, spreading the excitation along the MTT might even provoke the treatment effect [59]. Studies report that anisotropy can change the VTA by up to 18%, including VTA reductions and enlargements [34]. This essentially depends on how close the DBS lead is placed to an anisotropic white matter, but small displacements can drastically alter the shape of the VTA. Small distortions on the edges of the MTT are anomalies that are caused by the polygonal structure as shown in the Figure 40.

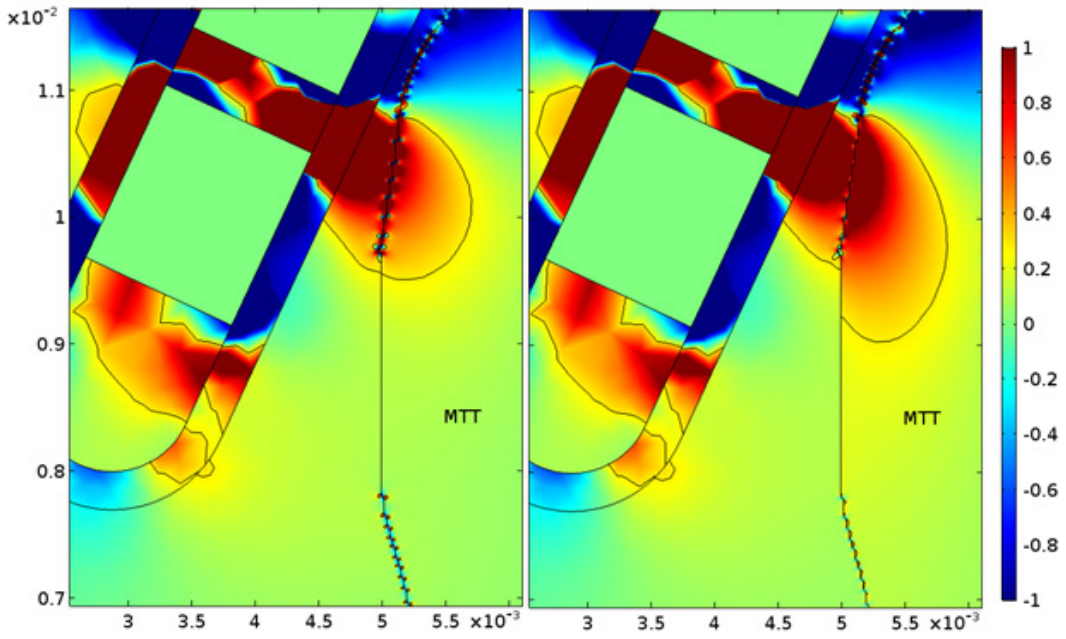


***Figure 40.*** *Effects of anisotropic white matter on VTA in monopolar stimulation. On the left image, MTT is isotropic and on the right image, it has anisotropic properties.*

Figure 41 shows three examples of the stimulations and how much of the ANT they cover. Area overlapped by the encapsulation tissue and the lead is not included into calculations. First image in the Figure 41 is -3 V monopolar stimulation. Middle image in the Figure 41 is also -3 V monopolar stimulation but the active electrode is centered in the middle of the ANT. In last image in the Figure 41, is a -3 V/3 V bipolar stimulation.

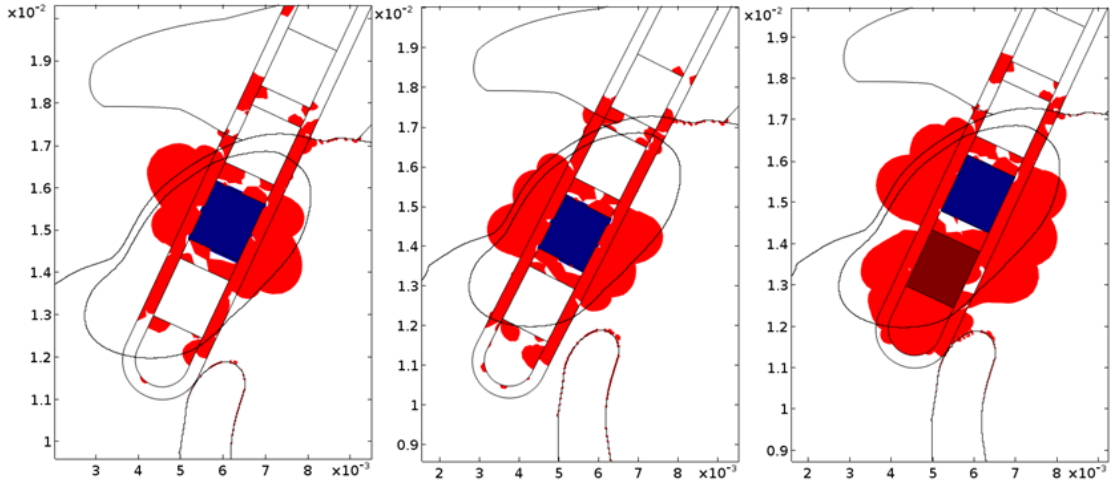

***Figure 41.*** *VTA of a -3 V monopolar stimulation, -3 V centered monopolar stimulation and -3 V/3 V bipolar stimulation.*

Figure 42 illustrates how large area of the ANT is covered when the amplitude is increased from -1 V to -5 V. Bipolar stimulation covers significantly more area, which is apparent from the graph and the images in Figure 41, since the two electrodes align with the shape of the ANT. In each stimulation the covered area plateaus already at relatively small amplitudes and further increasing the voltage won't have a huge impact on the ANT coverage.

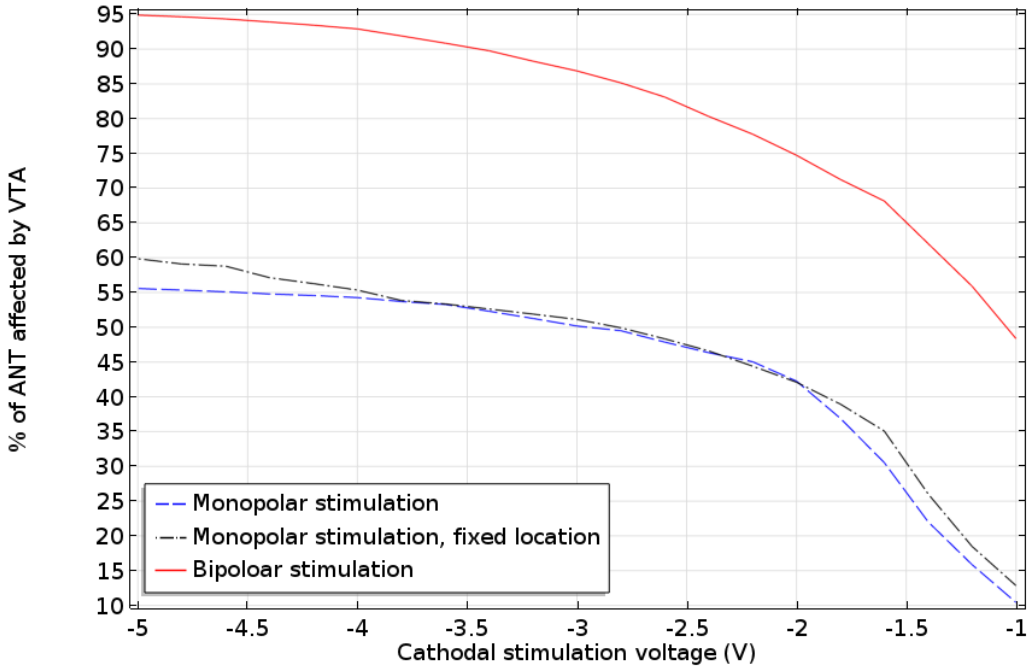


***Figure 42.*** *Stimulation voltage dependence on the ANT coverage.*

Figure 41 and Figure 42 represent situations where the electrode placement was near flawless. However, misplaced electrodes are a concern affecting every DBS procedure. Figure 43, represents a misplaced electrode that has been placed too far from the target and in a wrong angle. Hypothetical stimulation target is marked in the image as a red

dot and it is 1 mm from the encapsulation in a perpendicular line. Stimulation amplitude was increased from -1 V to -10 V, or until the activation function threshold was met at the target. In addition to increasing amplitude, active electrodes and different electrode configurations were explored, using three monopolar, three bipolar and one tripolar electrode configuration.

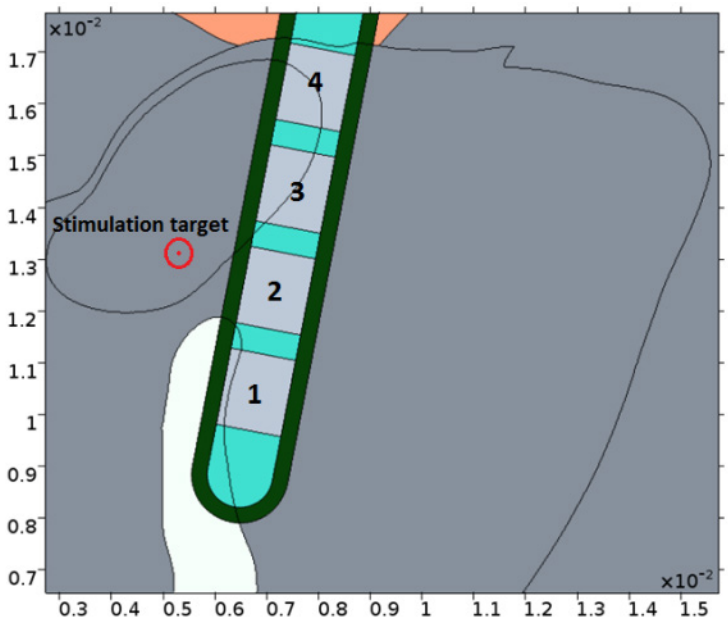


***Figure 43.*** *Hypothetical stimulation target and the misplaced electrode.*

Table 1 presents the electrode configurations and the results of the simulations. There are some important aspects that are pointing out from the results. Most notably, the activation did not occur at all in monopolar 1. This is because of the MTT and the attenuation it provides in the direction of low conductivity. In monopolar 2, the activation happened readily at a low voltage because the electrode is close to the target and also in the proper direction. From the Figure 41, it can be seen that VTA in the monopolar stimulation spreads more in the perpendicular direction with respect to DBS lead. Therefore, the active electrode in monopolar 3 was in an unfavorable direction and it took over twice the voltage to reach the activation threshold. Comparable situation may occur when the stimulation lead drifts lower from its original position. Even the smallest drift may then require considerable amplitude increase to maintain target coverage by VTA.

***Table 1.*** *Simulation results in the misplaced electrode simulations. Electrode number refers to figure 43 where (a) is the anode and (c) is the cathode. Voltage column is the stimulation amplitude when the target was activated and area column is the total VTA at that moment. Blank space is when the activation did not occur.*

| | Electrode nr. | Voltage (V) | Area ($mm^2$) |
|---|---|---|---|
| **Monopolar 1** | 1(c) | - | - |
| **Monopolar 2** | 2(c) | -3.37 | 6.0 |
| **Monopolar 3** | 3(c) | -7.50 | 14.8 |
| **Bipolar 1** | 1(a)+2(c) | -1.79 | 7.9 |
| **Bipolar 2** | 2(a)+3(c) | -2.16 | 9.6 |
| **Bipolar 3** | 1(a)+3(c) | -3.72 | 15.8 |
| **Tripolar 1** | 1(c)+2(a)+3(c) | -1.36 | 8.3 |

Each bipolar configuration achieved the activation but at very different amplitudes. In bipolar 1, the active cathode was closest to the target and thus the activation occurred at lower amplitude than in the other cases. Difference between bipolar 2 and 3 is most likely due the MTT affecting bipolar 3 more and the longer distance between active electrodes. Tripolar stimulation caused the activation at a very low voltage but as drawback it activated larger area than the best monopolar and bipolar stimulation option. When comparing these values, one has to take again into account that bipolar and tripolar stimulation requires an anode at the lead as well. Hence the voltage differences at the thalamus are twice as large as the table value.

Choosing the best stimulation option is not a straightforward decision. If the DBS lead is close to the target and at the same level as any of the electrodes, then the monopolar seems to be the best choice. Monopolar stimulation requires low voltages and activates the smallest area around the electrode, which may prevent some side effects to develop. If the electrode is behind fiber tracts, then the monopolar stimulation is more ineffective than other options. Monopolar stimulation also requires significant increase in amplitude if the target is off the electrode level. Bipolar stimulation with two adjacent electrodes is the most reliable choice. It is less affected by misplaced lead than the monopolar stimulation and it activates less area than bipolar with nonadjacent electrodes or tripolar stimulation. Tripolar stimulation should never be needed to use. Choosing a proper bipolar configuration can cover all the area around the DBS lead that a tripolar can. Because the activation occurs near each active electrode, tripolar stimulation also activates the largest area of unwanted tissue.

## 5.5 Model improvements

Model could be further improved by adding certain properties and details into it. First of all the, the anisotropy was calculated from an average value of the whole MTT and expecting that fibers run straight down towards the mammillary body. Few similar studies have used the DTI or DTI atlases superimposed on the MRI images to create a more accurate representation of the anisotropy. However, in most reports the DTI has been acquired with isotropic voxels despite the anisotropic MRI voxels, in addition to over 2 mm DTI voxel size [34, 21, 33]. MTT for example, has dimensions far smaller than 2 mm and DTI voxels of that size would include information about the surrounding tissues.

In this model, only ANT, MTT and lateral ventricle were separated from thalamus and its borders, but other nuclei and white matter could be added as well. For example stria medullaris is very close to the ANT and may affect the stimulation. Planar model could be expanded into three dimensional model of the thalamus, but it would require considerable time investment and knowledge of the slice thicknesses in the atlas.

Electrochemical double layer is another detail that exists between the electrodes and the encapsulation tissue. Electrochemical double layer forms on the tissue-metal interface and is few micrometers thick and its conductivity depends on the stimulation parameters, such as pulse frequency. Electrochemical double layer is not included in most models either, but some studies claim that it has a noticeable impact [30].

Another improvement for the model would be to take the α-dispersion into account. Dispersion in biological matters describes the frequency dependence of conductivity and permittivity. At frequencies between 1 Hz to 100 kHz α-dispersion is the dominant dispersion method. Its causes are still slightly unclear, but it is believed to arise from the counter-ion polarizations at the membrane surface or from the polarization of the internal membrane structures. It has a significant impact on the membrane permittivity which can go up to thirtyfold increase. Therefore choosing the literature values of permittivity closest to simulation frequencies, might affect the electric field propagation drastically. [11, 61, 62]

If the electrochemical double layer and the α-dispersion would be included in the model, then the quasistatic approximation had to be discarded. Adding more details and variables into the model will also increase the uncertainty of the results. Model details that have a negligible impact on the results should be avoided, as the uncertainty in them has a tendency to multiply in the end results [35].

# 6. CONCLUSION

The objective of this thesis was to create a model that could be used to observe the electrical behavior of the deep brain stimulation. Effect of the stimulation was evaluated with the concept of volume of tissue activated (VTA), which describes the level of neuronal activation. 3D model was first created to give insight into complex VTA volumes. Then the effects of tissue response in the form of an encapsulation were observed. Additionally, a 2D model of the thalamus was created to illustrate stimulation interactions with different tissue types and to create a more realistic sense of the areas that can be affected with the DBS.

Exact quantification of the VTA is an extremely complex task. Numerous variables concerning the electrical properties of the tissue types and individual variations in tissue geometry increase the uncertainty of the results. Activation functions are dependent on stimulation parameters and axonal geometry, which may have infinite combinations. Using average values regarding to tissue properties and stimulation, gives a rough estimate on how the DBS affects the target and the surrounding neurons.

Misplaced electrodes are one of the major concerns in DBS surgeries and 1/3 mm misplacement may correspond to a few volts in amplitude increase. Encapsulation is always present and affects stimulation performance greatly. Growing of the encapsulation tissue within the first weeks after the implantation may eventually require stimulation amplitudes to be increased by over 100% of the initial value.

Presence of different tissue types introduces huge conductivity variations. These changes in electrical properties can significantly alter the shape of the VTA. Anisotropic fiber tracts have a similar effect. Clinicians are always balancing between the treatment results, the adverse effects and power consumption. Instead of increasing the stimulation amplitude to spread the VTA into target region, changing the stimulation polarity or active electrode, may produce a more efficient outcome. Overall, the simulations were in accordance with other similar studies and clinical reports.

# REFERENCES


[1] D. Tarsy, J. L. Vitek, P. A. Starr and M. S. Okun, Deep Brain Stimulation in Neurological and Psychiatric Disorders, Totowa, NJ: Humana Press, 2008.

[2] World Health Organization, "WHO Fact sheets: Epilepsy," [Online]. Available: http://www.who.int/mediacentre/factsheets/fs999/en/. [Accessed 5 2016].

[3] C. H. Halpern, U. Samadani, B. Litt, J. L. Jaggi and G. H. Baltuch, "Deep Brain Stimulation for Epilepsy," *Neurotherapeutics,* pp. 59-67, 2008.

[4] A. M. Kuncel and W. M. Grill, "Selection of stimulus parameters for deep brain stimulation," *Clinical Neurophysiology,* no. 115, pp. 2431-2441, 2004.

[5] P. Brodal, Central Nervous System: Structure and Function, Oxford University Press, 2010.

[6] C. R. Noback, N. L. Strominger, R. J. Demarest and D. A. Ruggiero, The Human Nervous System Structure and Functions, Humana Press, 2005.

[7] R. Nieuwenhuys, J. Voogd and C. van Huijzen, The Human Central Nervous System, Springer Berlin Heidelberg, 2008.

[8] S. M. Sherman, "Thalamic relays and cortical functioning," *Progress in Brain Research,* no. 149, pp. 107-126, 2005.

[9] M. J. Aminoff and R. B. Daroff, Encyclopedia of the Neurological Sciences (Second Edition), Academic Press, 2014.

[10] M. D. Binder, N. Hirokawa and U. Windhost, Encyclopedia of Neuroscience, Springer, 2009.

[11] H. Nyberg and K. Jokela, Sähkömagneettiset kentät, Helsinki: Säteilyturvakeskus, 2006.

[12] S. M. Sherman, "Tonic and burst firing: dual modes of thalamocortical relay," *TRENDS in Neuroscience,* no. 24, pp. 122-126, 2001.

[13] J. Malmivuo and R. Plonsey, Bioelectromagnetism: principles and applications of bioelectric and biomagnetic fields, New York: Oxford University Press, 1995.

[14] J. R. Reitz, F. J. Milford and R. W. Christy, Foundations of electromagnetic theory, Reading, MA: Addison-Wesley, 1992.

[15] M. N. Sadiku, Numerical techniques in electromagnetics with MATLAB, Boca Raton, FL: CRC, 2009.

[16] W. H. Smithson and M. C. Walker, "What is Epilepsy," in *ABC of Epilepsy*, Blackwell Publishing Ltd., 2012.

[17] K. M. Hartikainen, L. Sun, M. Polvivaara, M. Brause, K. Lehtimäki, J. Haapasalo, T. Möttönen, K. Väyrynen, K. H. Ogawa, J. Öhman and J. Peltola, "Immediate effects of deep brain stimulation of anterior nuclei on executive functions and emotion-attention interaction in humans," *Journal of Clinical and Experimental Neuropsychology,* no. 36, pp. 540-550, 2014.

[18] V. Krishna, N. Kon Kam King, F. Sammartino, I. Strauss, D. M. Andrade, R. M. Wennberg and A. M. Lozano, "Anterior Nucleus Deep Brain Stimulation for Refractory Epilepsy: Insight Into Patterns of Seizure Control and Efficacious Target," *Neurosurgery,* no. 0, pp. 1-10, 2016.

[19] D. Denys, M. Feenstra and R. Schuurman, Deep Brain Stimulation A New Frontier in Psychiatry, Amsterdam: Springer, 2012.

[20] Medtronic, Inc., "Medtronic DBS Implant manual," Medtronic, Inc., Minneapolis, MN, 2014.

[21] C. C. McIntyre, S. Mori, D. L. Sherman, N. V. Thakor and J. L. Vitek, "Electric field and stimulating influence generated by deep brain stimulation of the subthalamic nucleus," *Clinical Neurophysiology,* no. 115, pp. 589-595, 2004.

[22] R. Fisher, V. Salanova, T. Witt, R. Worth and T. Henry, "Electrical stimulation of the anterior nucleus of thalamus for treatment of refractory epilepsy," *Epilepsia,* pp. 899-908, 2010.

[23] J. Buhlmann, L. Hofmann, P. A. Tass and C. Hauptmann, "Modeling of a segmented electrode for desynchronizing deep brain stimulation," *frontiers in NEUROENGINEERING,* no. 4, 2011.

[24] A. F. Sadikot, M. M. Chakravarty, G. Bertrand, V. V. Rymar, F. Al-Subaie and D. L. Collins, "Creation of computerized 3D MRI-integrated atlases of the human basal ganglia and thalamus," *frontiers in NEUROSCIENCE,* no. 5, 2011.

[25] Allen Institute for Brain Science, "Allen Human Brain Atlas," [Online]. Available: http://www.brainspan.org/static/atlas. [Accessed 8 2016].

[26] T. Möttönen, J. Katisko, J. Haapasalo, T. Tähtinen, T. Kiekara, V. Vähärä, J. Peltola, J. Öhman and K. Lehtimäki, "Defining the anterior nucleus of the thalamus (ANT) as a deep brain stimulation target in refractory epilepsy: Delineation using 3 T MRI and intraoperative microelectrode recording," *NeuroImage: Clinical,* no. 7, pp. 823-829, 2014.

[27] J. Volkmann, E. Moro and R. Pahwa, "Basic Algorithms for the Programming of Deep Brain Stimulation in Parkinson's Disease," *Movement Disorders,* no. 21, pp. 284-289, 2006.

[28] K. Lehtimäki, T. Möttönen, K. Järvenätausta, J. Katisko, T. Tähtinen, J. Haapasalo, T. Niskakangas, T. Kiekara, J. Öhman and J. Peltola, "Outcome based definition of the anterior thalamic deep brain stimulation target in refractory epilepsy," *Brain Stimulation,* 2015.

[29] W. M. Grill and T. Mortimer, "Electrical Properties of Implant Encapsulation Tissue," *Annals of Biomedical Engineering,* no. 22, pp. 23-33, 1994.

[30] M. Djilas, A. Mercanzini, P. Harbi, A. Dransart and S. Jezernik, "Influence of Encapsulation Tissue Reaction on the Volume of Tissue Activated with Deep-Brain Stimulation Electrodes: A Simulation Study," in *7th Annual International IEEE EMBS Conference on Neural Engineering*, Montpellier, France, 2015.

[31] W. M. Grill and J. T. Mortimer, "The Effect of Stimulus Pulse Duration on Selectivity of Neural Stimulation," *IEEE Transactions on Biomedical Engineering,* no. 43, pp. 161-166, 1996.

[32] C. R. Butson, C. B. Mask and C. C. McIntyre, "Sources and effects of electrode impedance during deep brain stimulation," *Clinical Neurophysiology,* no. 117, pp. 447-454, 2006.

[33] C. R. Butson, S. E. Cooper, J. M. Henderson and C. C. McIntyre, "Patient-specific analysis of the volume of tissue activated during deep brain stimulation," *NeuroImage,* no. 34, pp. 661-670, 2007.

[34] M. Åström, J.-J. Lemaire and K. Wårdell, "Influence of heterogeneous and anisotropic tissue conductivity on electric field distribution in deep brain stimulation," *Medical and Biological Engineering and Computing,* no. 50, pp. 23-32, 2012.

[35] C. Cobelli and E. Carson, Introduction to modeling in physiology and medicine, London: Academic Press, 2008.

[36] COMSOL AB, *COMSOL Multiphysics User's Guide,* 2012.

[37] K. H. Matucha, Materials Science and Technology A Comprehensive Treatment: Structure and Properties of Nonferrous Alloys, Weinheim: Wiley-VCH, 1996.

[38] D. O. Kipp, Plastic Material Data Sheets, MatWeb, LLC, 2010.

[39] P. A. Hasgall, F. Di Gennaro, C. Baumgartner, E. Neufield, M. C. Gosselin, D. Payne, A. Klingenböck and N. Kuster, "IT'IS Database for thermal and electromagnetic parameters of biological tissues," 9 2015. [Online]. Available: www.itis.ethz.ch/database. [Accessed 8 2016].

[40] C. C. McIntyre, A. G. Richardson and W. M. Grill, "Modeling the Excitability of Mammalian Nerver Fibers: Influence of Afterpotentials on the Recovery Cycle," *Journal of Neurophysiology,* no. 87, pp. 995-1006, 2001.

[41] MathWorks, Inc., *Matlab Image Processing Toolbox User's Guide,* Natick, MA, 2015.

[42] T. Hanekom, "Modelling encapsulation tissue around cochlear implant electrodes," *Medical and Biological Engineering and Computing,* no. 43, pp. 47-55, 2005.

[43] W. M. Grill and T. Mortimer, "Electrical Impedance of Electrode Encapsulation Tissue," in *14th Annual International Conference of the IEEE, Engineering in Medicine and Biology Society*, 1992.

[44] V. S. Polikov, P. A. Tresco and W. M. Reichert, "Response of brain tissue to chronically implanted neural electrodes," *Journal of Neuroscience Methods,* no. 148, pp. 1-18, 2005.

[45] N. Yousif, R. Bayford and X. Liu, "The influence of reactivity of the electrode-brain interface on the crossing electric current in theraoeutic deep brain stimulation," *Neuroscience,* no. 156, pp. 597-606, 2008.

[46] J. Latikka, T. Kuurne and H. Eskola, "Conductivity of living intracranial tissues," *Physics in Medicine and Biology,* no. 46, pp. 1611-1616, 2001.

[47] L. A. Geddes and L. E. Baker, "The specific resistance of biological material—A compendium of data for the biomedical engineer and physiologist," *Medical and biological engineering,* no. 5, pp. 271-293, 1967.

[48] S. B. Baumann, D. R. Wozny, S. K. Kelly and F. M. Meno, "The Electrical Conductivity of Human Cerebrospinal Fluid and Body Temperature," *IEEE Transactions on Biomedical Engineering,* no. 44, pp. 220-223, 1997.

[49] R. Sadleir, "A Bidomain Model for Neural Tissue," *International Journal of Bioelectromagnetism,* no. 12, pp. 2-6, 2010.

[50] J. C. Kolecki, "An Introduction to Tensors for Students of Physics and Engineering," National Aeronautics and Space Administration, Cleveland, OH, 2002.

[51] H. G. Kwon, J. H. Hong and S. H. Jang, "Mammillothalamic tract in human brain: Diffusion tensor tractography study," *Neuroscience Letters,* no. 481, pp. 51-53, 2010.

[52] D. M. Koh and H. C. Thoeny, Diffusion-Weighted MR Imaging, Springer Berlin Heidelberg, 2010.

[53] D. S. Tuch, V. J. Wedeen, A. M. Dale, J. S. George and J. W. Belliveau, "Conductivity tensor mapping of the human brain using diffusion tensor MRI," *Proceedings of the National Academy of Sciences,* no. 98, pp. 11697-11701, 2001.

[54] F. Rattay, "Analysis of Models for External Stimulation of Axons," *IEEE Transactions on Biomedical Engineering,* pp. 974-977, 1986.

[55] J. B. Ranck, "Which elements are excited in electrical stimulation of mammalian central nervous system: A review," *Brain Research,* no. 98, pp. 417-440, 1975.

[56] D. Liewald, R. Miller, N. Logothetis, H.-J. Wagner and A. Schüz, "Distribution of axon diameters in cortical white matter: an electron-microscopic study on three human brains and a macaque," *Biological cybernetics,* no. 108, pp. 541-557, 2014.

[57] M. Åström, E. Diczfalusy, H. Martens and K. Wårdell, "Relatioship between Neural Activation and Electric Field Distribution during Deep Brain Stimulation," *IEEE Transaction on Biomedical Engineering,* no. 62, pp. 664-72, 2015.

[58] D. Poole, Linear algebra: a modern introduction, Belmont, CA: Thomson, 2006.

[59] L. Sun, J. Peräkylä, M. Polvivaara, J. Öhman, J. Peltola, K. Lehtimäki, H. Huhtala and K. M. Hartikainen, "Human anterior thalamic nuclei are involved in emotion-attention interaction," *Neuropsychologia,* no. 78, pp. 88-94, 2015.

[60] C. Back, F. Alesch and H. Lanmüller, "Postoperative Monitoring of the Electrical Properties of Tissue and Electrodes in Deep Brain Stimulation," *Neuromodulation,* no. 6, pp. 248-253, 2003.

[61] J. D. Bronzino, The Biomedical Engineering Handbook, Second Edition, CRC Press, 1999.

[62] S. Grimnes and O. G. Martinsen, "Alpha-dispersion in human tissue," in *14th International Conference on Electrical Bioimpedance*, Gainesville, FL, 2010.

# APPENDIX A: MONOPOLAR VTA CONSTITUENTS

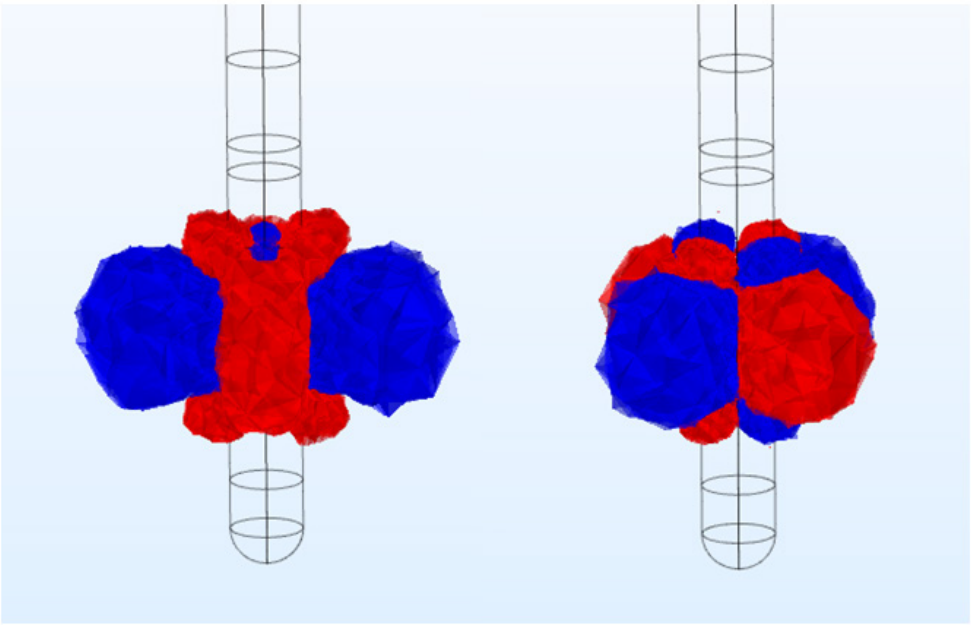

***Figure A-1.*** *VTA constituents of a monopolar stimulation in a homogenous and isotropic medium. $\partial x \partial x$ component on the left and $\partial x \partial y$ component on the right. Red volumes represent depolarization and blue volumes represent hyperpolarization.*

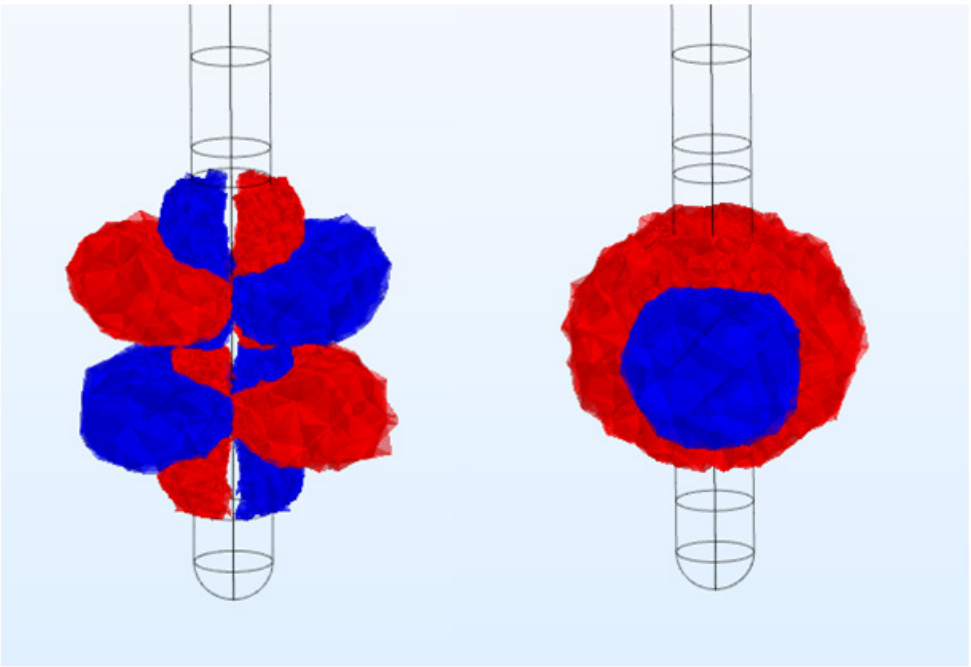

***Figure A-2.*** *VTA constituents of a monopolar stimulation in a homogenous and isotropic medium. $\partial x \partial z$ component on the left and $\partial y \partial y$ component on the right. Red volumes represent depolarization and blue volumes represent hyperpolarization.*

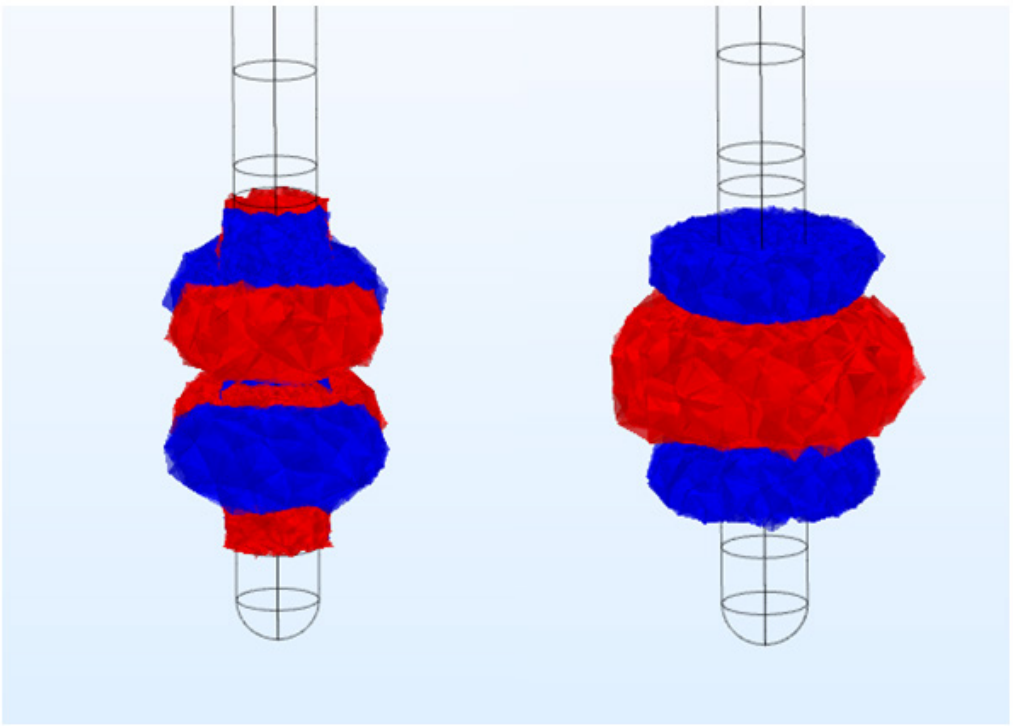

***Figure A-3.*** *VTA constituents of a monopolar stimulation in a homogenous and isotropic medium. $\partial y \partial z$ component on the left and $\partial z \partial z$ component on the right. Red volumes represent depolarization and blue volumes represent hyperpolarization.*

# APPENDIX B: BIPOLAR VTA CONSTITUENTS

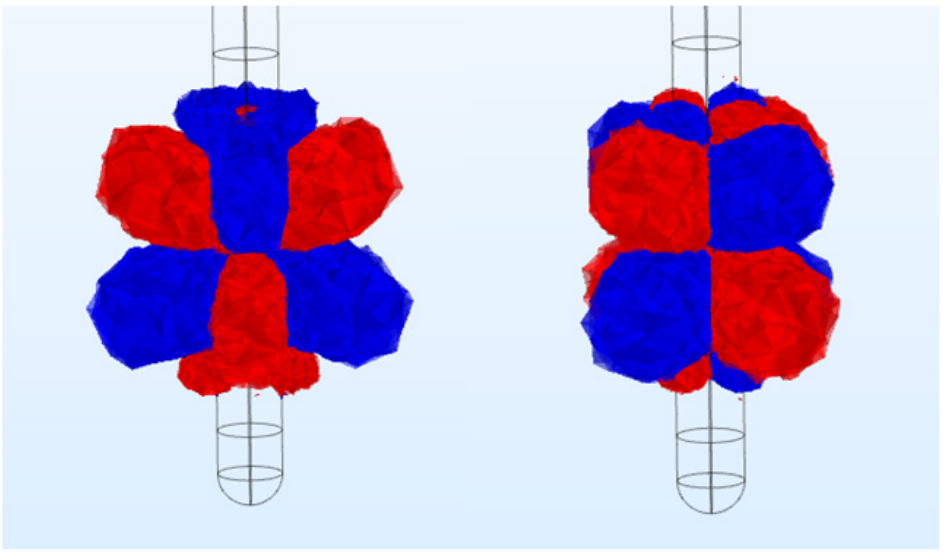

***Figure B-1.*** *VTA constituents of a bipolar stimulation in a homogenous and isotropic medium. $\partial x \partial x$ component on the left and $\partial x \partial y$ component on the right. Red volumes represent depolarization and blue volumes represent hyperpolarization.*

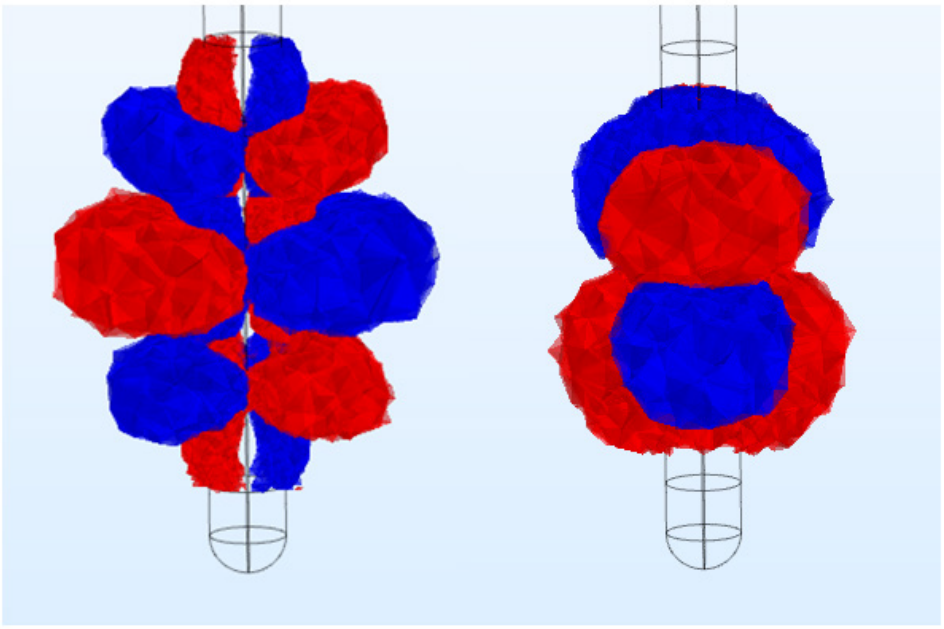

***Figure B-2.*** *VTA constituents of a bipolar stimulation in a homogenous and isotropic medium. $\partial x \partial z$ component on the left and $\partial y \partial y$ component on the right. Red volumes represent depolarization and blue volumes represent hyperpolarization.*

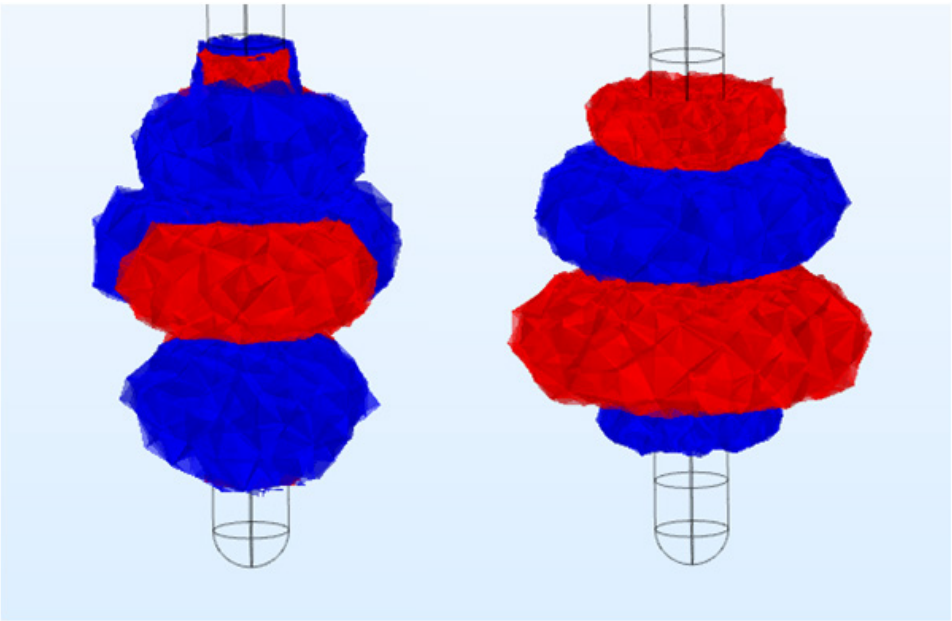

***Figure B-3.*** *VTA constituents of a bipolar stimulation in a homogenous and isotropic medium. ∂y∂z component on the left and ∂z∂z component on the right. Red volumes represent depolarization and blue volumes represent hyperpolarization.*